Durham E-Theses

Bright galaxy number counts

Marr, J.H.

How to cite:

Marr, J.H. (1995) *Bright galaxy number counts*, Durham theses, Durham University. Available at
Durham E-Theses Online: http://etheses.dur.ac.uk/5373/

Use policy

Declaration

This thesis is submitted for approval for the degree of MSc at the University of Durham. I confirm that this work is wholly my own work and no part of the material offered has previously been submitted by me for a degree at this or any other university.

J. H. Marr

March 1995

BRIGHT GALAXY NUMBER COUNTS

Thesis for M.Sc. by J.H. Marr

Supervisor: Dr. T. Shanks

Department of Physics,

University of Durham,

Durham DH1 3LE,

England.

Dedicated to Ann

"The opposite of a deep truth is also a deep truth" - Bohr

Abstract

The value of a plot of galaxy number counts per unit area of sky against magnitude as a probe of the early universe is well known, being influenced by both the curvature of expanding space and the deceleration parameter. The observations are complicated by changes which almost certainly have taken place in the intrinsic brightness of the distant galaxies over the long time periods involved, through both evolution and possible galaxy mergers over this time. In the blue band surveys fainter than $\sim 22^m$, the counts exceed the theoretical non-evolving models by a factor of 2–4, which at present is accounted for by requiring strong evolution in the models. An additional observational problem in determining the extent of such possible evolution is the observed under-density of counts over the brighter end of the curve ($\sim 12 - 18^m$) compared to the numbers at fainter magnitudes. This thesis details the theoretical models on which the predictions are based, re-examines several recent surveys to evaluate how well these can be fitted to assumed luminosity functions of the Schechter type, then examines number counts over this brighter range to look for possible causes for the observed discrepancy. Four possibilities are considered to account for this: (1) Photometric anomalies and technical problems, (2) Incomplete surveys over this range, (3) The presence of voids or strong inhomogeneities in this region, (4) The effect of evolutionary changes on the shape of the theoretical models. It is concluded that the survey data is reasonably robust, and the number count models may require merging evolution to account for the bright- end discrepancy as well as the faint–end anomalies.

CONTENTS

1. Introduction

1.1 Historical perspective - homogeneous models and inhomogeneous observations

An excellent historical account of the progressive development of galaxy number counts is provided by Peebles (1980), who gives a full discussion of the progress of successive observations and their interpretation as the observations achieved ever fainter magnitudes, and I am indebted to this work for many of the historical references.

In 1917, the phrase 'the large-scale distribution of matter' was taken to mean the distribution of stars in the Milky Way. The star counts were found to be different in different directions of the sky, and to increase less rapidly with increasing limiting magnitude than the simple Euclidean proportionality $N(m) \propto 10^{0.6m}$ had predicted. The implication was that the solar system was near the edge of a disk–like system.

In his early paper of 1917, Einstein argued that a homogeneous world model fitted well into general relativity theory and the requirements of Mach's principle. Hubble (1926) was the first to ask whether the counts of faint spiral nebulae are consistent with the assumption of uniform distribution through space. He applied Seares' (1925) estimate of the limiting magnitude $m \approx 16.7$ to the data of Fath (1914) and found the number of faint nebulae to agree well with that expected from extrapolation of the Euclidean slope at $m < 12$. This was an impressive success, for there are 600 times more galaxies in the deep survey as at $m < 12$, and this came as a complete contrast to the behaviour of the star counts. The implication was that observations of stars reached the edge of the finite volume of space containing them, whilst observations of galaxies gave no suggestion of any edge or other inhomogeneity.

It is now known that Hubble's early results were largely fortuitous, since galaxies at $\lesssim 12^m$ are not a fair sample. Even in 1931 and 1934 when Hubble extended his magnitude limits to $\sim 19^m.1$ and $19^m.6$, the ratio of counts agreed well with the $10^{0.6m}$ law, as did the ratios of these counts to those of Shapley-Ames (1932), this time through the fortuitous presence of the local supercluster. Then in 1936 Hubble considered counts to 5 limiting magnitudes in the range $18^m.5 - 21^m.0$. He now found the counts to increase less rapidly with m than the $10^{0.6m}$ law, with a discrepancy amounting to a factor of 1.8 over this range of magnitudes. He tentatively concluded that the discrepancy was larger than might be expected in a relativistic model, and suggested that relativity theory might be incorrect. Hubble's main point however remains valid: to the depth of the survey there

1

is no evidence of an edge to the universe of the galaxies, and most theorists were quick to accept this evidence. Thus Einstein (1933) wrote: 'Hubble's research has shown that these [galaxies] are distributed in space in a statistically uniform fashion, by which the schematic assumption of the theory of a uniform mean density receives experimental confirmation', and Robertson (1935) in an influential review said: 'we accept the data, due primarily to Hubble and Shapley, on the uniform distribution of matter in the large within the visible universe, and we extrapolate them to the universe as a whole'.

It is no coincidence that a first note of caution was sounded by a theoretician who was also an astronomer; in 1932, de Sitter wrote 'It should not be forgotten that all this talk about the universe involves a tremendous extrapolation, which is a very dangerous operation'. During the 1930's there was a running debate between Hubble and Shapley over the relative importance of departures from homogeneity. Both clearly recognised that the galaxy distribution is strongly clumped on relatively small scales. For example, Hubble (1934) found that the frequency distribution of galaxy counts in different telescopic fields is not Poisson, as would be expected if the galaxies were randomly distributed, and the general clumping makes for a considerable broadening of counts, and he made the interesting observation that the distribution of $\log N$ is remarkably close to Gaussian. However, to Hubble, the main observation was the uniform distribution on large scales as revealed by very deep counts averaged over many sample fields. Shapley (1938) in contrast emphasised the great irregularities in the galaxy distribution: 'the irregularities are obviously too pronounced to be attributed to chance; they are rather a demonstration of evolutionary tendencies in the metagalactic system'. Having the use of smaller telescopes than Hubble, Shapley and his colleagues could only study galaxy distribution to a shallower depth, but they studied it in greater detail across the sky. He noted a considerable difference in the numbers of Shapley–Ames galaxies in the northern and southern galactic hemispheres, and suggested that this north–south asymmetry might amount to as much as 50% at $17^m.0$. The data also suggested that galaxy density might vary by a factor of ~ 2 on scales $\sim 30°$ at $\sim 18^m$, though there were problems in transferring magnitude standards across the sky. This led Shapley (1938) to believe the galaxy distribution might not be close to uniform even when averaged over large scales, and he suggested that the deviation from the $10^{0.6m}$ law in Hubble's data might be the result of large–scale density irregularities, not a failure of relativity theory. Eddington (1939) and Tolman (1949) also suggested that large–scale inhomogeneity might account for Hubble's results.

Modern ideas expect relativity theory to be correct, and presume systematic errors in magnitude estimates plus required K–corrections to account for Hubble's discrepancy, and by the 1950's the possibilities of large scale inhomogeneities was largely ignored by cosmologists in the debate over homogeneous world models — especially steady state versus evolving, and possible values of parameters such as the cosmological constant, Hubble's constant and the time scale, the deceleration parameter, and open versus closed models. Thus Bondi's 1952 book on cosmology specifically rejected the suggestion of Eddington and Tolman as unprofitable. However, de Vaucouleurs (1971) has made the interesting point that 'If the universe really is close to homogeneous on the scale of the horizon cH_0^{-1}, it is a remarkable break with the state of affairs on smaller scales: from subatomic particles on up we deal with objects – localised structures.' He went on to note that this tendency to clump continues to scales at least as large as the local supercluster (the concentration of galaxies around the Virgo cluster, of which we are part), and he cited indications of irregularities on still larger scales, such as the large-scale correlation of rich clusters found by Kiang and Saslaw (1969), pointing to strong clustering on scales $\sim 100h^{-1}$ Mpc.

1.2 The bright n(b) problem

This difficulty in reconciliation between the observational inhomogeneities of the visible universe of the astronomer on the one hand, and the requirement for homogeneity insisted on by most theoreticians on the other, remained a central problem of cosmology. Over recent years, the plots of galaxy number counts have been extended to increasingly fainter magnitudes. One such curve from Shanks (1990) is shown in Fig. 1.1. This includes error bars for the Durham COSMOS survey, and a Euclidean $10^{0.6m}$ law slope (solid), described later in §2.1. The Revised Shapley–Ames (RSA) survey (1932) contains bright local galaxies to an apparent magnitude depth of 12.0, and is biased by an excess of galaxies in the local Virgo cluster. Discounting this, the plot of galaxies over the magnitude range $14 - 20$ is remarkably linear, and fits the theoretical Euclidean slope well.

Two further curves by Shanks are shown in Figs. 1.2a and 1.2b, based on other surveys detailed in his paper (1990), with a theoretical non–evolving model curve (solid). The problem with normalising the curves is now apparent. The first section of the theoretical curve (to $b_J \sim 17^m.5$) approximates well to the Euclidean curve, but if normalised at $\leq 17^m$ it is too low above this range, while if normalised over the range

Figure 1.1. The plot of five bright surveys: The Durham redshift survey (DARS), Durham COSMOS survey, Collins *et al.* , APM (Maddox *et al.*), and RSA. Also shown are the Euclidean $10^{0.6m}$ law slope and a theoretical curve for a non-evolving model. From Shanks (1990).
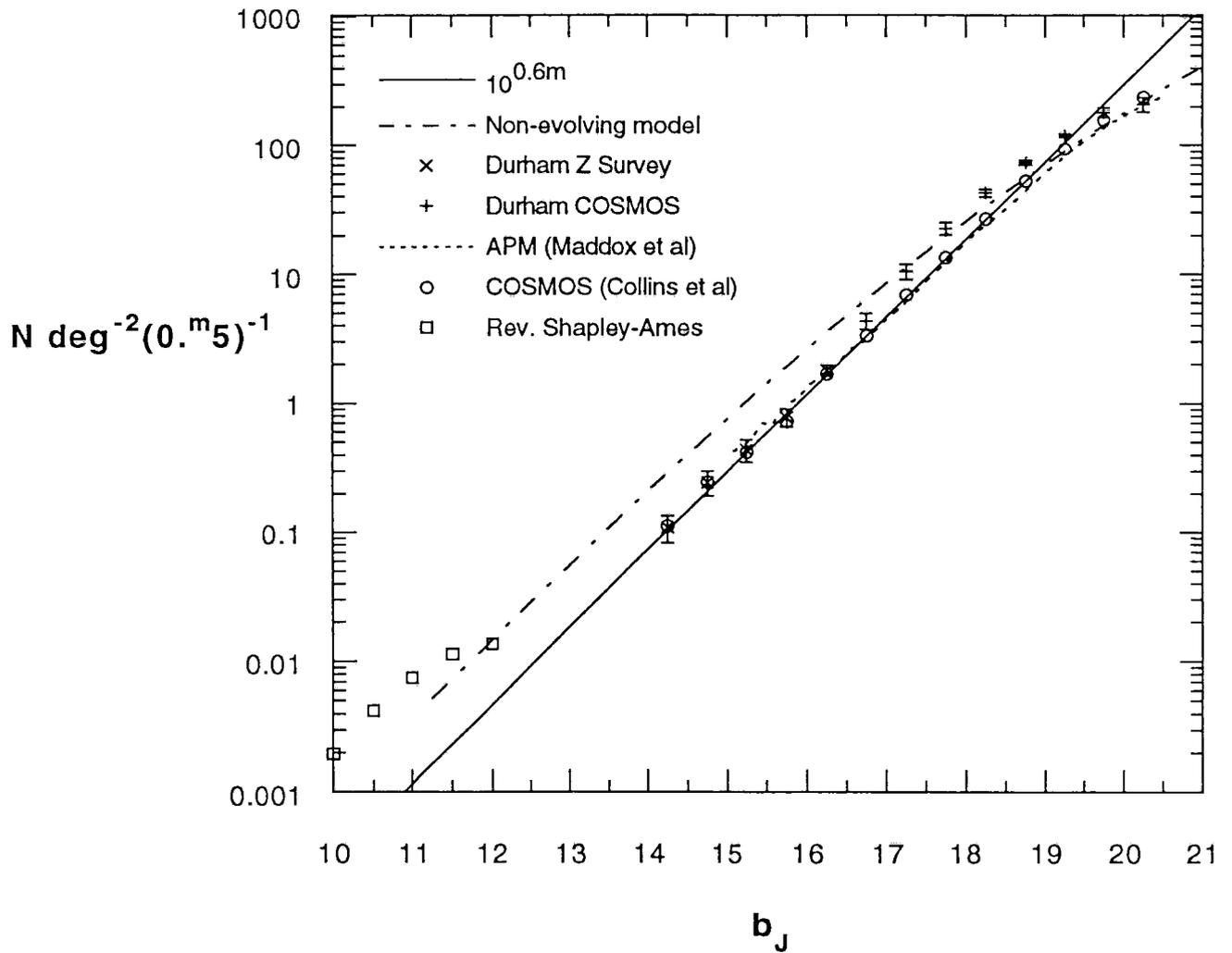
Fig. 1.1

Figure 1.2a. A fainter plot incorporating the surveys of Figure 1.1 with additional surveys of RC2, Zwicky, and the Durham CCD plots, compared to a theoretical non-evolving model and (Figure 1.2b) a curve showing the APM data of Maddox *et al.* , the Durham COSMOS data, Durham redshift survey data (Z SURVEY) and Collins *et al.* COSMOS survey against the theoretical non-evolving model, emphasising the number count deficit over the range $15 - 18^m$. From Shanks (1990).

N

Bccd

Fig. 1.2a

Legend:
- □ Nens
- ● NZwi
- △ RC2)
- — model
- □ Ndars
- □ Nccd
- — Bq.02noevc

$N \ deg^{-2}(0.^m5)^{-1}$

- —— Non-evolving model
- × Durham Z Survey
- + Durham COSMOS
- ---- APM (Maddox et al)
- ○ COSMOS (Collins et al)
- □ Rev. Shapley-Ames

b_J
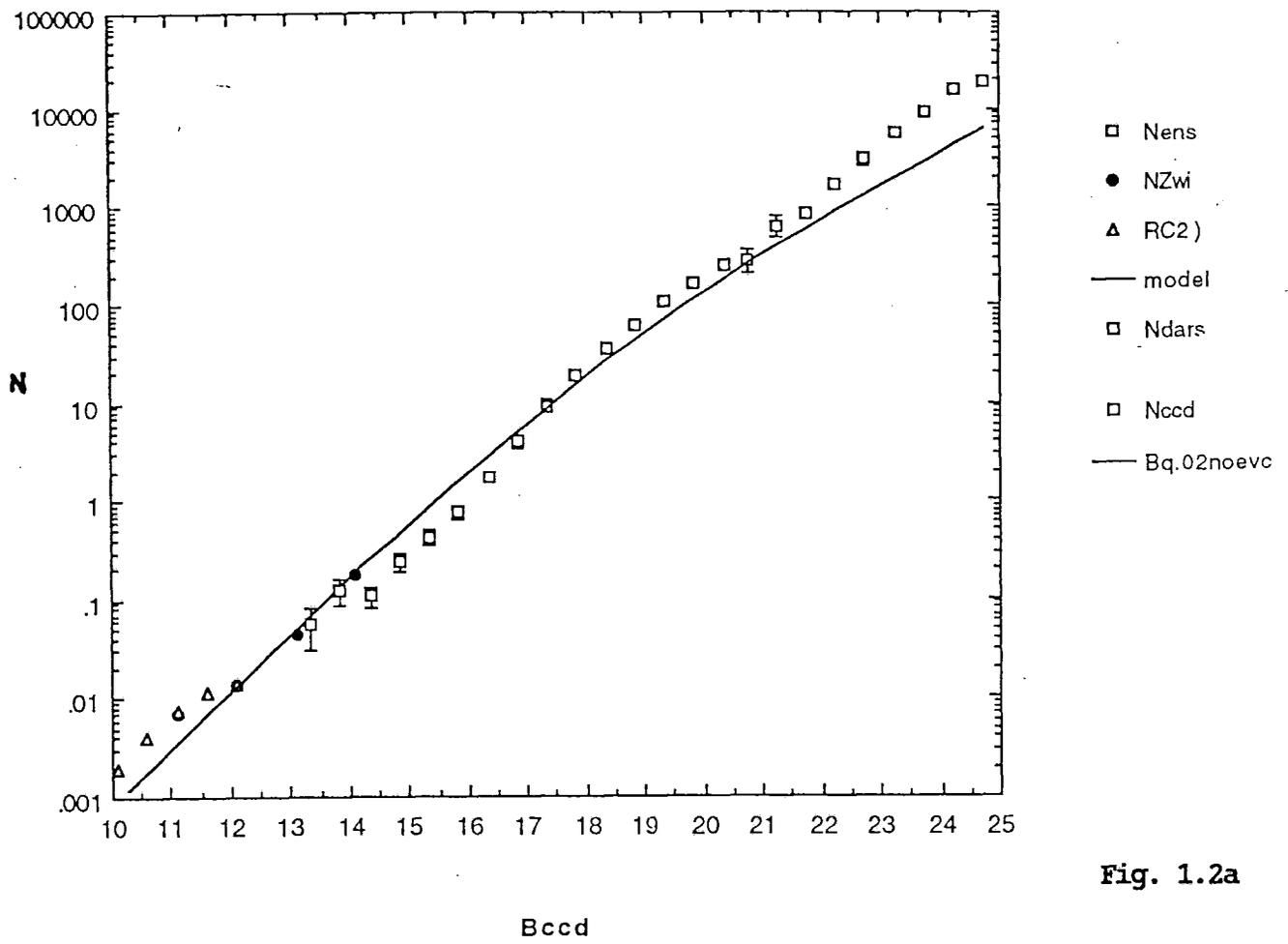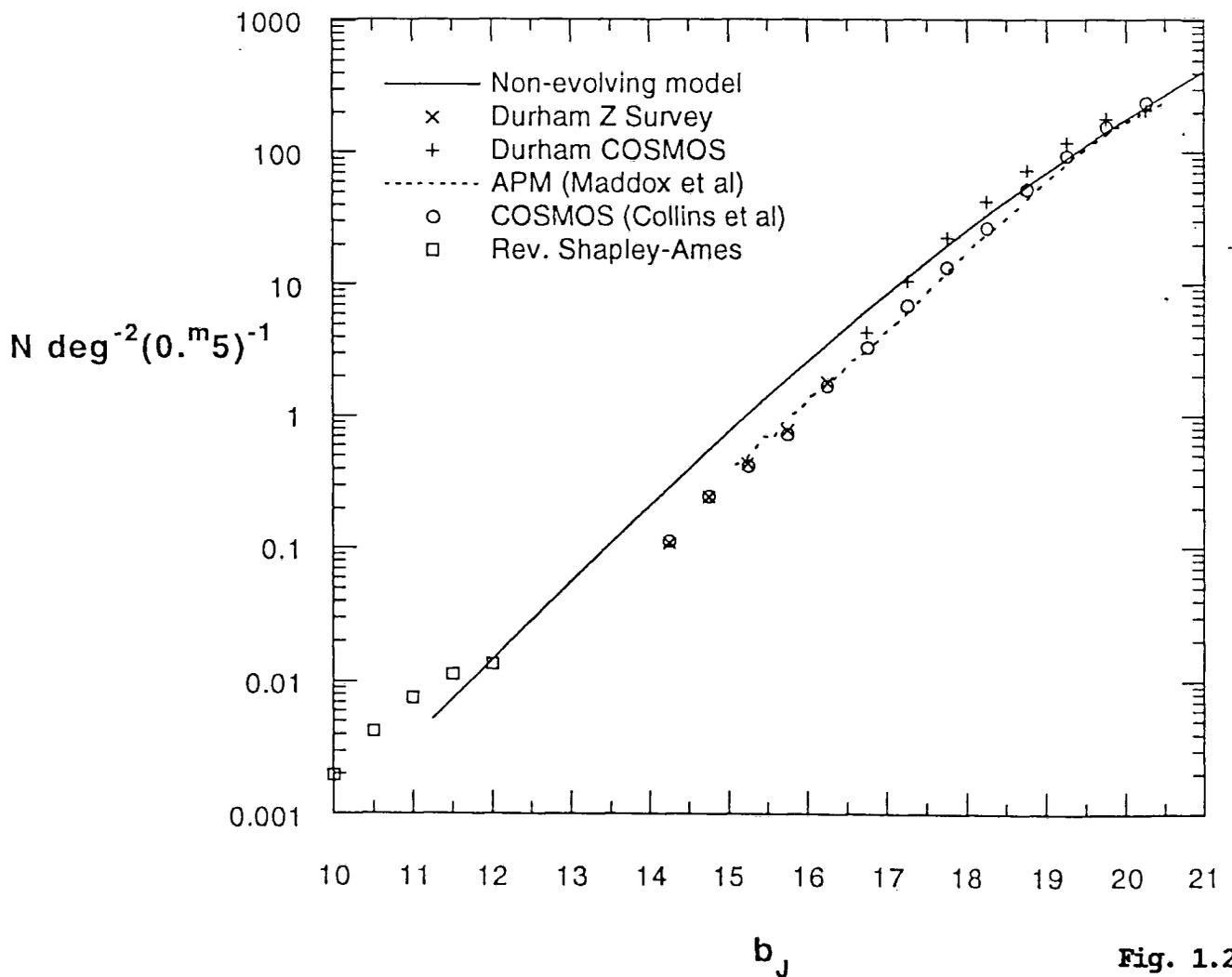
Fig. 1.2b

$18 - 20^m$ there is an apparent deficiency in the number counts in the brighter range; even with this normalisation there remains a considerable excess in blue counts beyond $\sim 22^m$. The departure from the models at faint magnitude/high number density is well known, and continues to produce considerable debate about possible causes such as: galaxy evolution (ie galaxies were brighter in the past, with active star formation, so more can be seen to greater depth in the b_J range); an increase in absolute galaxy numbers in the past through merging models; low density models ($q_0 < 0.5$) which give a greater volume of space with look–back distance; and 'exotic models' with non-zero Λ.

A more extensive plot with results from several disparate surveys is shown in Fig. 1.3, with two theoretical curves for $q_0 = 0.02$ (solid line) and $q_0 = 0.5$ (dotted line), corresponding to 'open' and 'flat' non–evolving models in conventional FRW dust universes with zero expansion parameter, Λ. The theory underlying these curves is considered in §2.2. The absolute normalisation of the curves to the observational data is arbitrary, as any theoretical normalisation awaits better models of the evolution of galaxy luminosity and merging. In general the homogeneity of the universe is a function of scale and is expected to become more homogeneous over larger volumes and, for this reason, it has become usual practice to normalise the curves at the fainter range, $\sim 17 - 22^m$. Thus Shanks (1990) normalises in the range $18^m \leq B_j \leq 22^m$, which has the advantages of being conservative and requiring less evolution at the fainter end; but normalisation in this range has the effect of introducing a deficit or under–count in the brighter range ($\sim 14 - 17^m$) followed by the local excess brighter than $\sim 12^m$. Over the range $18.0 < b_J < 25^m$, the observed number counts are closely log–linear with a slope 0.45 ± 0.02 (Metcalfe *et al.* 1987, Tyson 1988). Models assuming no evolution, and based on local properties of the galaxy population, yield slopes of $\sim 0.3 - 0.35$. If the counts are normalised to the no-evolution model at $b_J = 18^m$, this difference in slopes gives an observed galaxy excess by factors of 1.6, 2.5 and 4 at $b_J = 20, 22$ and 24^m respectively. Faint number counts in the U passband have an even steeper slope, while those in the R and I are flatter and closer to the no–evolution model. Number counts in the K–band have been reviewed by Gardner *et al.* (1993) and indicate minimal excess, with the discrepancy in counts accounted for wholly by a change in colour at a redshift $z \sim 1$, beyond which galaxies become progressively bluer due to evolution.

4

Figure 1.3. A full plot of sixteen independent surveys, with two theoretical non-evolving curves for $q_0 = 0.02$ ('open') and $q_0 = 0.5$ ('flat') models.
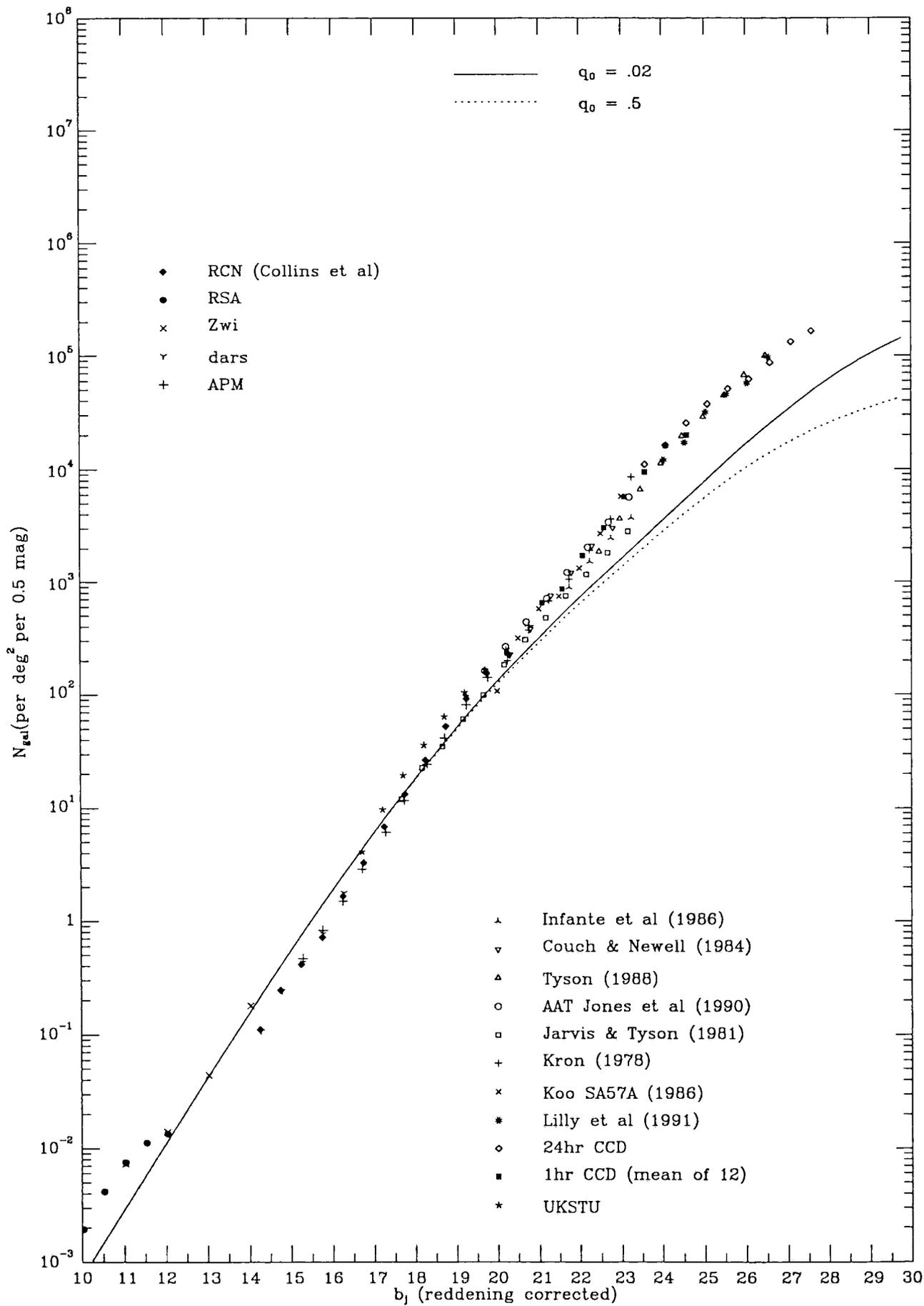
Fig. 1.3

1.3 Some possible solutions to the bright n(b) problem

In addition to theoretical uncertainty in the models, several practical problems contribute to the scatter in number-count normalisation (e.g. Tyson, 1988):

(1) The number of galaxies per area of sky near the 21st magnitude is approximately equal to the number of stars at this magnitude. The distinction is usually resolved using a star–galaxy classification algorithm, but different observers use different algorithms. It is therefore important to use an algorithm with a large dynamic range.

(2) Fields surveyed near the north galactic pole have an excess of galaxies correlated with the Virgo and Coma clusters. Some of the photographic–survey fields in Jarvis and Tyson (1981) suffered from this pollution.

(3) Each survey will lose some of its area to bright stars, galaxies, or plate defects. Some observers correct for this defect while others do not.

(4) Differences between observers in the type of photometry can contribute to an offset, while also affecting the slope at the faint end of the survey. For example, isophotal magnitudes will always result in an undercount at the faint end, unless a minimum area criterion is imposed, as faint- galaxy surface-brightness profiles eventually sink below the isophotal cutoff, whereas aperture magnitudes suffer a Malmquist bias due to noise scattering more faint objects into a fixed aperture than it scatters bright objects out.

1.3.1 Photometry errors

Several fundamental problems have caused the calibration of magnitudes to be fraught with uncertainties. Modern observations have progressed so rapidly in recent years, with the development of more sensitive CCD devices attached to ever larger mirrors, that it has been impossible to survey more than a few tiny areas of sky in any detail. Although the CCD devices offer the hope of consistent sensitivity, there is a problem in tying in these small areas with standard reference galaxies which were defined according to old photographic standards. An additional practical problem is that the CCD devices are so sensitive that brighter galaxies can either saturate them, or be so extensive in area that they are not contained on one CCD scan.

Photographic surveys suffer from well known problems of calibration, both internally (i.e. from field to field using the same emulsions and telescope) and externally, when adjacent fields are compared from different surveys. This has particularly been a problem between north and south sky surveys, and several methods of photometry are in use by

different investigators (see for instance Lilly, Cowie and Gardner 1991), which it is important to consider when comparing results on a common plot.

One such method is aperture photometry, where a fixed circular aperture is applied to all objects in all passbands. This has the advantages of simplicity since only the centre of each image is specified, and repeatability as the aperture is the same for all objects. If the seeing is the same for images at different wavebands, then it can produce accurate colours. Disadvantages are the contaminating effect of close neighbour galaxies, and the different fraction of light included in the aperture for objects with different profiles or physical sizes.

A second method is isophotal magnitudes, where the light is integrated out to some fixed limiting magnitude. This overcomes the problems of differing image profiles, but there is a strong redshift dependence on physical size, corresponding to a fixed isophote, because of: (a) the cosmological dimming effect, which goes as $(1 + z)^4$; (b) strong K–correction effects; and (c) for fainter objects, the light enclosed by the isophote may dim suddenly, especially when the isophotal limit becomes comparable to the seeing disk. A meaningful colour determination is also difficult, as the application of isophotal magnitudes in all passbands requires the use of potentially large and poorly understood corrections to the derived colours (e.g. Tyson 1988) and, since the isophote is determined for each object separately, interpretation of quoted magnitudes can be difficult.

A third method is the use of apertures that are determined by the shape of the light profile. If this is independent of waveband, then the fraction of light enclosed within a 'characteristic radius' should be independent of redshift; however the problems in the determination of colours from isophotal magnitudes also apply with this technique.

Overlap from fields in these surveys onto those in the standard reference catalogues is generally done by extrapolation using a curve of growth, but there are some incompatibilities between these surveys from both the measuring techniques and differing automated counting methods. The APM method removes bright peaks and measures integrated density; on a scale of 0-7 (corresponding to the photographic range of unexposed to full saturation), the night–sky brightness is usually set to a scale of 1 for sky-limited plates (corresponding to the beginning of the linear photographic emulsion exposure/log intensity plot), while the COSMOS plate analyser cuts off all images darker than a scale level of 2. The overall result is that spirals and ellipticals should be offset relative to each other in terms of their scan magnitude, as ellipticals have steeper, sharper profiles.

This can be done from their colours and from photographic data, and may introduce an estimated error of $\sim 0^m.1$. In addition, there is a departure from linearity at the brighter end on translating COSMOS magnitudes into CCD magnitudes. This is slight for spiral galaxies, but can be as great as $0^m.5$ for the bright ellipticals (brighter than $\sim 14^m$). Machine saturation becomes severe for galaxies brighter than $b_J \leq 15$, and the APM image analyser and software used by Maddox *et al.* (1990) to scan their Schmidt plates is unreliable for images larger than ~ 1mm on the plate (equivalent to $\sim 1'$). This means that the correction for galaxies is not strictly correct and makes calibration of APM magnitudes at $b_J < 15$ uncertain.

Correlation of the various surveys is best done with fields of overlap or fields in common, but there are few good ones. The best tested one (Metcalfe) is the GSM field, and the recent CCD results of Metcalfe are now placed within ~ 0.2 mag of each other.

The available CCD photometry data (Metcalfe *et al.* 1989) suggests that these problems are not too serious in the range $b_j \geq 14^m$. Overall, there is an estimated error of $\sim 0.2 - 0^m.3$ in field-to-field correlations which, though important in itself, is insufficient to account for the count deficit in the range $13 - 17^m$, where the observed disparity is as large as $0^m.8$.

1.3.2 Incomplete surveys

This problem was hinted at in previous sections, and there are three causes for it. Firstly, there is statistical incompleteness caused by the paucity of data for the brightest galaxies, and the known inhomogeneities of the universe even in deep surveys, which always leave a question mark in the mind of the observer, who wonders how typical his particular survey actually is. However, recent transforms of the Zwicky magnitudes (e.g. review in Appendix I) suggest that the Zwicky counts also show good agreement for $b_j \leq 14^m$, and the field to field error bars shown in Fig. 1.1 suggest that the count deficit is a very significant effect, and unlikely to be due to statistical fluctuation.

Secondly, there is the well documented problem of selection bias and incompleteness. As stated in §1.3, at $\sim 21^m$, the number of galaxies equals the number of stars in a field and inevitably there will be a residual percentage of misclassified objects. When we consider models to mimic the observations, some form of luminosity function has to be assumed which in turn relies on the accurate measurement of redshift for many objects; this requires readily identifiable line spectra, which is another source of observer error.

Similarly, the models have to assume certain parameters for evolution and merging. Some attempt to quantify these from observations and from theoretical modelling of galaxy dynamics has been made, but inevitably there is considerable uncertainty and at the faintest end of the number count curves, theoretical effects of evolution (such as luminosity, star-burst models and merging) are generally employed to account for the excess galaxy numbers. A typical resultant curve using one of the Bruzual (1981) models is shown in Fig. 1.4, while Fig. 1.5 is derived from a $(1 + z)^3$ merging model normalised to 19^m.

Thirdly, each new survey inevitably goes to the observational limit of the telescope and CCD. This limit is invariably reached just short of the point where noise becomes indistinguishable from data, usually just where the data would become most interesting, being then still unknown. The very faintest surveys must always therefore be treated with caution, possibly pointing the way ahead, but awaiting confirmation from other workers before too much reliance can be placed on their theoretical implications.

1.3.3 The effects of large–scale structure on the surveys

The Copernican principle leads us to expect that the part of the universe we inhabit is probably typical of the universe at large. Observation shows that the universe is populated by hierarchical clustering, with extensive voids between the observable clusters and superclusters. We need not therefore be surprised if we note an excess of galaxies in our vicinity, as indeed we do with the Virgo cluster. The question then arises, are we separated from other superclusters by significant voids and, if so, what statistical effect will these have on our observations of galaxy counts? That there is large–scale structuring is well understood, and part of this thesis examines how this might influence $n(b)$. Figs. 1.6 and 1.7 show the type of curves that can be produced to mimic the bright-end observations. Fig. 1.6 assumes a simple local overdensity ($\phi^* = 2.0\phi_0$) out to $25h^{-1}$Mpcfollowed by a void ($\phi^* = 0.2\phi_0$) to $75h^{-1}$Mpc. Fig. 1.7 models a local overdensity ($\phi^* = 1.5\phi_0$ to $25h^{-1}$Mpc) followed by a void ($\phi^* = 0.5\phi_0$ out to $300h^{-1}$Mpc), represented in these models by simple step-functions.

Two further aspects of void simulation may be mentioned. Fig. 1.8 shows the effect of a homogeneous void of $\phi^* = 0.5\phi_0$ out to $180h^{-1}$Mpc, which follows the observations quite closely. Here two different values of α (-1.2 and -1.5) were looked at, but both gave the same result. Fig. 1.9 was derived via a different route; by generating Monte Carlo simulations using homogeneous and void fields (again with $\phi^* = 0.5\phi_0$ out to

Figure 1.4. A fit to the data using Bruzual evolutionary models for two values of q_0 (0.05 and 0.5).
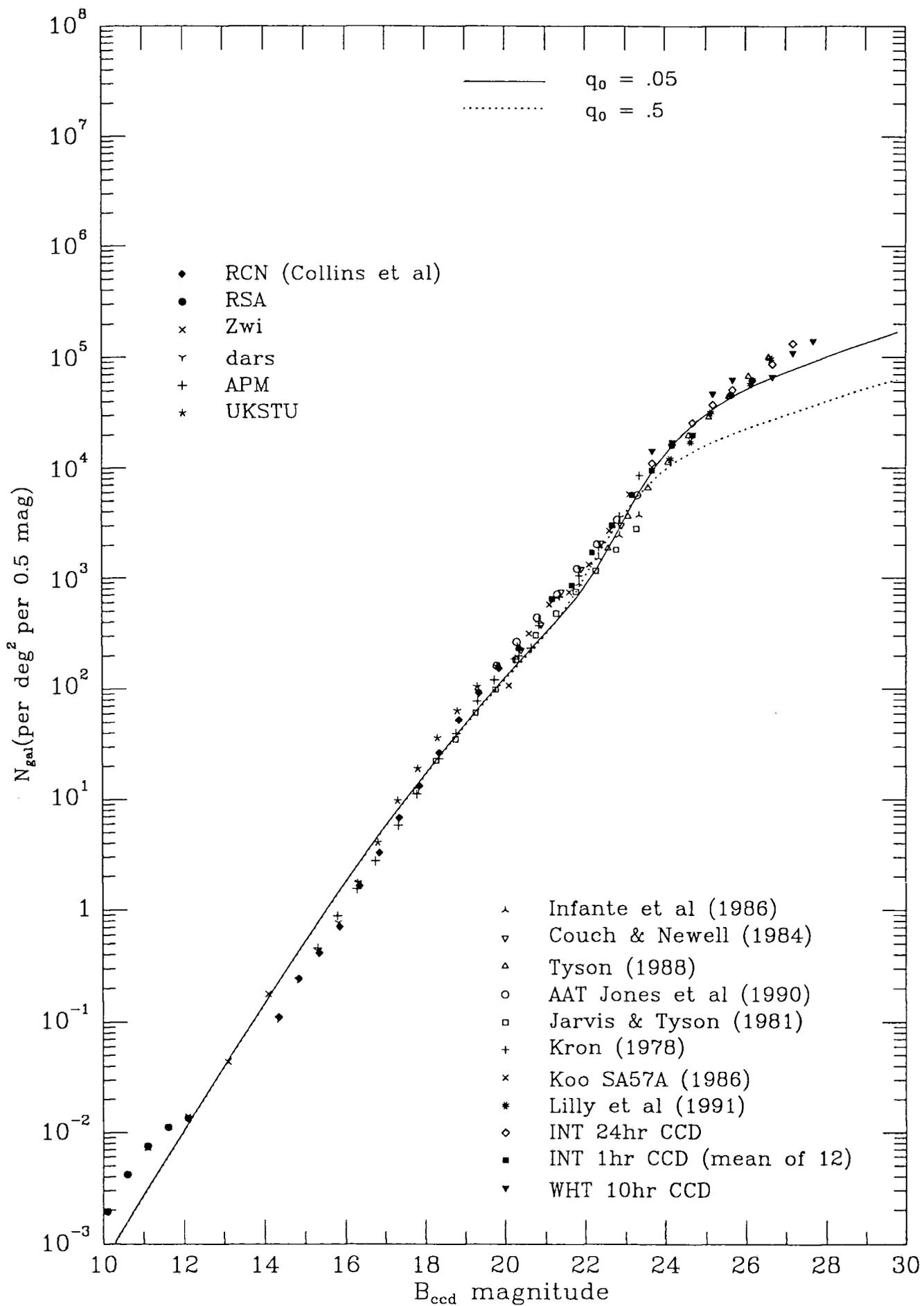
Fig. 1.4

Figure 1.5. A derived density–merging model for $q_0 = 0.5$ and using the merging parameter $(1 + z)^3$. Comparison curves are for the standard models with $q_0 = 0.02$ and $q_0 = 0.5$, all normalised to 19^m.
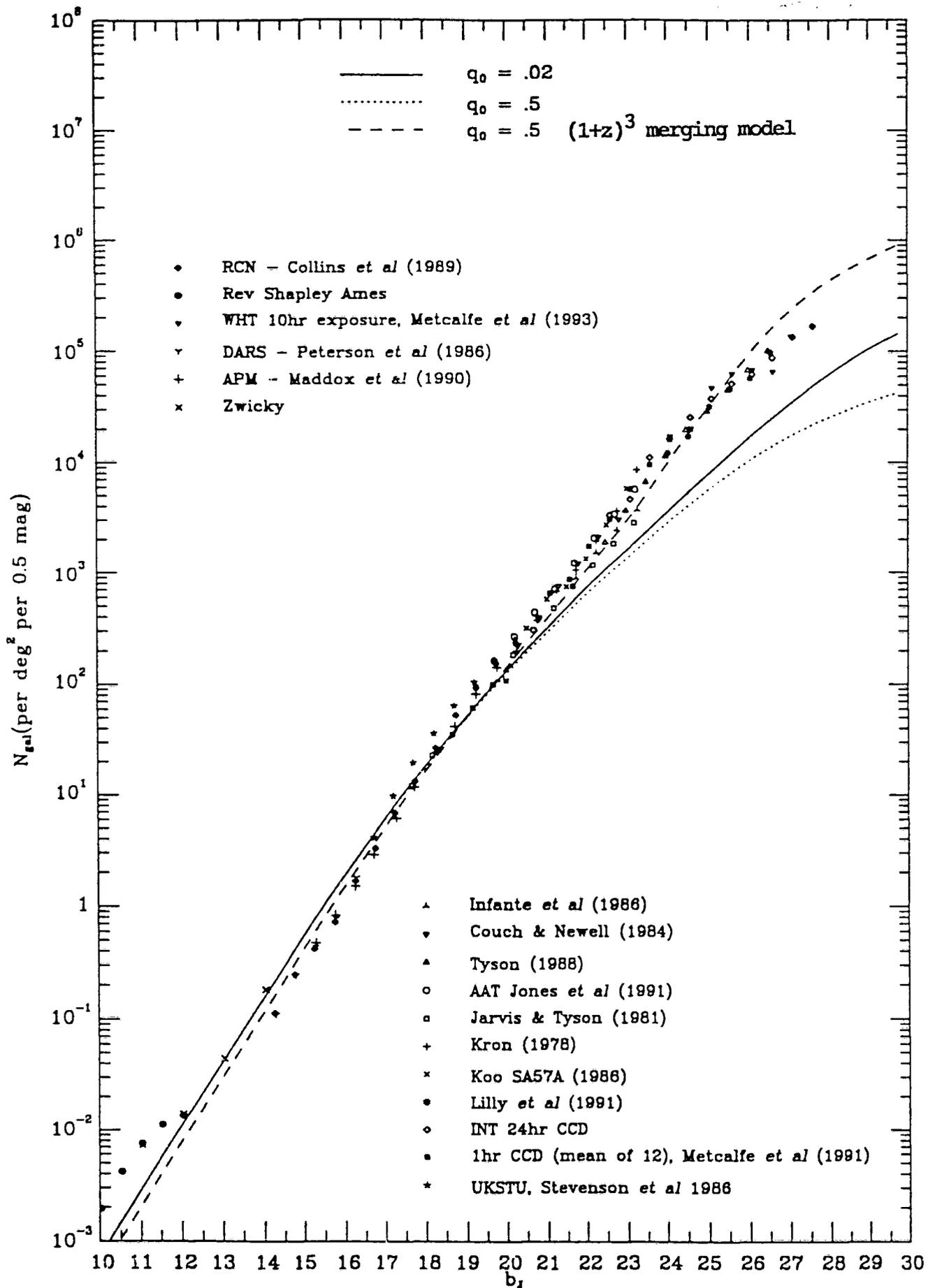
Models for 5 galaxy types from Metcalfe, Shanks, Fong and Jones (1991)

Fig. 1.5

Figure 1.6. A modest degree of local over density ($\phi^* = 2.0\phi_0$) to a depth of $25h^{-1}$ Mpc followed by an under density ($\phi^* = 0.2\phi_0$) to a distance of $75h^{-1}$ Mpc
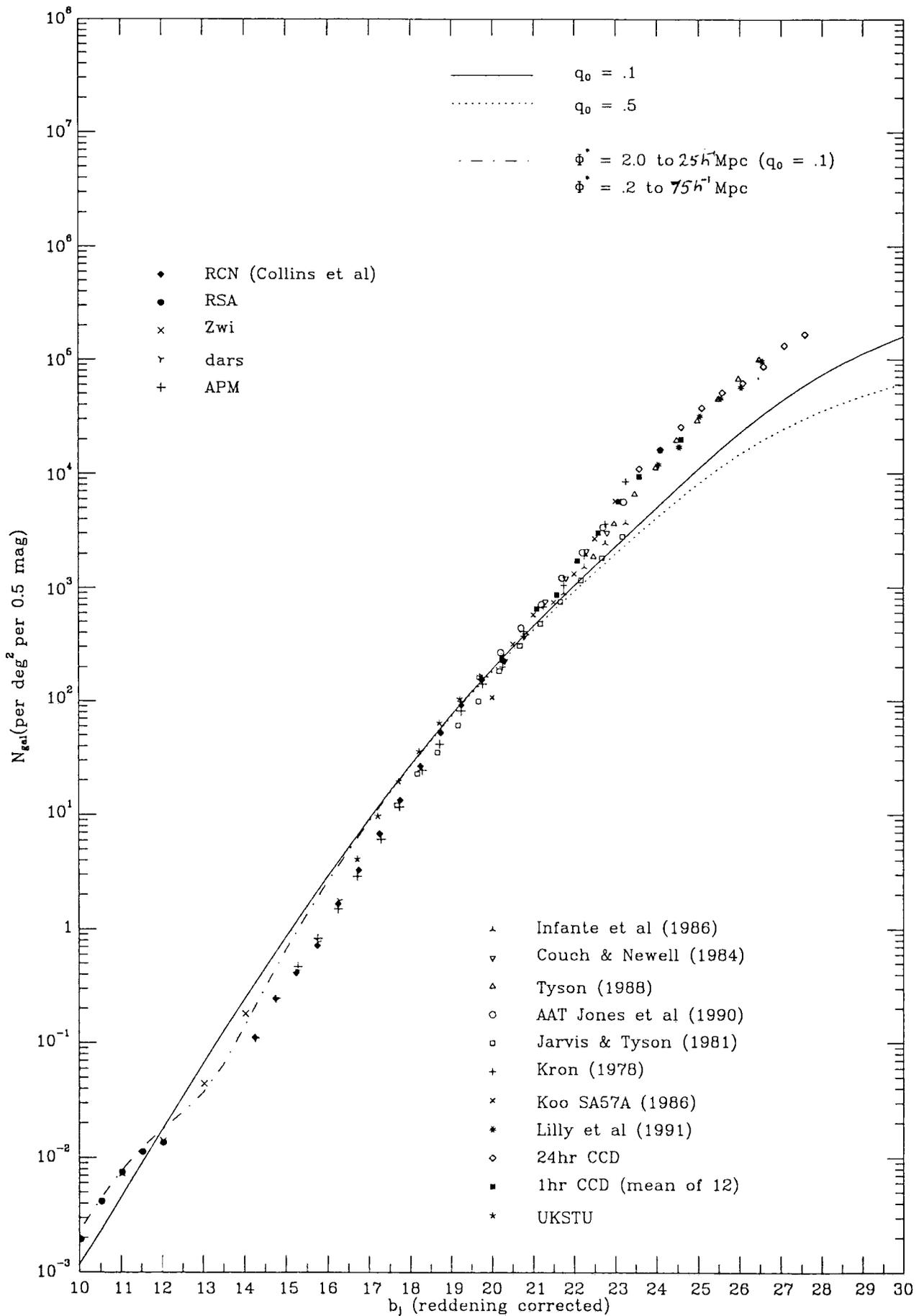
Fig. 1.6

Figure 1.7. As Fig. 1.5, but with the overdensity $\phi^* = 1.5\phi_0$ to $25h^{-1}$ Mpc and an under density of $0.5/phi_0$ to $300h^{-1}$ Mpc.
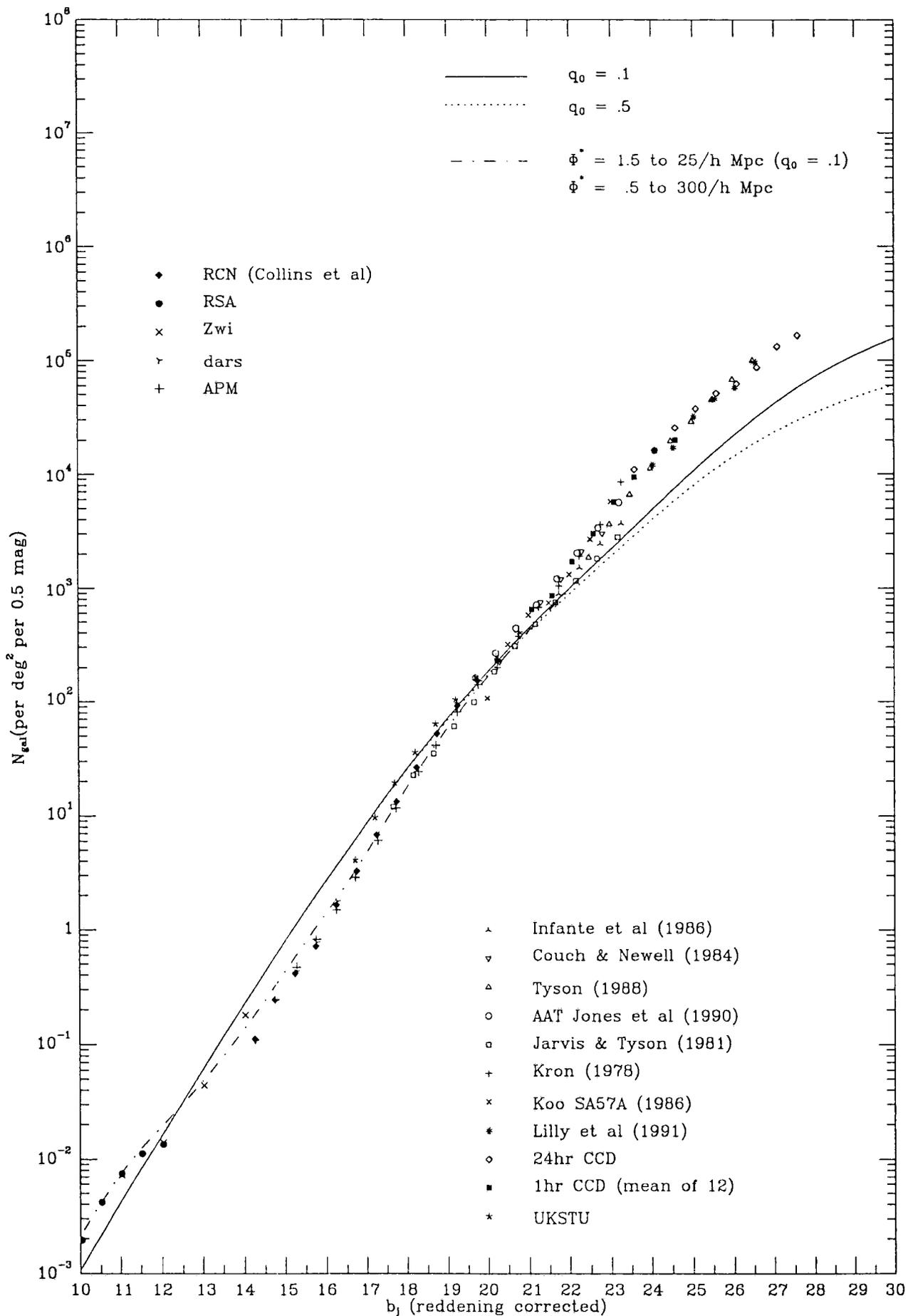
Fig. 1.7

Figure 1.8. A plot emphasising the brighter galaxy observations to $20^m.0$, and showing the exact equivalence of two void models (dashed lines) with $M^* = -19.9$, $\alpha = -1.5$ and $M^* = -19.6$, $\alpha = -1.2$ respectively. For both, the void put in was $\phi^* = 0.5\phi_0$ to $180h^{-1}$ Mpc. The comparison curve (solid) is for a $q_0 = 0.5$ model with K-correction $= 3z$, $M^* = -19.9$ and $\alpha = -1.5$.

$M^{\bullet} = -19.9$, $\alpha = -1.5$: Voids with $\Phi^{\bullet} = 0.5$ to $180h^{-1}$ Mpc

$M^{\bullet} = -19.6$, $\alpha = -1.2$

$q_0 = .5$ model, K-corr $= 3z$, $M^{\bullet} = -19.9$, $\alpha = -1.5$

1000

100

10

1

.1

.01

.001

N_g (deg^{-2} 0^m.5^{-1})

RCN – Collins *et al* (1989)

APM – Maddox *et al* (1990)

DARS – Peterson *et al* (1986)

Zwicky

Revised Shapley–Ames

Jarvis & Tyson (1981)

UKSTU, Stevenson *et al* 1986

10   11   12   13   14   15   16   17   18   19   20

b_j (reddening corrected)
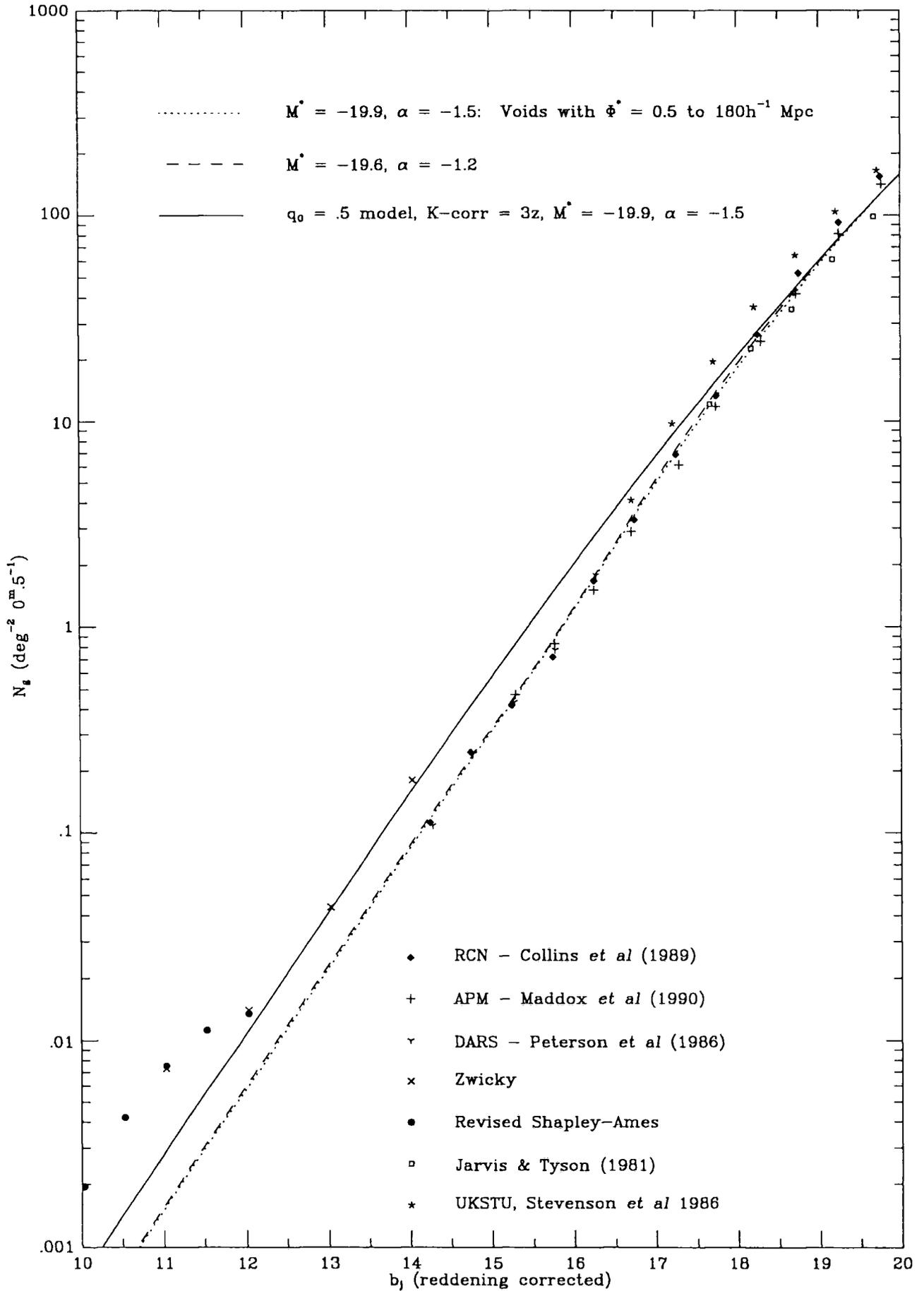
Plot of simulated fields, comparing homogeneous to void distributions.

Fig. 1.8

Figure 1.9. Monte Carlo plots for homogeneous fields and a void simulation with $\phi^* = 0.5\phi_0$ out to $180h^{-1}$. Brighter than $12^m.5$, the error bars due to the small numbers swamp the counts.
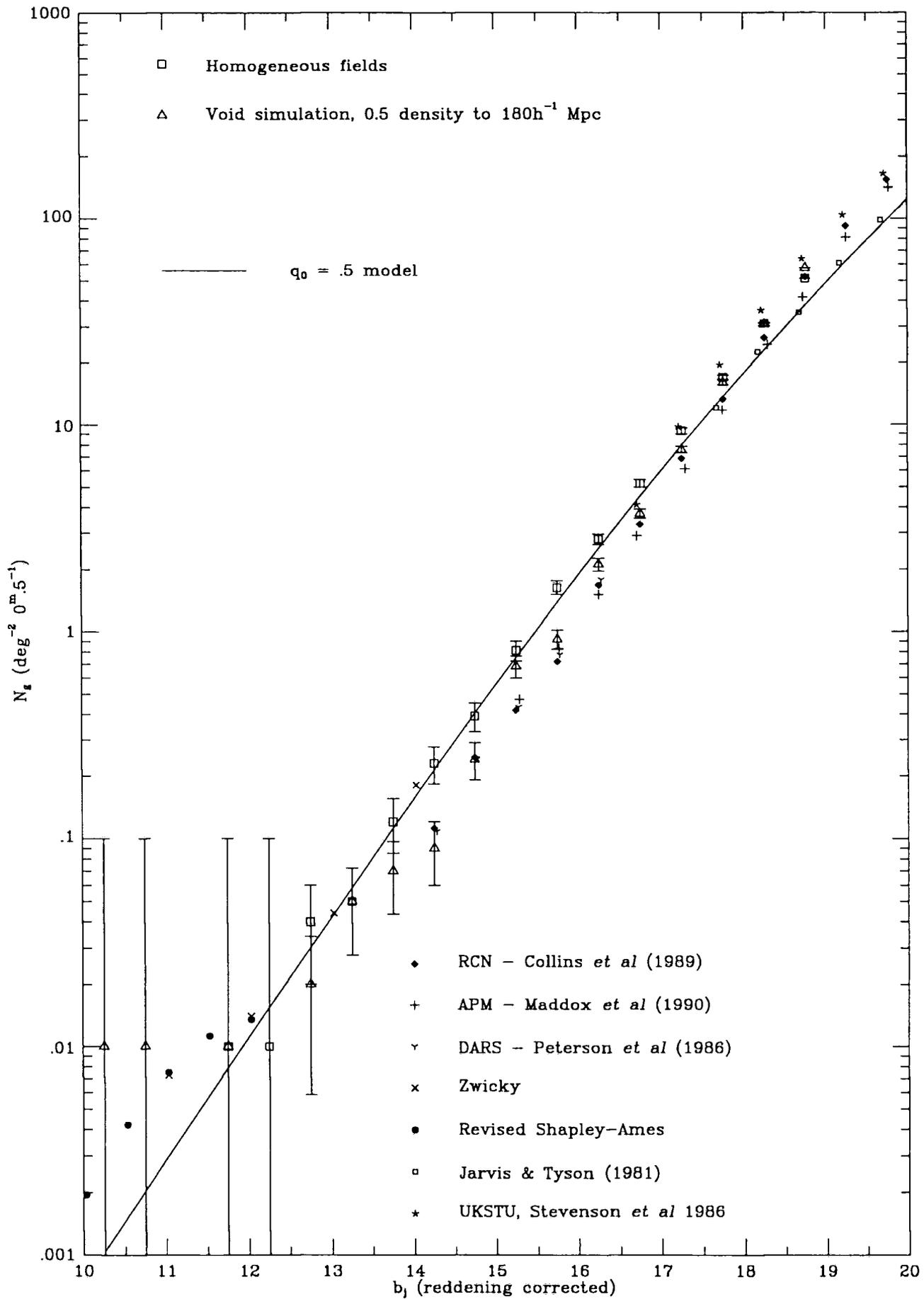
Plot of simulated fields, compared to real data fields of Figure 3.

Fig. 1.9

180h^{-1}Mpc) and supperimposing these over the observed field data. Error bars are included, and confirm the significance of the low counts over the range $b_j = 14 - 17^m$.

Whether such massive and homogeneous voids can be supported by the observational evidence is one of the subjects to be considered by this thesis.

1.3.4 Evolutionary effects on bright number counts

One final possibility that should be included in this review is that evolution might account for changes in luminosity and hence the observed number counts in each apparent magnitude bin. However, the luminosity functions are now well described for galaxies out to $b_j = 21^m.5$, and show little evidence for evolution in their form. Also the redshifts of the objects comprising these counts have been determined, and are generally found to be low. On both these grounds therefore, it is unlikely that luminosity evolution has any part to play in accounting for the number count enigma.

2. Theoretical curves

2.1 The Euclidean interpretation of number counts

The Euclidean model is of an ideal static universe with uniform density distribution extending to infinity, in which we initially consider a homogeneous distribution of galaxies with number density Φ_n and equal luminosity L.

The luminosity is related to the apparent magnitude m by the relationship:

$$m = A_0 - 2.5 \log \left(\frac{L}{4\pi r^2} \right) \tag{2.1.1}$$

The arbitrary normalisation constant A_0 is conveniently replaced by an absolute magnitude M, defined as the magnitude a source of brightness L would appear to have if at a distance of 10 parsec. This gives the relationship between m and r as:

$$m = M + 5 \log r + 25 \tag{2.1.2}$$

where r is now in h^{-1}Mpc. Expressing r in terms of m:

$$r = \text{dex} \left[0.2(m - M - 25) \right] \tag{2.1.3}$$

i.e.

$$r^3 = \text{dex} \left[0.6(m - M - 25) \right] \tag{2.1.4}$$

and

$$dr = 0.2 \, ln(10) r \, dm \tag{2.1.5}$$

The number of galaxies n contained in a shell of thickness δr at distance r and subtending solid angle $\delta\Omega$ is then

$$n = \Phi_n \, r^2 \, dr \, \delta\Omega \tag{2.1.6}$$

Substituting for r and dr, taking logs and differentiating,

$$\frac{d(\log n)}{dm} = 0.6 \tag{2.1.7}$$

which is the classic Euclidean slope for number counts in increments of m.

It may readily be seen that this is independent of absolute magnitude, and hence independent of any actual probability distribution of M. All that is required is that there be a uniform distribution of galaxies over the large scale, and that space be Euclidean.

2.2 The Standard G-R Model

There are only two practical methods for distance measurement of an object in cosmology: if we know its absolute luminosity we can compare this to its apparent luminosity, or — if we know its true diameter — this can be compared to its observed angular diameter. These give the luminosity distance (d_L) and the angular diameter distance (d_A) respectively. Weinberg (1972) additionally defines a third distance, d_P, the 'proper motion distance', where $d_P = R_0 r_e$; R_0 is the usual scale factor and r_e the comoving coordinate of the galaxy. For objects $\lesssim 10^9$ lt. yrs ($\lesssim 300$ Mpc) these distances are virtually identical to the familiar proper motion distance and parallax distances of standard astronomy; beyond these limits, however, cosmological effects are more pronounced and it becomes necessary to use the curvature corrections of general relativity.

The volume element in cosmology is usually quoted from the relationships of Weinberg derived from the Robertson-Walker line element (e.g. Phillipps *et al.* 1978; Yoshii and Takahara, 1988; Broadhurst *et al.* 1988; Colless *et al.* 1990):

$$d V = \sqrt{g}\, d\, r\, d\, \theta\, d\, \phi = R^3(t)(1 - kr^2)^{-\frac{1}{2}} r^2\, d\, r\, \sin\theta\, d\, \theta\, d\, \phi$$

$$\text{i.e.} \qquad d V = \frac{R_0^3 r_e^2\, d\, r\, d\, \Omega}{(1 - kr^2)^{\frac{1}{2}}} \qquad (2.2.1)$$

where $d\,\Omega$ is the solid angle of sky and k is the usual curvature constant. It may then be shown (eg Narlikar 1983, White 1990) that

$$R_0 r_e = \frac{z q_0 + (1 - q_0)(1 - y)}{(1 + z) q_0^2} \qquad (2.2.2)$$

where z is the observed redshift, $q_0 = \Omega_0/2$ is the deceleration parameter and $y = (1 + 2 q_0 z)^{\frac{1}{2}}$. It is then easily shown (Weinberg §14.4) that the luminosity distance and angular distance are given by: $d_L = R_0 r_e (1 + z)$ and $d_A = R_0 r_e /(1 + z)$ respectively,

$$\text{i.e.} \quad d_A = \frac{d_L}{(1 + z)^2}$$

$$= \left(\frac{c}{H_0}\right) \times \frac{z q_0 + (1 - q_0)(1 - y)}{(1 + z)^2 q_0^2} \qquad (2.2.3)$$

The comoving distance is defined by the line integral, with the substitution $x = (1+z)^{-1}$:

$$\int_0^{r_e} \frac{dr}{(1 - kr^2)^{\frac{1}{2}}} = \int_{t_1}^{t_0} \frac{dt}{R(t)}$$

$$= -\frac{1}{R_0 H_0} \int_1^x \left[1 - 2 q_0 + \frac{2 q_0}{x}\right]^{-\frac{1}{2}} \frac{dx}{x} = \{\cdots\} \qquad (2.2.4)$$

11

Differentiating both sides with respect to r, and substituting $dx = -(1+z)^{-2}dz$:

$$\frac{1}{(1-kr^2)^{\frac{1}{2}}} = \frac{d}{dx}\Big\{\cdots\Big\}\frac{dx}{dz}\frac{dz}{dr}$$

$$\text{ie} \qquad \frac{dr}{(1-kr^2)^{\frac{1}{2}}} = \frac{1}{H_0 R_0}\frac{dz}{(1+z)y} \qquad (2.2.5)$$

Then (remembering $1\,\text{deg}^2 = 3.0462 \times 10^{-4}$ radians), the differential comoving volume dV_c for 1 sq deg, is:

$$\frac{dV_c}{dz} = \left(\frac{c}{H_0}\right) \times 3.0462 \times 10^{-4}\, d_A^2\, \frac{(1+z)}{y}\, dz \qquad (2.2.6)$$

which is the model usually quoted when deriving theoretical curves in magnitude–number count plots, multiplied by a normalised number–density, n_0. Fig. 2.1 shows how differential volume varies with redshift for differing values of q_0.

.

Figure 2.1. Differential volume element/sq deg/unit redshift as a function of q_0.
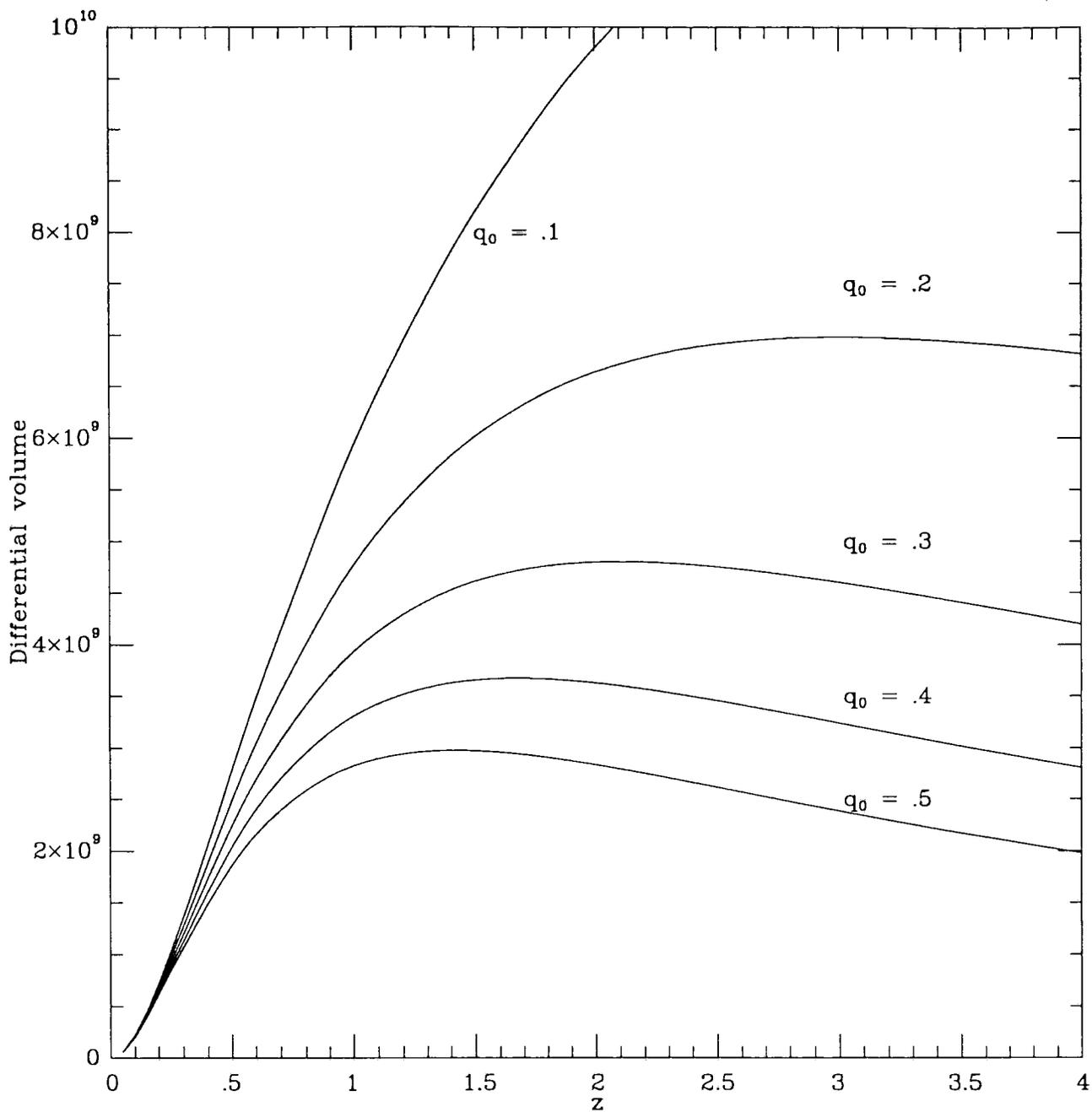
Differential volume element/sq deg/unit redshift (h^3 Mpc^3)

(as a function of q_0)

Fig. 2.1

2.3 K-corrections

K-corrections have to be introduced to allow for the cosmological reddining in a galaxy's spectrum at large distances, which brings a different part of the galaxy's spectrum into the observer's passband as compared to a zero redshift galaxy. The B-band (and to a lesser extent the R-band) K-corrections therefore need to take account of measurements of the spectral flux energy distribution of galaxies in the UV. These measurements can only be taken by satellite observatories, and the relevant observations from OAO-2, ANS and IUE satellites are summarised by Ellis (1982). King and Ellis (1985) compared the spectra of elliptical galaxies with 18 broad-band UV satellite measurements, and the UV spectra of later types with the average of 40 broadband UV observations from the OAO-2 and 70 from the ANS satellites. They found reasonable agreement between different observations for all morphological types to wavelengths down to 1500 Å, and concluded that the B-band K-corrections should be reliable to $z = 1.5$, and the R-band K-corrections to $z = 3.0$.

The following coefficients (Table 2.1) for the B-band K-correction polynomials were adopted for five galaxy types after King and Ellis, and these are plotted in Fig. 2.2.

Table 2.1 B-band K-correction coefficients used in the models

Galaxy type	a_0	a_1	a_2	a_3	a_4
E/S0	4.92	4.565	0.178	-1.744	0.703
Sab	2.08	4.316	-1.539	-1.029	0.502
Sbc	1.433	3.587	-1.894	-0.273	0.244
Scd	0.846	3.305	-3.203	1.301	-0.256
Sdm	0.248	1.935	-1.708	0.541	-0.126

Figure 2.2. K-corrections used in the models for five galaxy types: E/S0, Sab, Sbc, Scd, and Sdm.
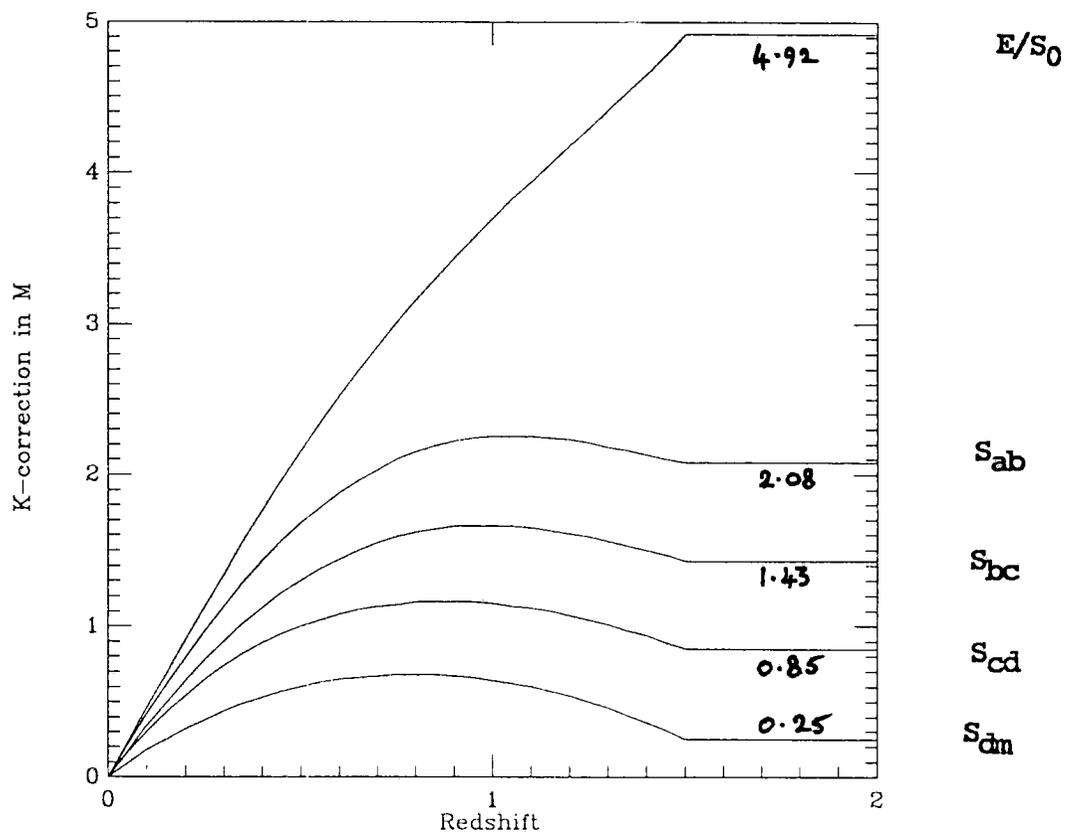
Fig. 2.2

2.4 The Luminosity Function

The mean number of galaxies/unit volume of space is conceptually straightforward, but has little value in observational astronomy. There are two principle reasons for this: a) with decreasing absolute magnitude, the number of galaxies/unit volume appears to increase continuously within the observational limit, and b) with increasing apparent magnitude, the actual number of galaxies observed per unit volume decreases as only those very close to us can actually be seen.

For a specific sample of galaxies, S, it is helpful to refer to a luminosity distribution given by Schechter (1975), defined as $n_s(L)$ galaxies per unit luminosity for the sample. For a given sample size, the volume of the sample will vary with the luminosity and can be defined as $V_s(L)$. Then

$$n_s(L)\,\delta L \equiv \text{ no of galaxies in } S \qquad (2.4.1)$$

in luminosity interval δL centred on L, and the luminosity function $\phi_s(L)$ of the sample S has the units of number of galaxies per unit luminosity per unit volume and is defined as

$$\phi_s(L)\delta L \equiv n_s(L)\delta L / V_s(L) \qquad (2.4.2)$$

Assuming the universe to be homogeneous on the large scale, Schechter defined a universal luminosity function $\phi(L)$ which is reached in the limit of $V_s(L) \rightarrow \infty$. Then for a random sample volume, the luminosity distribution will be

$$n(L)\delta L \equiv \phi(L)\,\delta L\,V_s(L) \qquad (2.4.3)$$

Schechter used the whole sky for his initial sample volume, excluding a zone $\pm 30°$ about the galactic equator where dust extinction is too high for accurate measurements. A further exclusion zone was taken within $6°$ of the Virgo cluster because of the high velocity dispersion in this field; this introduces an error in the volume of $< 1\%$ and is generally ignored. Schechter took his sample from the First Reference Catalogue of Bright Galaxies (de Vaucouleurs 1964, RC1) for galaxies brighter than $m_{B(0)lim} = 11.75$, and with well-defined (though sometimes independently obtained) redshifts. This gave him a sample of 184 galaxies for which he calculated d_L using $d_L = cz/H_0$, taking $H_0 = 50$ km sec^{-1} Mpc^{-1} with

$$M_{B(0)} = m_{B(0)} - 25 - 5\log d_L - A_b \times \csc b \qquad (2.4.4)$$

14

The highest redshift in his survey was $z \sim 0.014$, with a corresponding $d_L \sim 84$ Mpc and $M_{B(0)} \sim -23$, using $H_0 = 50$.

To calculate the volume, consider a small element at distance R from ourselves and elevation b to the galactic plane. Then the volume element is

$$\delta V = 2\pi R^2 \cos b \, \delta b \, \delta R \qquad (2.4.5)$$

and integrating over both hemispheres

$$V = 2 \int_0^{R^*} \int_{b_{lim}}^{90^\circ} 2\pi R^2 \cos b \, db \, dR \qquad (2.4.6)$$

$$= \frac{4\pi}{3} \int_{b_{lim}}^{90^\circ} R^{*3} \cos b \, d\, b \qquad (2.4.7)$$

where R^* is the limiting radius for any given intrinsic brightness $M_{B(0)}$, being the maximum distance out to which the galaxy may be seen. This can be defined in terms of the limiting apparent magnitude, $m_{B(0)lim}$, where $m_{B(0)}$ is related to d_L, the luminosity distance, by

$$m_{B(0)} = M_{B(0)} + 5\log(d_L) - 5\log(D) + A_b \csc b \qquad (2.4.8)$$

where the additional term is due to extinction by dust in the plane of our galaxy. Schechter assumed a value for A_b of 0.12 (Peterson 1970), and he limited the sample volume to $|b_{lim}| = 30^\circ$.

Rearranging (and remembering that $D = 10$ parsec $= 10^{-5}$ Mpc)

$$d_L = \text{dex}\left[0.2(m_{B(0)} - M_{B(0)} - 25 - A_b \csc b)\right] \qquad (2.4.9)$$

and substituting the limiting value for d_L into (2.4.7),

$$V[M_{B(0)}] = \frac{4\pi}{3} \int_{b_{lim}}^{90^\circ} \text{dex}\left[0.6(m_{B(0)lim} - M_{B(0)} - 25\right]$$
$$\times \cos b \, \text{dex}\left(-0.6 A_b \csc b\right) db \qquad (2.4.10)$$

The integral is an incomplete gamma function which may readily be computed to a value of 0.3987.

Schechter defined his luminosity function as

$$\phi(L)dL = \phi^*(L/L^*)^\alpha \exp(-L/L^*) \, d(L/L^*) \qquad (2.4.11)$$

but the standard figures and best–fit values are done in terms of a characteristic absolute magnitude, M^*. Rewriting (2.4.11) in terms of absolute magnitude, and from (2.4.3), this yields:

$$n_s(M)dM = K\phi^* \text{dex}\left[0.4(\alpha + 1)(M^* - M)\right] \exp\left\{-\text{dex}\left[0.4(M^* - M)\right]\right\}$$
$$\text{dex}\left[0.6(m_{lim} - M - 25)\right]dM \qquad (2.4.12)$$

with $K = 4\pi/3 \times 0.3987 \times 0.4 \times \ln(10)$. Schechter gave the following best fit values for his expression:

$$\phi^* V^* = 216 \pm 6$$

$$\phi^* = .005(H_0/50)^3 \text{Mpc}^{-3}$$

$$M^* = -20.6 + 5\log(H_0/50) \pm 0.11$$

$$\alpha = -1.24 \pm 0.19$$

Schechter next showed that his general luminosity function is also applicable to cluster galaxies. A composite luminosity function was constructed using 13 of the 15 rich clusters studies by Oemler (1974) to produce 13 bins of galaxies and each cluster was assumed to occupy a constant, though unknown, volume V_c which depended on where the cluster limit is drawn and the distance and richness of the cluster. Abell (1958) defined the richness of a cluster to be the number of galaxies in the two magnitude interval following the third brightest galaxy in a circle of radius 1.72 z^{-1} arc min., though Oemler counted galaxies out to two or three Abell radii.

Then using

$$n(L) \equiv \phi(L)\delta L\, V_s(L) \qquad (2.4.13)$$

$$n_s(M)\, dM = K\phi^*\, V_c\, \exp\{K(\alpha + 1)(M^* - M)$$
$$- \text{dex}\left[K(M^* - M)\right]\}\, dM \qquad (2.4.14)$$

(with $K = 0.4\ln 10$). Schechter gave the values:

$$\phi^* V_c = n^* = 910 \pm 120$$

$$M^*_{J(24.1)} = -21.41 \pm 0.10$$

$$\alpha = -1.24 \pm 0.05$$

The shape of the Schechter luminosity curve is one of a double exponential; this has great observational significance as the number of very bright galaxies is predicted to fall precipitously with increasing absolute magnitude. It is on this basis that the possibility of using the brightest galaxies of rich clusters as standard candles to give one indication of distance has been suggested, though observations suggesting that CD galaxies do not fit a Schechter function may limit this.

Schechter's work has received considerable subsequent attention and refinement. Garilli, Maccogni and Vettolani (1991) use the maximum likelihood method to estimate M^* and α in the medium red-shift southern cluster of galaxies A 3639, and obtain comparable results though with a large allowed range of values. Ramella, Geller and Huchra (1989) found about 58% of groups in their $m_{B(0)} \leq 15.5$ survey contained three or more galaxies brighter than M^*. de Lapparent, Geller and Huchra (1989) calculated the luminosity function for two complete slices of the extension of the Center for Astrophysics (CfA) survey and found the shape of the luminosity function could be approximated by a Schechter function. Efstathiou, Ellis and Peterson (1988) presented a detailed analysis of the field-galaxy luminosity function for five magnitude limited redshift surveys and conclude that the field luminosity function was well described by a Schechter function. Tully (1988) obtained a good Schechter correlation with $M^* = -20.18 + 1.25(1 + a) + 5\log(H_{75})$, and $\alpha = -1.0$, and Phillipps and Shanks (1987) confirmed the luminosity function with $M^*_{(B_J)} = -19.8$ and $\alpha = -1$.

Other workers calculated the luminosity function for a number of differing galaxy types, and generally found Schechter's function well approximated. Reshetnikov (1986) studied Seyfert galaxies; Oegerle, Hoessel and Ernst (1986) and Oegerle, Hoessel and Jewison (1987) studied nearby Abell clusters; Choloniewski (1985) studied E and S0 galaxies, and Turner and Gott (1976) determined the luminosity function of galaxies in small groups by combining the data on 63 groups. These workers noted several suggestive differences and, although no statistically significant variation was found initially between either rich-cluster and small-group or early and late morphological types, more recent work (e.g. Metcalfe, Shanks, Fong and Jones 1991) suggests that a real difference is becoming apparent.

Some workers have queried the standard Schechter form. Thompson and Gregory (1980) studied Coma cluster galaxies and found evidence that the ellipticals taken separately did not fit the simple Schechter function over the entire magnitude interval.

Ferguson and Sandage (1991) found that composite giant+dwarf luminosity functions did not well fit the function, and Huchra (1985) measured the cluster luminosity function for 471 galaxies in the Virgo cluster brighter than $m_{pg} = 15.5$, finding the function surprisingly flat at the faint end.

On balance, although there has been considerable variation in the actual parameters, the Schechter function has received good experimental conformation. There has also been some theoretical justification such as by Schaeffer (1987) who showed from a model of the non-linear matter distribution of rich clusters and their correlations that the luminosity function has the Schechter form, and Cole (personal communication) who has computed a theoretical luminosity function from star formation models. Other workers such as Kirshner, Oemler and Schechter (1979) and Kirshner, Oemler, Schechter and Shechtman (1983) (commonly known as KOS and KOSS) were able to normalise the Schechter function for the nearer galaxies by looking out to larger redshifts and fainter absolute magnitudes. KOS looked out to a limiting apparent magnitude of 14.9, using eight fields from the Second Reference Catalogue of Bright Galaxies (de Vaucouleurs, de Vaucouleurs and Corwin 1976) containing 155 galaxies. The CfA redshift survey (Davis *et al.* 1982) increased by a factor of four the volume of space in which the redshifts of galaxies is known, and KOSS used samples from this survey (matched to give similar numbers to KOS) to give a two magnitude increase in the depth of their analysis.

The work of Schechter and others to determine a luminosity function for galaxies distributed randomly through space was invaluable in determining a standardised function to predict the number of galaxies which should be visible in any magnitude-limited survey of the sky. The significance of the Schechter function is its ability to predict the number density of galaxies in the remote universe in order to compare the expected density with that actually observed which is of prime importance in determining how close together the early universe was, and consequently deducing the early rate of expansion of the universe and its curvature.

The models used as a basis for the number–magnitude count plots are based on five galaxy types, each with its own locally determined Schechter function and appropriate K–correction (Metcalfe *et al.* 1991 §2.3). These galaxy types are: E/S0, Sab, Sbc, Scd and Sdm and Fig. 2.3 is a combined plot of these five types using the best recent values for their relative abundances (ϕ^*) and showing (solid curve) the composite Schechter–type function, though it should be noted that this resultant function is not a true Schechter curve, as they do not obey algebraic addition. Fuller details of the major redshift surveys and their assumptions and conclusions are given in Appendix 1.

Figure 2.3. The derived Schechter functions for the five galaxy types assumed in the models, and the resultant composite curve.
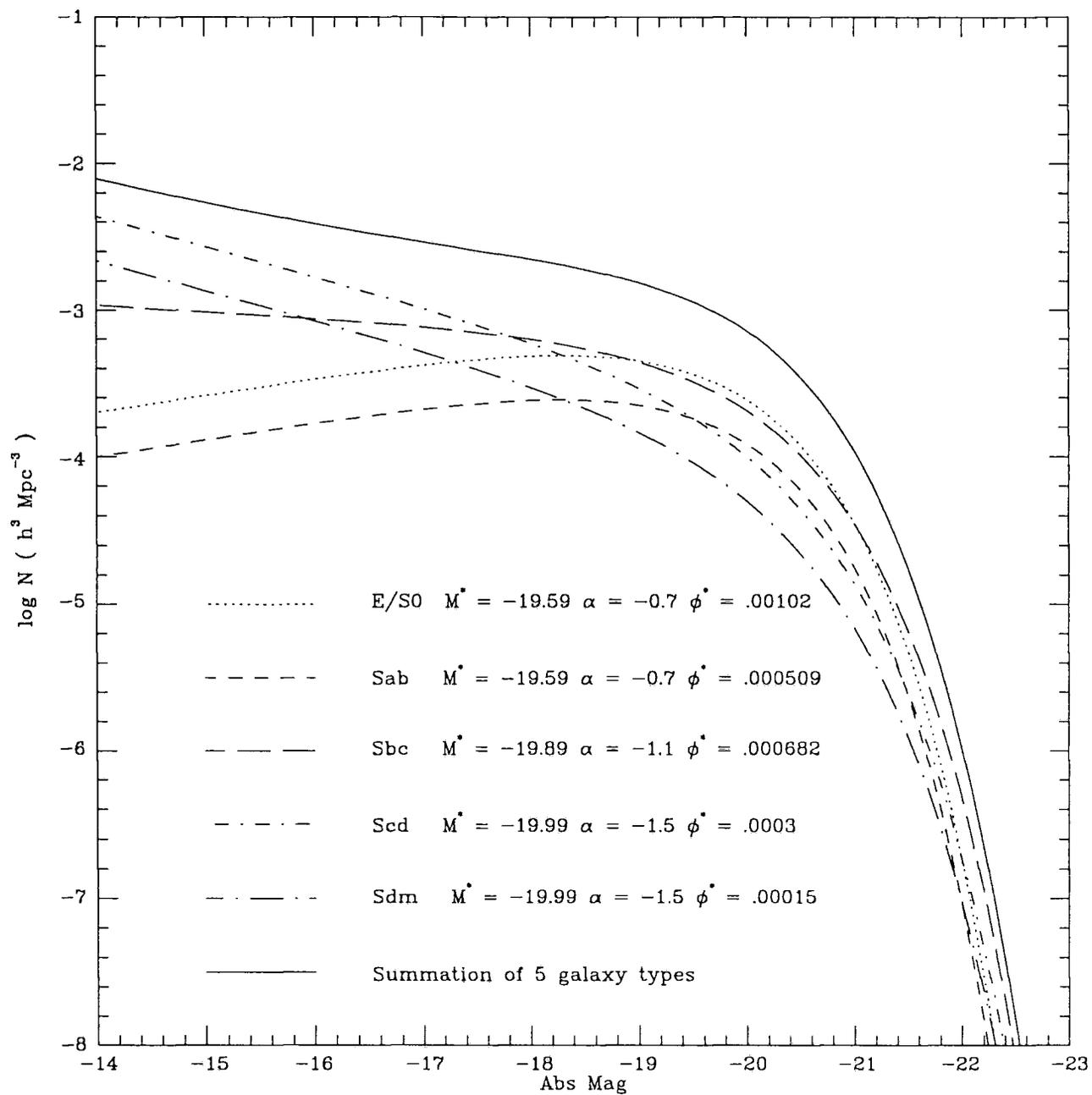
Derived Schechter distribution for 5 galaxy types ($H_0 = 100$)

Fig. 2.3

2.5 Clustering and the two-point correlation function

A full discussion of the statistical measures available for a description and analysis of galaxy distributions is given by Peebles (1980). He lays emphasis on the use of the autocorrelation function, and considers several historical approaches: Bok's statistic is an integral over the two-point correlation function, looking at the variance of the counts N in cells; Zwicky's index of clumpiness is the ratio of the variance of N to what would be expected for a uniform random distribution. Rubin used estimates of the variance of N to measure the spatial galaxy autocorrelation function; Limber estimated the auto-correlation function of galaxy counts from the Lick survey, and showed there is a linear integral equation relating this angular correlation function to the corresponding spatial correlation function $\xi(r)$. Limber's function is of considerable practical importance, as the translation from one to the other is fairly straightforward, and equally important it makes it easy to say how the statistical estimates ought to scale with the depth of the survey.

The autocorrelation function $\xi(r)$ is not useful to characterise the abundance of rare extreme fluctuations like the Abell clusters. Abell considered the frequency distribution of the counts N of clusters found in cells of fixed angular size. If the clusters were placed at random, N would have a Poisson distribution, and Abell used the deviation of the observed distribution from Poisson as a measure of clustering of the objects. The two-point correlation function $\xi(r)$ determines the second moment of this distribution; to predict the third moment, one needs the three-point correlation function, and to predict the full shape of the distribution in N one would need to know all orders of the correlation functions. Thus Abell's statistic is sensitive to different aspects of the clustering than revealed by $\xi(r)$ alone. Peebles summarises the position by suggesting that $\xi(r)$ is satisfactory if the data is limited, as was the position in the 1950s. With the completion of the Zwicky and Lick surveys and the advent of high speed computers, the situation changed and more complete statistical information could be obtained by using higher order correlation functions. With this proviso, the two-point correlation function provides a straightforward and useful model to test for clustering or voids, and this is the model developed here in considering the significance of voids in the large scale distribution of galaxies.

2.5.1 The two-point spatial correlation function $\xi(r)$

The probability of finding an object in the volume element δV is:

$$\delta P = n \, \delta V \tag{2.5.1}$$

where the mean number density n is independent of position. The mean number of objects found within the finite volume V is the integral of (2.5.1):

$$\langle N \rangle = nV \tag{2.5.2}$$

The two-point correlation function ξ is defined by the joint probability of finding an object in both of the volume elements δV_1 and δV_2 at separation r_{12}:

$$\delta P = n^2 \, \delta V_1 \, \delta V_2 [1 + \xi(r_{12})] \tag{2.5.3}$$

The function ξ is a function of separation alone, consistent with homogeneity and isotropy. The factor n^2 makes the correlation function dimensionless. In a uniform random Poisson distribution, the probabilities of finding objects in δV_1 and δV_2 are independent, and in this case $\xi = 0$, with

$$\delta P = n^2 \, \delta V_1 \, \delta V_2 \tag{2.5.4}$$

If the object positions are correlated, $\xi > 1$; if the positions are anticorrelated, $-1 \leq \xi < 0$. If an object is chosen at random from the ensemble, the probability of finding that it has a neighbour at distance r in δV is

$$\delta P = n \, \delta V [1 + \xi(r)] \tag{2.5.5}$$

The mean number of neighbours within distance r of a randomly chosen object is then the integral of (2.5.5):

$$\langle N \rangle_p = \frac{4\pi}{3} r^3 n + n \int_0^r \xi(r) \mathrm{d}V \tag{2.5.6}$$

For the moments of counts, the central moment in the two-point correlation function is given by:

$$\langle (N - \langle N \rangle_p)^2 \rangle_p = \langle N \rangle_p + n^2 \int \int_V \xi(r_{12}) \, \mathrm{d}V_1 \, \mathrm{d}V_2 \tag{2.5.7}$$

There are two interesting cases where P_N can be estimated from the two-point correlation function. In the limiting case of V larger than the maximum clustering length, P_N approaches a Gaussian. If V is small, P_N rapidly decreases at large N and

an approximation method can be used. The galaxy two-point correlation function is then a close approximation to a power law:

$$\xi \propto r^{-\gamma}, \qquad \gamma \approx 1.8 \tag{2.5.8}$$

over a large range of r. Peebles shows that this power law may be expanded as a Fourier transform of ξ, with the zero of ξ at

$$r_0 = \lambda_0 \tan \pi/(2+n) \tag{2.5.9}$$

Peebles takes the power spectrum to be

$$\langle |\delta_k|^2 \rangle = A k^n e^{-\lambda_0 k}, \qquad n > -3 \tag{2.5.10}$$

and it is apparent that $\xi(r)$ must pass through zero, and the limit $k \to 0$ gives:

$$\int_0^\infty d^3 r \xi(r) = 0, \qquad n > 0 \tag{2.5.11}$$

because the spectrum given by (2.5.10) vanishes at $k = 0$. Since $\xi(0)$ must be positive (because ξ is the autocorrelation function of a continuous function), $\xi(r)$ must pass through zero; hence the objects must be anticorrelated at some r. With higher orders, there is oscillation through r, depending on the detailed shape of the short wavelength cutoff of the spectrum.

As a complement to the autocorrelation function, Watson and Rowan-Robinson (1993) describe the use of the void probability function (VPF) in flux-limited samples. The VPF is defined as follows: if a test sphere of volume V is placed into a distribution of points of number density n, then the VPF, $P_{0,n}(V)$, is the probability that the volume will be found to contain no galaxies. Similarly, $P_{p,n}(V)$ is the probability that the sphere will be found to contain p galaxies. Even points set down entirely at random will be found to contain some large empty spaces. From Poisson statistics, considering a random point distribution with average number density n, the probability that a volume of size V will be found to be completely empty is given by

$$P_{0,n}(V) = e^{-nV} \tag{2.5.12}$$

For a clustered distribution, the probability that any particular volume will be empty must include terms that describe the actual form of the clustering present.

The problem of magnitude limited surveys is that the number density n is then not constant across the volume; this problem has been approached for the CfA survey (Geller and Huchra 1988) by using apparent brightness and redshift information to isolate volume–limited sub–samples.

The VPF method of Watson and Rowan-Robinson incorporates the selection function for a flux–limited sample allowing use of the bulk of the information contained in a galaxy survey. They make particular reference to the QDOT survey and go on to show that a simulated CDM calalogue may credibly reproduce the observed void. Although not developed specifically in this paper, the method does suggest that further information may be obtained from redshift catalogues to derive estimates for the excess void in local space from clustering, when compared to that which might be expected on grounds of Poisson statistics alone.

Bonometto *et al.* (1993) describe the evaluation of three- and four-point correlation functions from the Perseus–Pisces galaxy redshift sample, and suggest that in the range of distances from 1 to $10h^{-1}$Mpc, these do not agree with the expectation values of hierarchical clustering models. Such findings result in the partial modification of the picture of the large-scale matter distribution obtained from early two-dimensional samples such as those detailed above. They suggest a gradual passage from a linear to a nonlinear regime with support for a biased theory of galaxy formation with a bias factor for bright galaxies $\sim$2–2.5.

3. Obtaining the luminosity function

3.1 Modelling the Schechter function

One problem affecting the plot of number counts is its dependence on some form of the Schechter function to give the probable distribution of galaxies in a given magnitude range. In particular, the predicted faint end slope (governed by α) may be quite sensitive to inhomogeneities in the experimentally observed fields used to determine α. The Schechter function is generally built up by looking at a number of galaxies of similar type, but to obtain significant numbers one needs to look at ever increasing distances. This feeds back into the problem because we live in a galaxy which is itself part of a cluster; therefore there is contamination from the effects of both the richness of our own local group, and possible voids between our group and more distant clusters.

Before looking in detail at actual galaxy surveys, consideration was given to various models of galaxy distribution built up from an ideal Schechter form. A local void was then introduced to examine the effect of such a void on calculations to try to reobtain the original parameters of α and M^* put into the model. Three values of α were considered: namely, -1.1, -1.5, and -1.8, this last having a particularly high slope to see what effect a void might have in masking the presence of such large numbers of faint galaxies.

The model was examined for its effectiveness by simulating an area of sky $\sim 6.6 \times 6.6°$sq, containing a nominal 1000 galaxies out to a limiting apparent magnitude of $B = 17^m.0$. A simple form of K–correction was incorporated, using $K = 3z$ as a first approximation. No clustering was built into this model, and Fig. 3.1 is a 'cone' plot showing the random distribution of the galaxies in z–space using $\alpha = -1.1$ and $M^* = -20.0$. The models were checked subjectively by binning the galaxies (z–bins $= .005$) and plotting the resulting counts against the theoretical curve for $N - Z$ distributions. Figs. 3.2, 3.3 and 3.4 show the curves for a normal density distribution for $\alpha = -1.1$, -1.5 and -1.8 models respectively.

Fig. 3.5 is for a void under-density of $\phi = 0.5\phi_0$ out to $150h^{-1}$Mpc (with $\alpha = -1.5$) while for completeness, Fig. 3.6 shows the presence of a dense cluster at 150Mpc; all these use $M^* = -20.0$, except for Fig. 3.4 which has $M^* = -19.0$. The histogram plots are compared with theoretical curves for the give values of α and M^*, normalised to the total count density of 1000 galaxies, so the integrated area of the curve equals the area of the histograms. It may readily be seen that increasing the faint end slope results in the $N - z$ plots becoming increasingly skewed towards low redshift. The presence of a

Figure 3.1. A diagrammatic representation of the $6.6 \times 6.6°$ field, $17^m.0$ limited Monte Carlo sample used for the homogeneous simulations, showing redshift against angular distribution in the sky.

Angle (degrees)
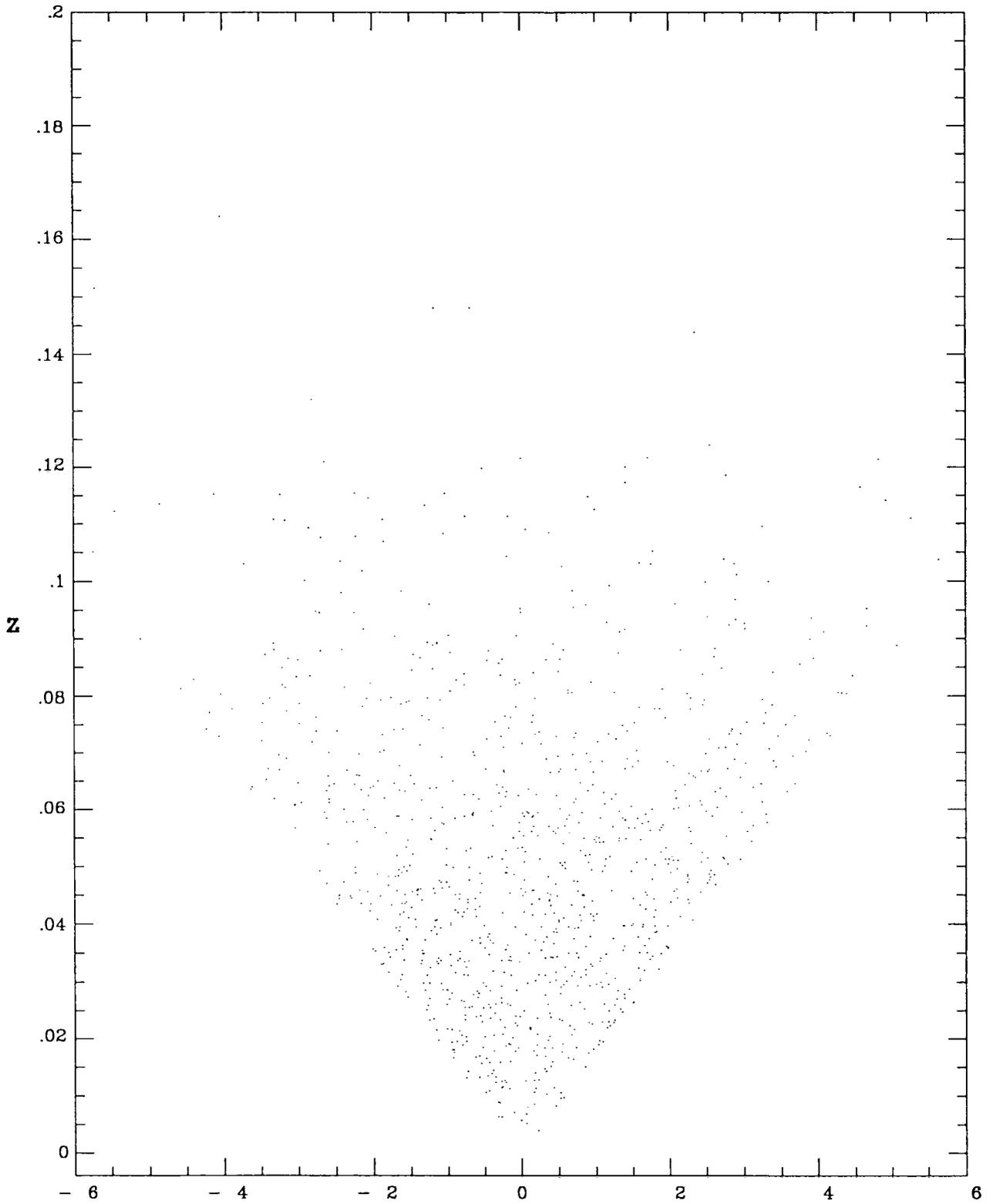
6.6° simulation, homogeneous distribution

Fig. 3.1

Figure 3.2. Number/redshift $(n - z)$ plot for the galaxies of Fig. 3.1. $(M^* = -20.0, \alpha = -1.1)$.
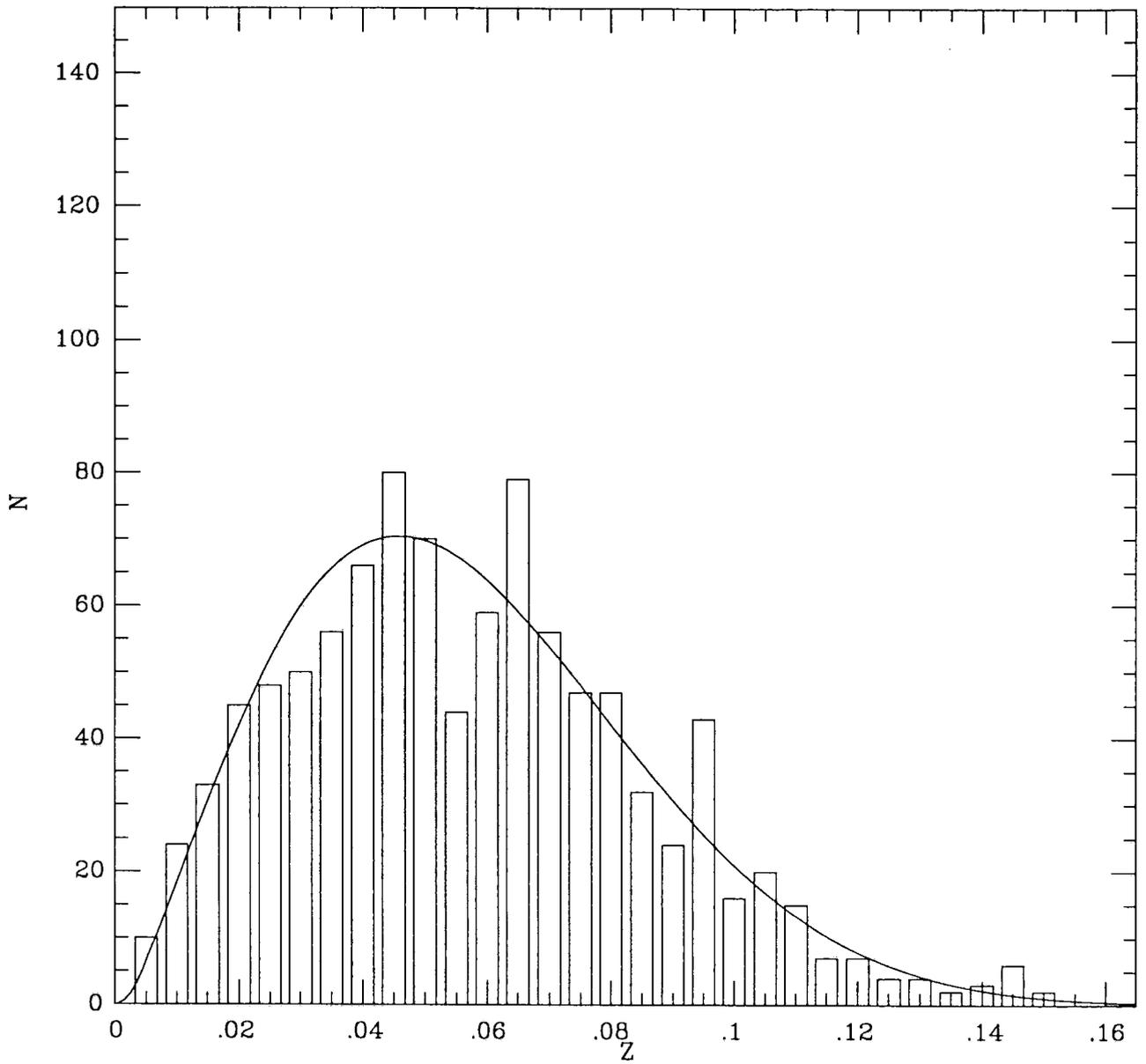
Number / Redshift plot (1000 galaxies) — Uniform density

17_m limited Monte Carlo plot ($\alpha=-1.1$, $M^{\bullet}=-20.0$)

Fig. 3.2

Figure 3.3. As Fig. 3.2, but with a steeper $\alpha = -1.5$.
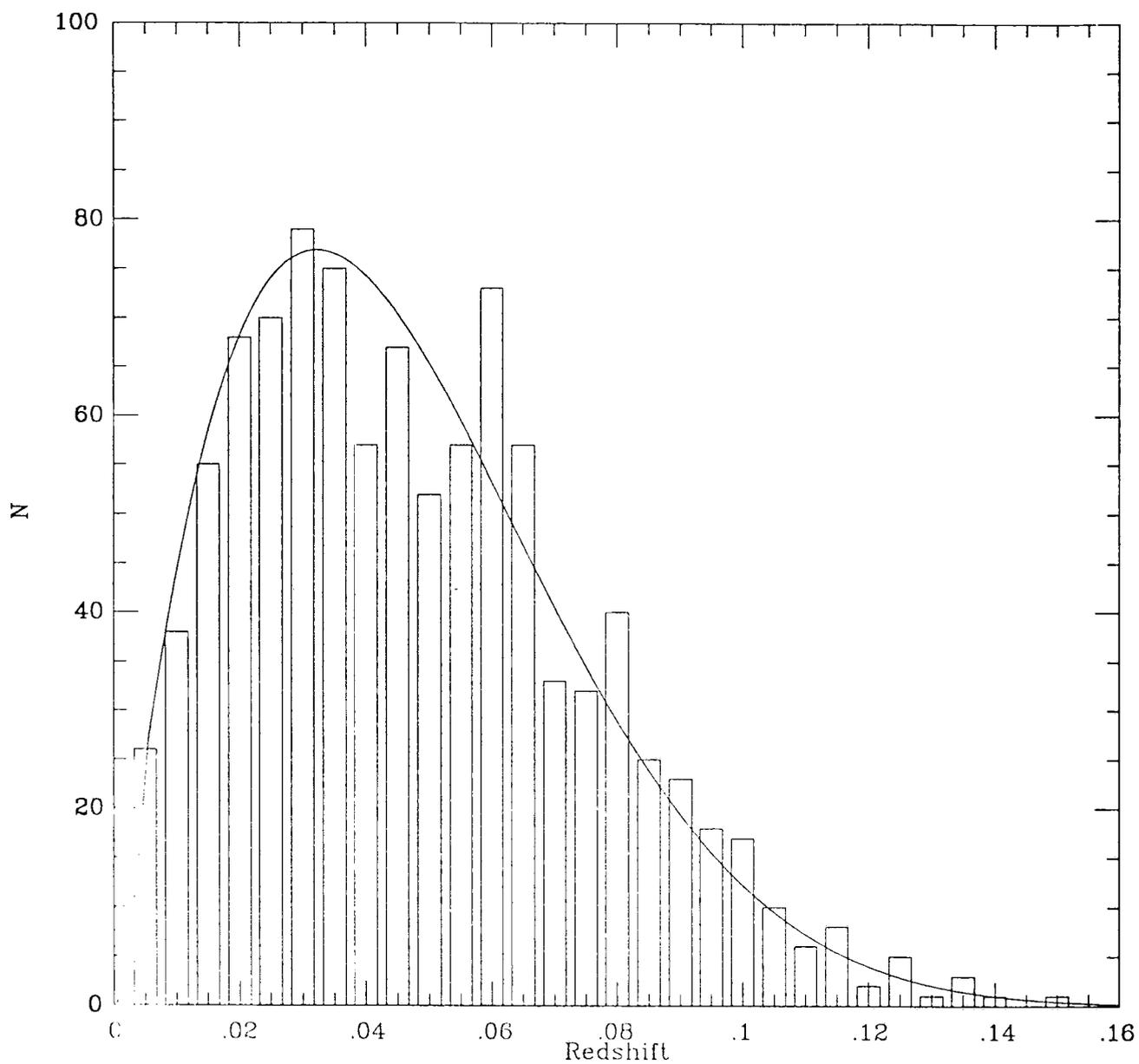
Number / Redshift plot (1000 galaxies) – Uniform density

17_m limited Monte Carlo plot ($\alpha=-1.5$, $M^{\cdot}=-20.0$) – Run#TS1

Fig. 3.3

Figure 3.4. As Fig. 3.2 and Fig. 3.3 with a still steeper $\alpha = -1.8$.
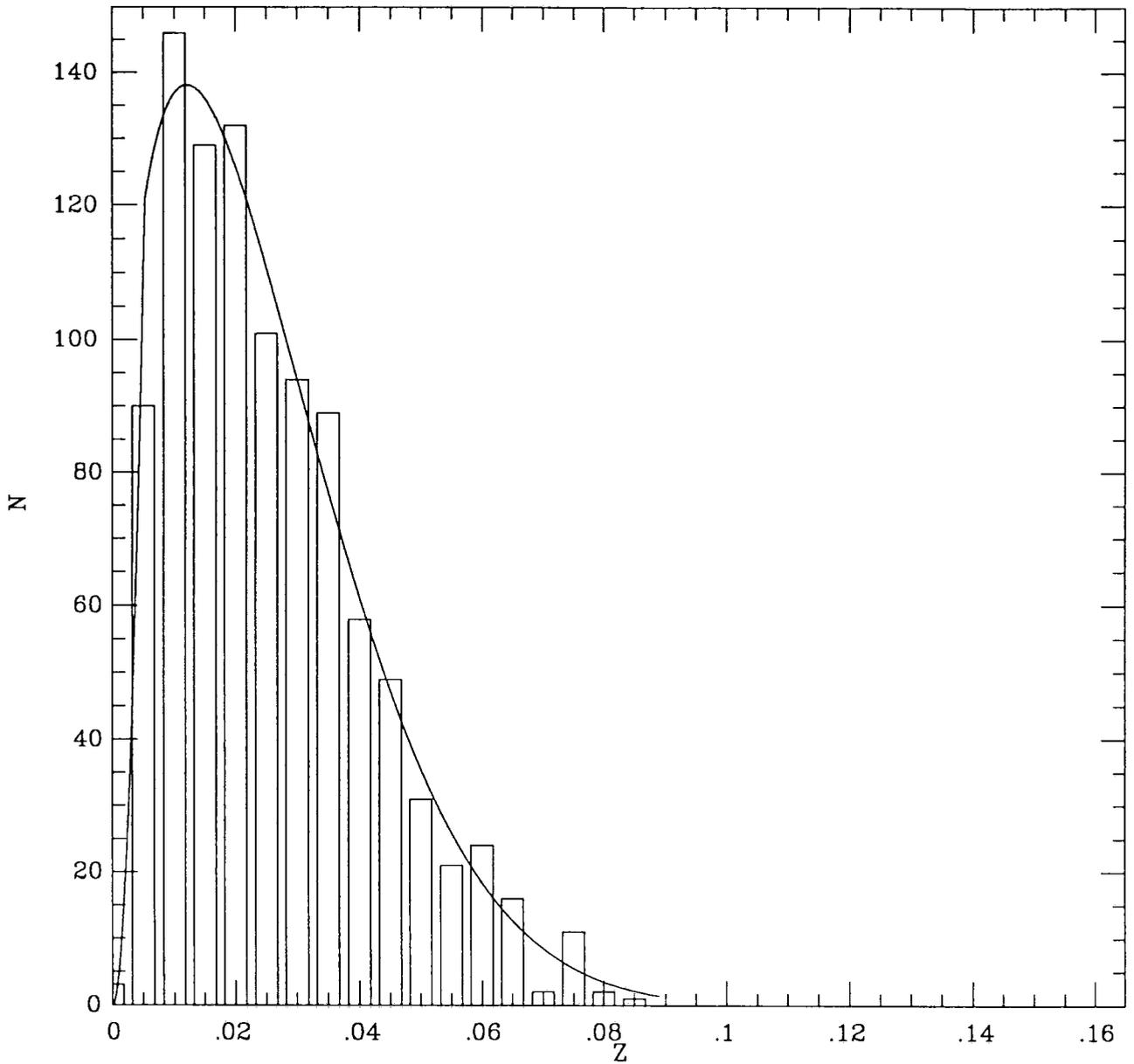
Number / Redshift plot (1000 galaxies) — Uniform density

17_m limited Monte Carlo plot ($\alpha=-1.8$, $M^*=-19.0$)

Fig. 3.4

Figure 3.5. $n - z$ plot of Monte Carlo simulation with a void of $\phi^* = 0.5\phi_0$ out to $150h^{-1}$ Mpc, $\alpha = -1.5$. The count deficit is clearly visible against the homogeneous theoretical curve, followed by a compensating count excess (the theoretical curves are all normalised to the total galaxy count, *i.e.* the area under the curves are equal).
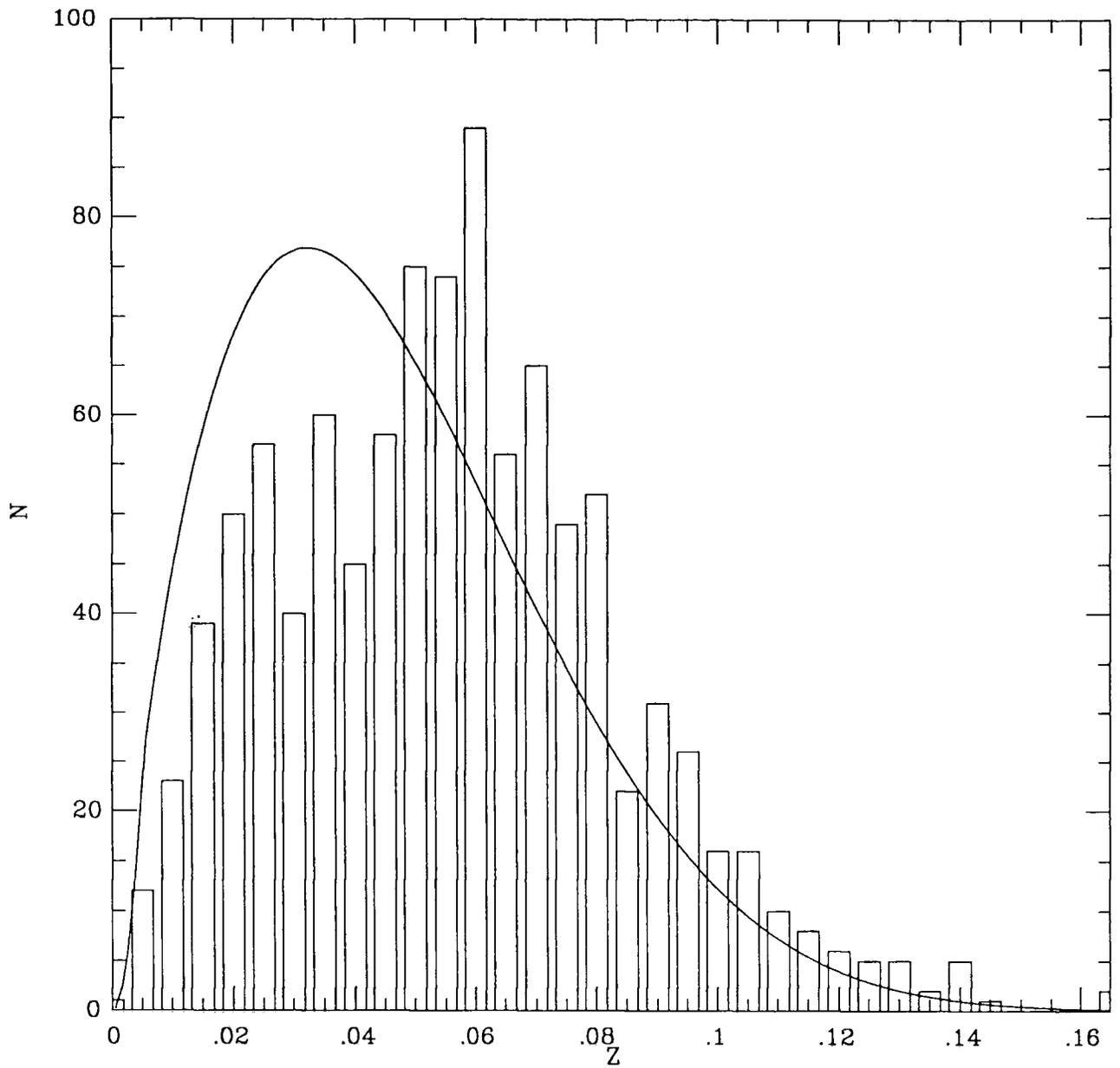
Number / Redshift plot (1000 galaxies) — Void (X0.5) to 150Mpc

17_m limited Monte Carlo plot ($\alpha=-1.5$, $M^{\bullet}=-20.0$)

Fig. 3.5

Figure 3.6. As Fig. 3.5, but now showing a Monte Carlo cluster model with a local excess of $\phi = \times 10\phi_0$. The resultant void is clearly seen against the predicted model curve from Sandage's method.
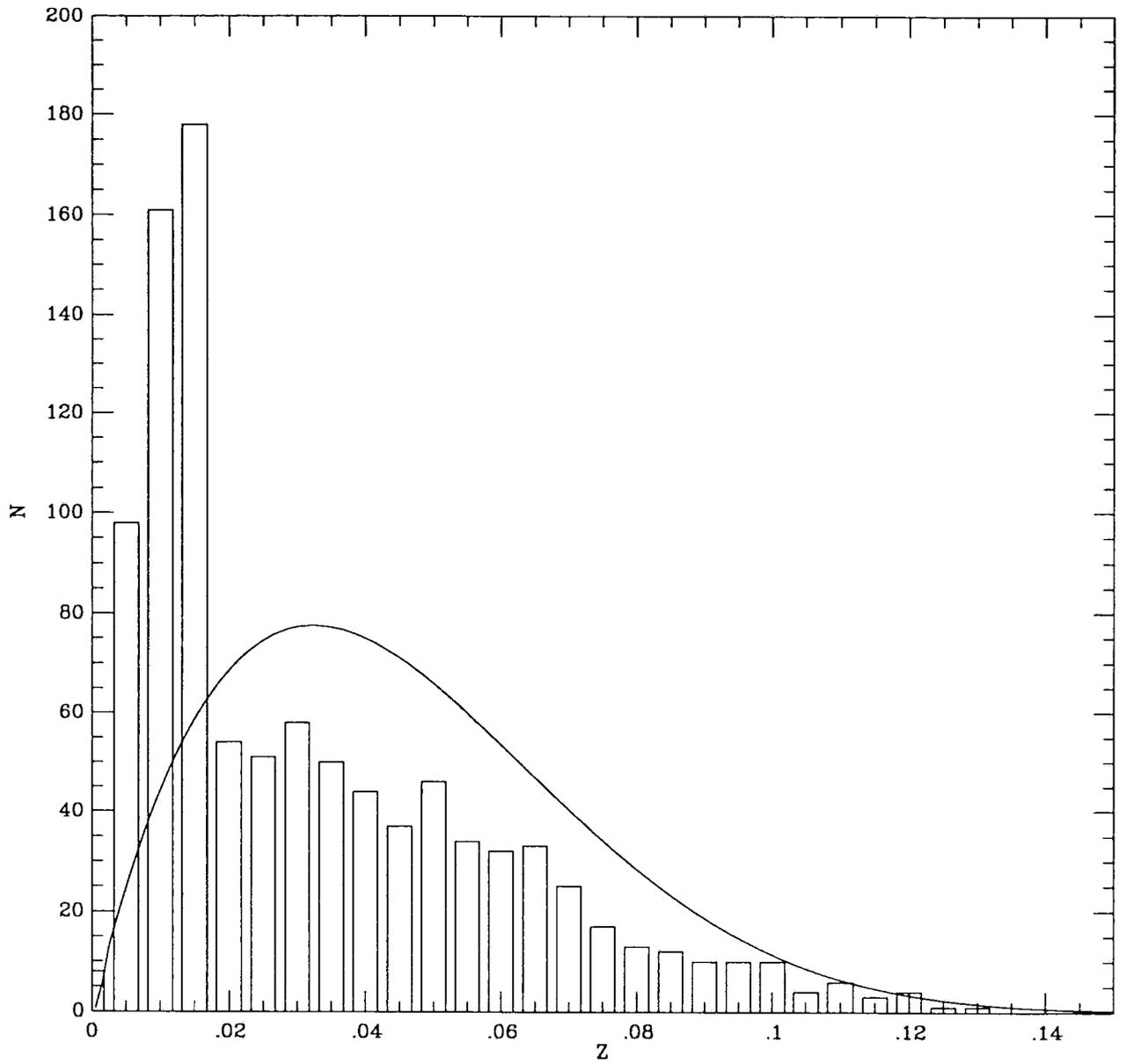
Number / Redshift plot, local cluster model ($\alpha = -1.5$)

Fig. 3.6

void is apparent, with a deficiency of low redshift objects and a relative excess of ones with higher redshift.

The resulting Monte-Carlo distributions were analysed using a $1/V_{max}$ method and a Maximum Likelihood method to look at their resulting shapes, and any discrepancies in the faint slopes.

3.2 The $1/V_{max}$ analysis

For each galaxy in the Monte-Carlo survey, given z and the apparent magnitude, we can calculate the absolute magnitude the galaxy would have, using the same K-correction $(3z)$ as that put into the model. The galaxies are then binned in absolute magnitude. We then calculate the actual volume out to the distance of the galaxy (V) and the maximum volume to which the galaxy can just be seen at the given limiting apparent magnitude (V_{max}); recalculating by a factor $N(m)/V_{max}$ then produces the number which should be seen in a complete sample out to the magnitude limit for any given absolute magnitude. Three typical runs from the simulations (one including Poissonian error bars) are shown in Fig. 3.7 for a uniform distribution, while Figs. 3.8 and 3.9 show a void distribution with $\alpha = -1.1$ and $\alpha = -1.5$ respectively. The fluctuations about the curve of the input function are apparent, becoming most severe at the faint end where the actual numbers of galaxies in the bins is particularly small, but again the emphasis of bright counts and the deficit for faint counts may be seen from examination of the void plots.

3.3 The Maximum Likelihood Estimator (M.L.E.) – Peebles' Method

Binning galaxies in absolute magnitude then multiplying each bin by the maximum volume to which that magnitude is visible at the given apparent magnitude limit provides a simple method to regenerate the Schechter function and estimate the three parameters ϕ^*, M^* and α. However, this is a relatively crude method and several more sophisticated methods have been suggested in the literature. One of these, the Maximum Likelihood Estimator, or M.L.E., was described by Bean (1983), after a method suggested by Peebles using log–likelihood intervals.

Suppose we have a sample of observations $(x_1, x_2, \ldots, x_n)$, where x_i is a realisation of the random variable X_i. Then let

$$g(x_1, x_2, \ldots, x_n; \theta) = P(X_1 = x_1, X_2 = x_2, \ldots, X_n = x_n) \qquad (3.3.1)$$

Figure 3.7. Three independent Monte Carlo runs shown against the Schechter curve ($M^* = -20.0$, $\alpha = -1.1$) from which they were generated, plotted using the V_{max} method. Error bars have been drawn for only one of the curves to avoid excess confusion.
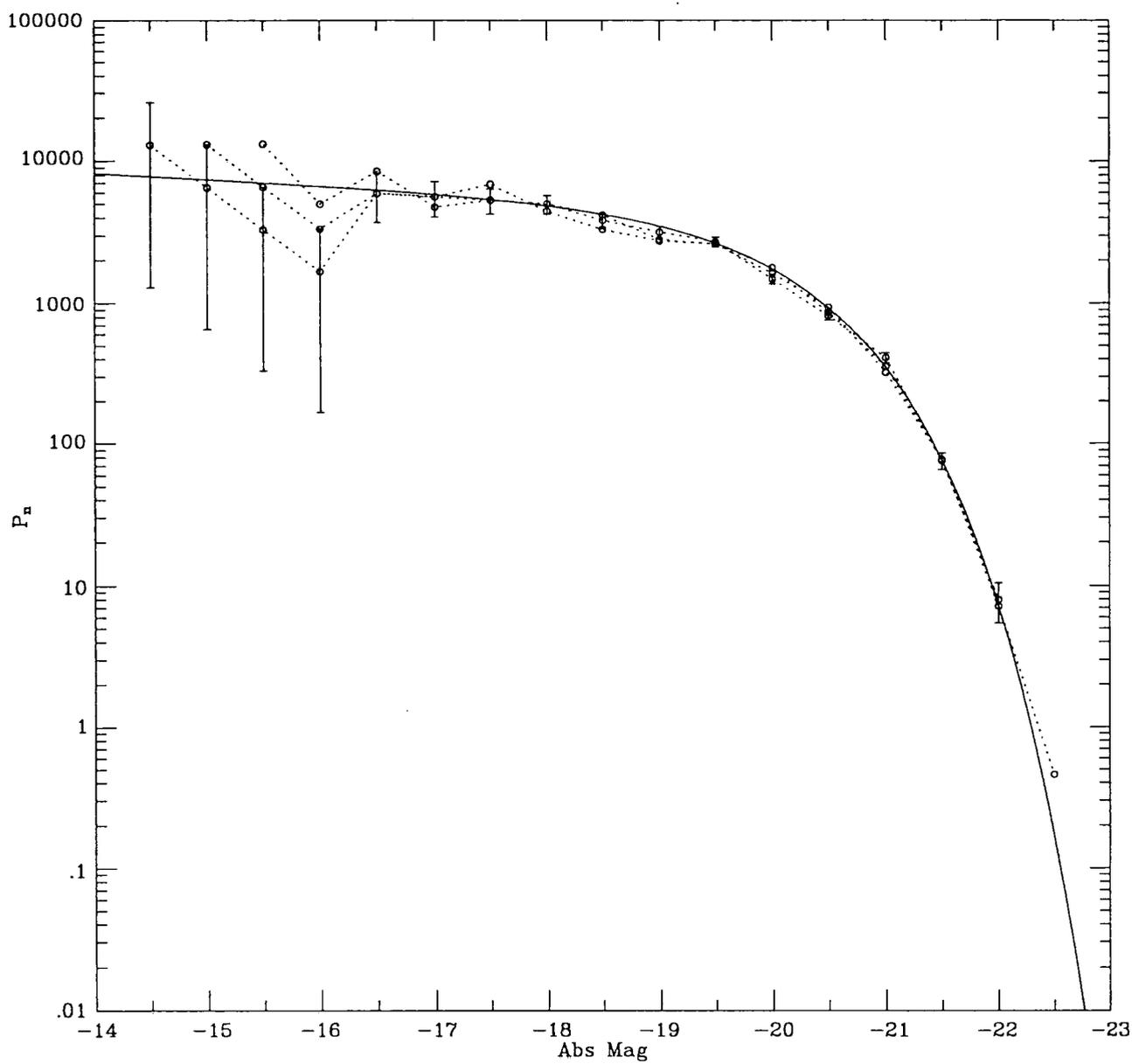
Schechter Curve for simulations ($\alpha = -1.1$, $M^* = -20.0$, $H_0 = 100$)

Apparent $mag_{lim} = 17$, K−correction = 3Z

Fig. 3.7

Figure 3.8. A void simulation plotted using the V_{max} method, showing the small deficit in counts over the fainter absolute magnitudes and a slight excess at the brighter end.
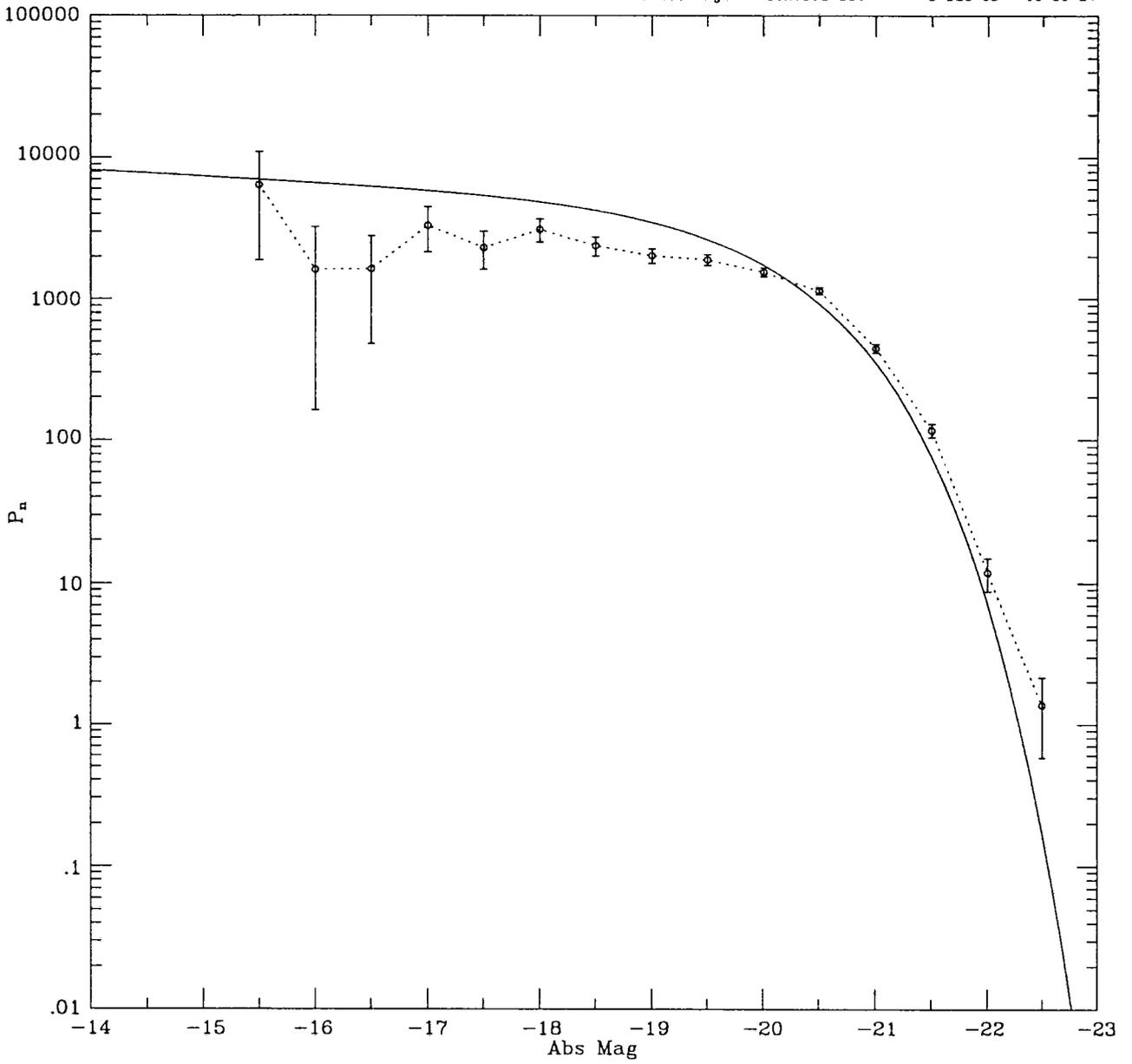
Schechter Curve for simulations ($\alpha = -1.1$, $M^* = -20.0$, $H_0 = 100$)

Apparent $m_{lim} = 17$,   K-correction = 3Z

(Void of 0.5 to 200 Mpc)

Fig. 3.8

Figure 3.9. As Fig. 3.8 with a void of $\phi^* = 0.5\phi_0$ to 150 Mpc, but with a steeper $\alpha = -1.5$.
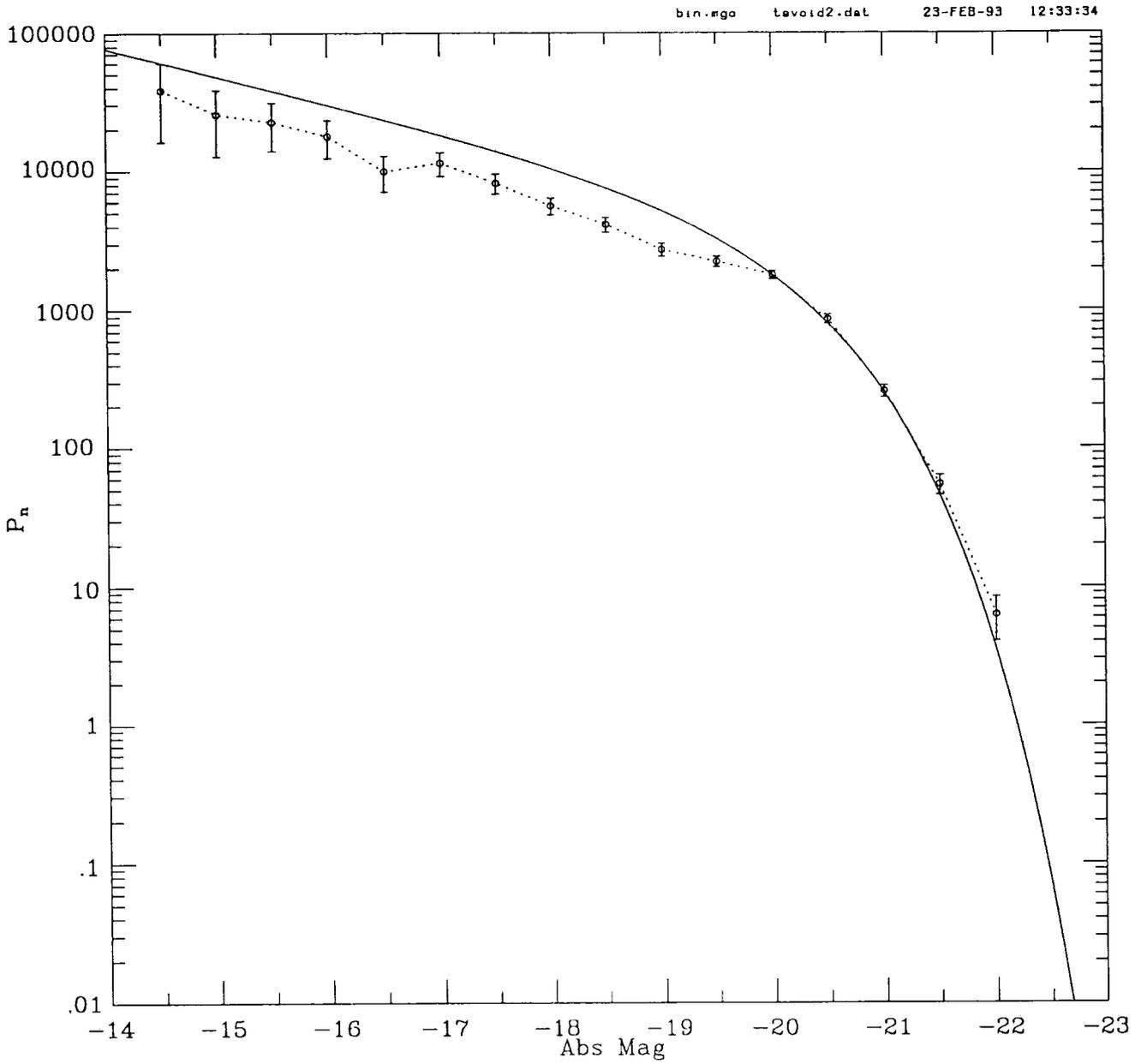
Schechter Curve for simulations ($\alpha = -1.5$, $M^{*} = -20.0$, $H_0 = 100$)

$\text{mag}_{\text{lim}} = 17$,   K−correction = 3Z, Void X0.5 to 150Mpc (run#TSVOID2)

(1000 galaxies, V/Vmax method)

Fig. 3.9

Here θ denotes the (scalar) parameter of the joint distribution of the X_is; in the multi-parameter case, θ is a vector. The likelihood function of θ is defined as

$$l(\theta) = ag(x_1, x_2, \ldots, x_n; \theta) \qquad (3.3.2)$$

where a is an arbitrary constant which depends on the observations x_i. No significance attaches to the absolute values of a likelihood, as it is concerned only with the comparisons of the values of the likelihood function at various values of θ, these comparisons being made in terms of ratios. In practice (3.3.2) is often replaced by the equivalent

$$l(\theta) \propto g(x_1, x_2, \ldots, x_n; \theta) \qquad (3.3.3)$$

If the x_i are independent and identically distributed variables (which is assumed to be true in the case of galaxy samples) then the likelihood function takes the simpler form

$$l(\theta) = l(x_1, x_2, \ldots, x_n; \theta) \propto \prod_1^n f(x_i, \theta) \qquad (3.3.4)$$

The log of a likelihood function is often easier to use because, if $l(\theta)$ has a maximum, then $\log l(\theta)$ also has a maximum at the same θ-value. We now need to apply a suitable probability function to the x_is to obtain the maximum likelihood for θ.

The Poisson distribution is sometimes known as the 'distribution of rare events', indicating that this distribution governs the number of occurrences of events having a small probability, so they occur in a small number of cases (say < 30) even in a large sequence of observations, and this is the probability function adopted here. It is given by

$$P_x^{\bar{z}} = e^{-\theta}\theta^x/x!, \quad x = 0, 1, \ldots \quad (\theta > 0) \qquad (3.3.5)$$

To form the likelihood function for a set of galaxies in a given sample, we bin them into two dimensional cells n_{ij} in absolute magnitude, i, and redshift j (though in practice, the distance modulus is more convenient and was found to be more accurate). The function θ is now a vector with two components,

$$\theta = \phi_i \rho_j = \langle \bar{n}_{ij} \rangle \qquad (3.3.6)$$

where ϕ_i is the differential LF and ρ_j is the product of the absolute number density of galaxies at that redshift bin and the appropriate volume element across the field. We may now rewrite the Poisson probability function of two dimensions as

$$P_{ij}^{\bar{n}_{ij}} = e^{-\bar{n}_{ij}}(\bar{n}_{ij})^{n_{ij}}/n_{ij}! \qquad (3.3.7)$$

26

From (3.3.4), the likelihood function is now

$$\mathcal{L} = \prod_{ij} P_{ij}^{\bar{n}_{ij}}$$

or

$$\log \mathcal{L} = \sum_{ij} [n_{ij} \log(\phi_i \rho_j) - \phi_i \rho_j - \log(n_{ij}!)] \tag{3.3.8}$$

Taking partial derivatives to maximise $\log \mathcal{L}$ (and hence $\mathcal{L}$):

$$\frac{\partial \log \mathcal{L}}{\partial \phi_i} = \sum_{j=1}^{j_{lim}} \left[\frac{n_{ij}}{\phi_i} - \rho_j \right] = 0 \tag{3.3.9}$$

and

$$\frac{\partial \log \mathcal{L}}{\partial \rho_j} = \sum_{i=1}^{i_{lim}} \left[\frac{n_{ij}}{\rho_j} - \phi_i \right] = 0 \tag{3.3.10}$$

giving two equations

$$\phi_i = \sum^{j_{lim}} n_{ij} / \sum^{j_{lim}} \rho_j \tag{3.3.11}$$

$$\rho_j = \sum^{i_{lim}} n_{ij} / \sum^{i_{lim}} \phi_i \tag{3.3.12}$$

where the summation limits j_{lim} and i_{lim} are functions of i and j respectively, because of the cut off in the selected sample of galaxies by apparent magnitude.

The scheme is illustrated in Fig 3.10 which shows the distribution of a random sample of 1000 galaxies with four contours of apparent magnitude at 10, 12, 14, and 16^m and the 17^m cutoff limit with one typical cell, n_{ij}, also indicated. Fig. 3.11 is the corresponding plot of absolute magnitude against distance modulus, while Fig. 3.12 shows a large cluster ($\times 10$ over–density) present. To solve for ϕ_i, one puts in a trial function ϕ_{i0} and estimates ρ_{j0} using (3.3.12) which is then put back into (3.3.11) to get a first solution for ϕ_{i1}, the iteration continuing until a stable solution is reached. Fig. 3.13 shows the result of the iteration, with arbitrary normalisation against the Schechter function. The first 4 iterations and the 10th are plotted, showing the rapid convergence of the estimates as the iteration proceeds. The effect of continuing the iterations beyond 10, with up to as many as 50 iterations, was looked at but gave no additional improvement in accuracy.

Figure 3.10. A simulated plot of absolute magnitude v redshift for 1000 galaxies, with an observational cutoff at $17^m.0$, and contours of apparent magnitude drawn at 2^m intervals. Also shown is a typical cell used for the Maximum Likelihood Estimator method of Peeble's.
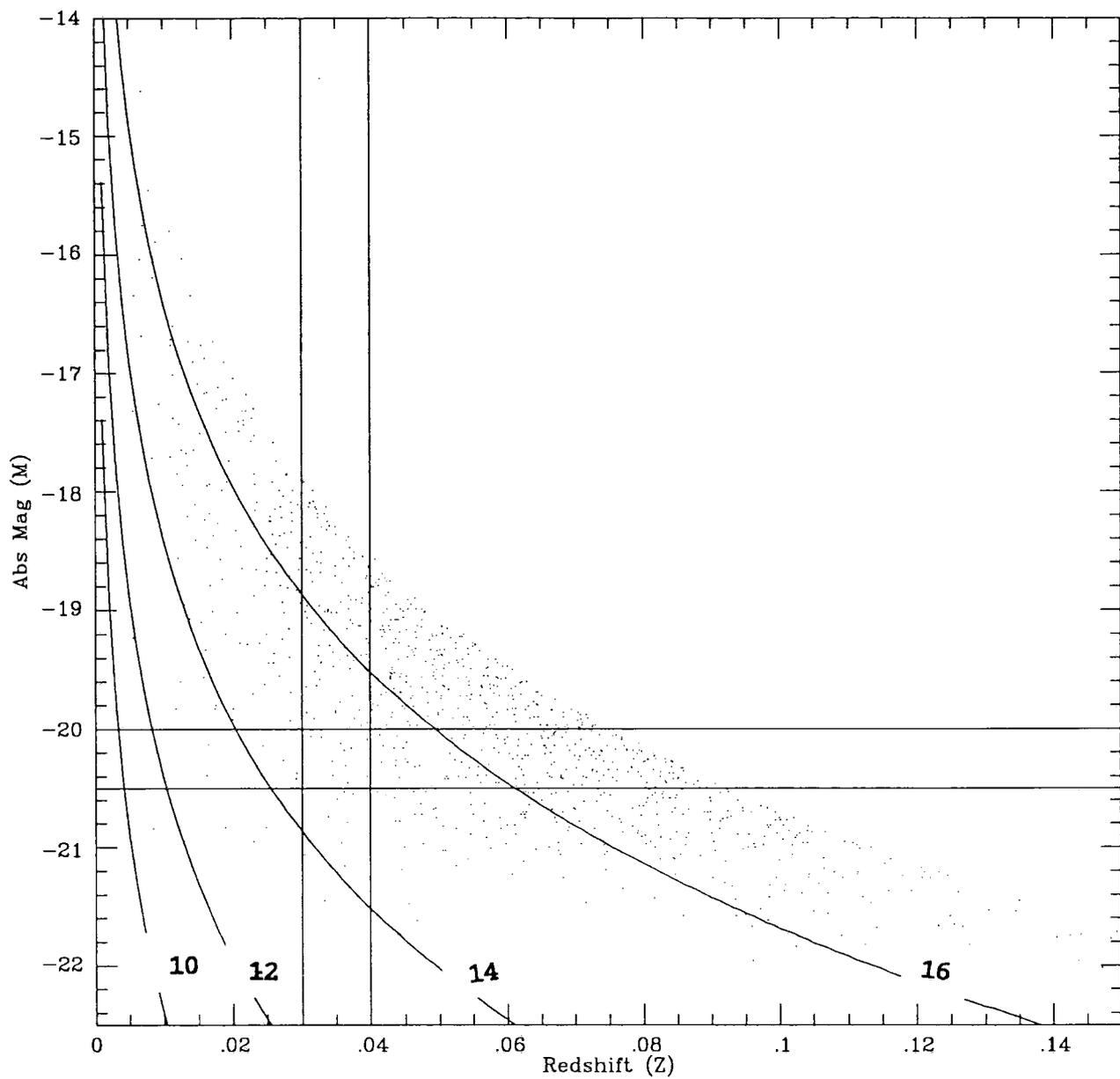
Absolute mag / Redshift plot (1000 galaxies)

17_m limited Monte Carlo plot

Fig. 3.10

Figure 3.11. The same simulation of Fig. 3.10, but redrawn as absolute magnitude v distance modulus, to show how the lines of equal apparent magnitude are now linear (*see text*).
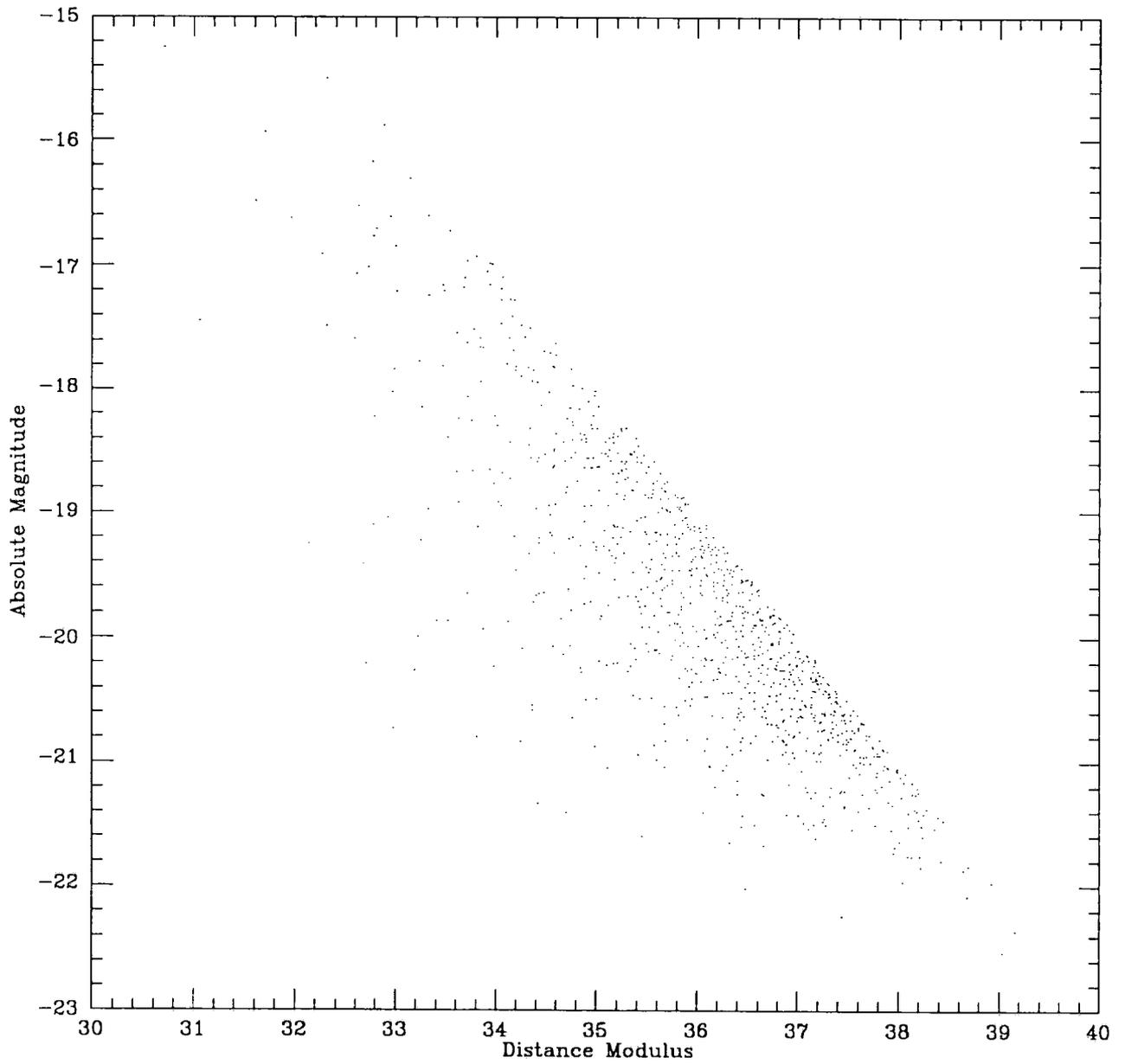
1000 galaxy simulation, homogeneous distribution

Fig. 3.11

Figure 3.12. As Fig. 3.11, but with a cluster of $\phi = \times 10 \phi_0$ density at a distance of 150 Mpc and cluster depth of 15 Mpc.
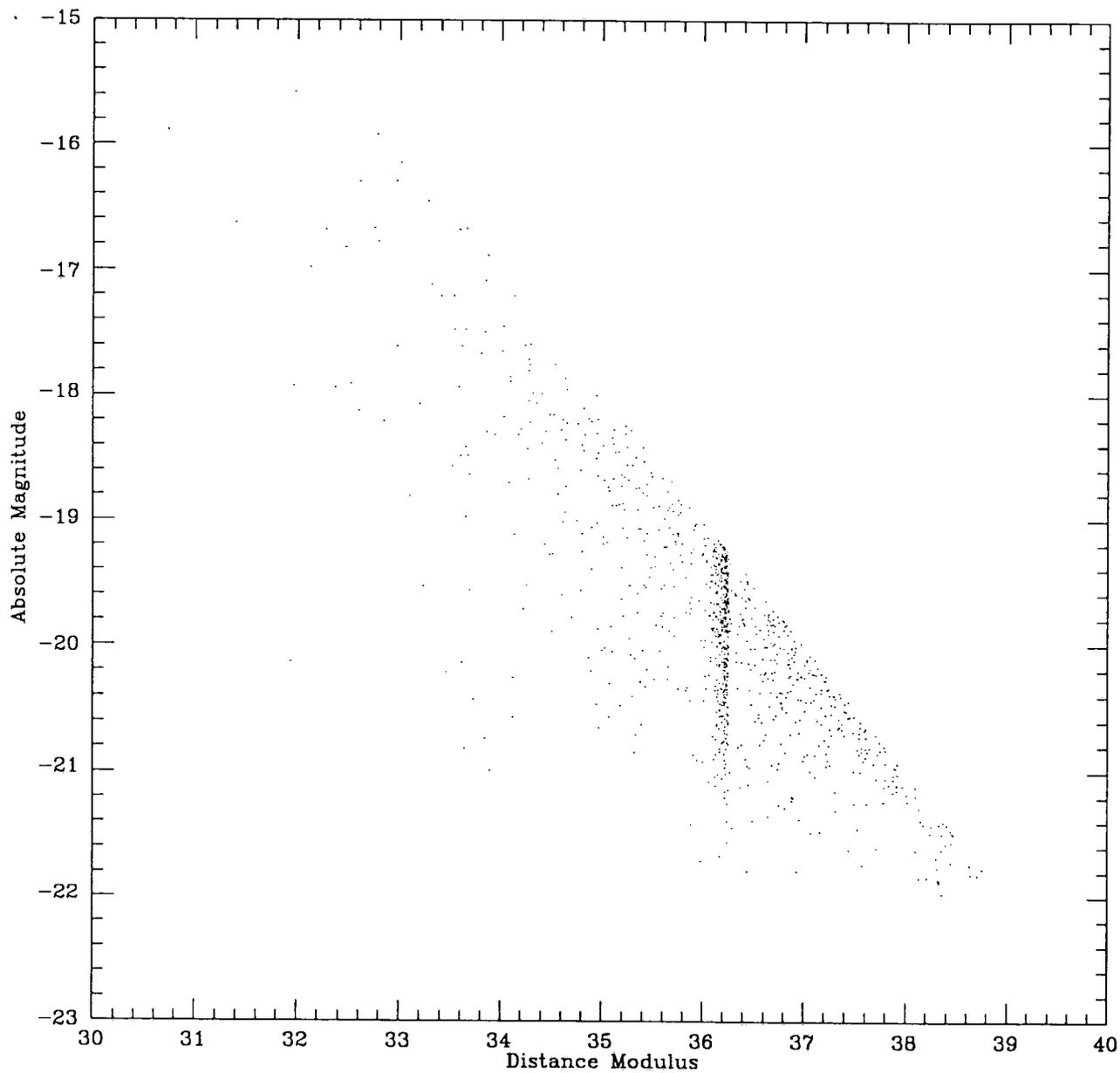
1000 galaxy cluster simulation, 10X density at 150Mpc, depth 15Mpc

Fig. 3.12

Figure 3.13. Results of ten consecutive runs using the Maximum Likeli-hood Method to reconstruct the original data put into the simulation.
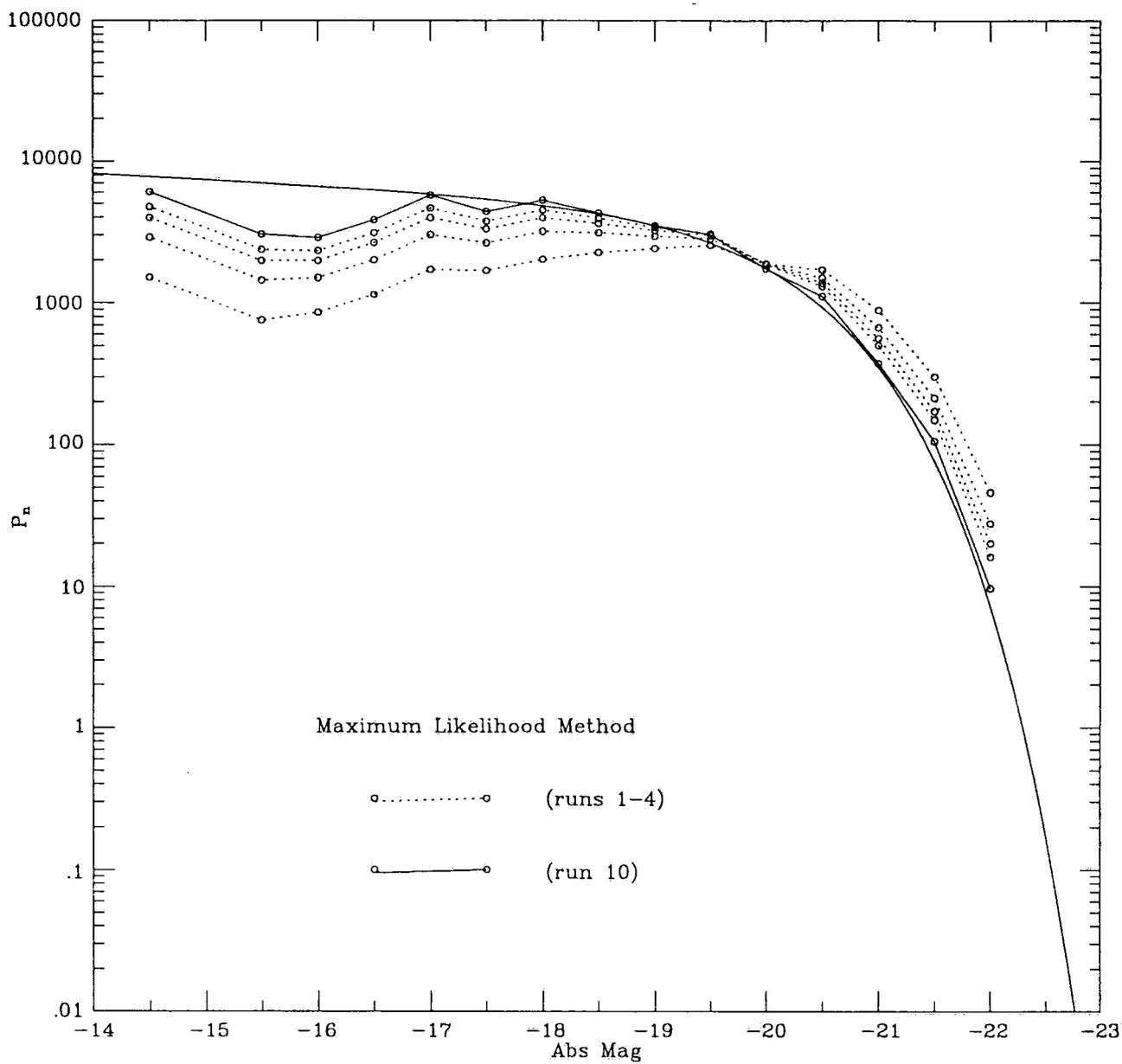
Schechter Curve for simulations ($\alpha = -1.1$, $M^* = -20.0$, $H_0 = 100$)

Apparent $m_{lim} = 17$, K−correction = 3Z

Fig. 3.13

3.3.1 Confidence Levels for the M.L.E.

For the one-parameter case of $l(\theta)$ as defined in (3.3.4), with estimate $\hat{\theta}$, the standard error ω is given by (Leidermann):

$$-1/\omega^2 = E\{\frac{d^2 \log \mathcal{L}}{d\,\theta^2}\}$$
$$\approx \frac{d^2 \log \mathcal{L}}{d\,\theta^2}\,|_{\hat{\theta}} \qquad (3.3.13)$$

which has its central 95% confidence interval in the range $\hat{\theta} \pm 2\omega$. Thus, taking the partial second derivative of ϕ_i in (3.3.9),

$$\frac{\partial^2 \log \mathcal{L}}{\partial \phi_i^2} = -\sum_j^{j_{lim}} \frac{n_{ij}}{\phi_i^2} \qquad (3.3.14)$$

$$\therefore \quad \omega = \phi_i/\sqrt{n} \qquad (3.3.15)$$

where n is the total count. The 95% confidence level for ϕ_i is then

$$\phi_i \pm 2\phi_i/\sqrt{n} \qquad (3.3.16)$$

3.4 The Maximum Likelihood Function (M.L.F.) – Sandage's Method

Sandage, Tammann and Yahil (1979) described another maximum likelihood method which provides an estimate of α and M^* for a given magnitude-limited sample without the need for binning the data, and independent of clustering or voids in the distribution. It does assume a pure Schechter distribution.

Given the Schechter L.F. distribution function, then the probability P_i that any particular galaxy i at a redshift z_i has an absolute magnitude M_i is given by:

$$P_i \propto \frac{\phi_s(M_i)}{\int_{-\infty}^{M_{lim}(z_i)} \phi_s(M)\,dM} \qquad (3.4.1)$$

where $M_{lim}(z_i)$ is the faintest absolute magnitude that would be visible at the given z_i. Multiplying probablities as with the M.L.E. method (3.3) gives the likelihood function $\mathcal{L}$:

$$\mathcal{L} = \prod_i P_i \qquad (3.4.2)$$

and taking logs:

$$\ln \mathcal{L} = \sum_i \ln P_i$$

$$i.e. \quad \ln \mathcal{L} = \sum_i (\alpha + 1) \ln K_i - \sum_i K_i$$
$$- \sum_i \ln \Gamma(\alpha + 1, \mathrm{dex}\,[0.4(M^* - M(z_i))]) \qquad (3.4.3)$$

where $K_i = \mathrm{dex}\,[0.4(M^* - M)]$. The function is maximised by stepping through all probable values for α and M^* to build up a table of results, then adding the probabilites for all the galaxies in the survey for each combination of α and M^* to look for a maximum probablity. The process is repeated by iteration using progressively smaller increments for the values of α and M^* until a sufficient accuracy is obtained, and this is the method usually employed to obtain these parameters for any magnitude–limited survey.

3.4.1 Confidence levels for the M.L.F.

The ideal M.L.E. steps through all possible values of M^* and α to obtain the least squares best fit for the overall function. The results are plotted out as percentage probabilities against a figure of 100 for the most probable combination, using a probability array with abscissa in α and ordinate in M^*. Such an array may be used to generate a parabola of uncertainty at the 1σ, 2σ, $\ldots n\sigma$ levels, as shown by the array and data below (Table 3.1) which was derived from a homogeneous population simulation using 300 objects generated with an absolute magnitude range $-14.0 \leq M \leq -23.0$. The values input into the simulation were $\alpha = -1.5$ and $M^* = -20.0$.

Table 3.1 Probability array in α / M^* for the M.L.F. method

$M^*\backslash\alpha$	-1.0	-1.1	-1.2	-1.3	-1.4	-1.5	-1.6	-1.7	-1.8	-1.9
-21.0	0	0	0	0	0	0	0	0	0	0
-20.9	0	0	0	0	0	0	0	0	0	0
-20.8	0	0	0	0	0	0	0	0	0	0
-20.7	0	0	0	0	0	0	0	0	0	0
-20.6	0	0	0	0	0	0	0	0	0	0
-20.5	0	0	0	0	0	0	0	0	0	0
-20.4	0	0	0	0	0	0	0	2	2	1
-20.3	0	0	0	0	0	0	3	8	6	2
-20.2	0	0	0	0	0	3	15	22	11	2
-20.1	0	0	0	0	1	16	45	40	12	1
-20.0	0	0	0	0	11	53	82	43	8	0
-19.9	0	0	0	4	38	100	87	27	3	0
-19.8	0	0	1	16	69	97	48	9	0	0
-19.7	0	0	4	28	61	47	13	1	0	0
-19.6	0	0	6	21	24	10	1	0	0	0
-19.5	0	0	3	6	3	0	0	0	0	0
-19.4	0	0	0	0	0	0	0	0	0	0
-19.3	0	0	0	0	0	0	0	0	0	0
-19.2	0	0	0	0	0	0	0	0	0	0
-19.1	0	0	0	0	0	0	0	0	0	0

The divergence from the array maxima may then be parameterised in terms of α and M^* to a stated degree of accuracy. Here, there is a 95% central confidence level in the range $\alpha = -1.5 + 0.05, -0.1$, $M^* = -19.9 + 0.15, -0.05$ or, taking median values, $\alpha = -1.52 \pm 0.04$, $M^* = -19.87 \pm 0.08$.

3.5 Monte Carlo simulations and analysis of methods

3.5.1 Homogeneous single-α populations

Many simulations were run to generate Monte Carlo type data fields which might mimic real data, with total galaxy counts ranging from 300 to 1000. The simulations

included homogeneous single Schechter type functions with flat and steep alphas (typically -1.0, -1.5 and -1.8 with an M^* of -20) and various combinations of void and cluster in these. In addition, mixed population models were studied, typically containing a predominant 'flat alpha' population, with a smaller high alpha subgroup. These simulations were all plotted on a $1/V_{max}$ plot to show the initial assumptions put into the model, and were then subjected to the Peebles' M.L.E. method to see how this compared to the V/V_{max} curves, and the M.L.F. method of Sandage to return values for alpha and M^* which could be compared to the input parameters.

The results of three independent runs using the $1/V_{max}$ method were shown in Fig. 3.7, with error bars for one of the runs, and compared to the base curve (solid) showing the original parameters put into the model, with $\alpha = -1.1$ and $M^* = -20$ ($H_0 = 100$). The K-correction throughout is taken as $3z$, and the apparent magnitude limit was 17^m. It may be seen that even this simple method gives a close approximation to the initial parameters over much of the range, with errors creeping in at the extremes (Abs Mag > -16.5 and Abs Mag < -21.5) where the numbers of galaxies are small. Fig. 3.14 shows a similar run for 1000 galaxies with a high slope tail ($\alpha = -1.5$) and the larger numbers of galaxies in the faint tail are now seen to reduce the errors considerably.

The M.L.F. method of Sandage *et al.* proved to be extremely effective at returning the parameters α and M^* originally put into the Monte Carlo simulations, returning values typically within 5% of the input values.

3.5.2 Inhomogeneous single-α populations

The inclusion of a significant under–density (void) of 0.5 to $150h^{-1}$Mpc   (Fig. 3.9 with a high–alpha tail) shows its presence clearly in the fainter galaxies (Abs Mag > -20). If the presence of a void here were not known, this method would produce a lower value for alpha than is really the case. The M.L.E. method is good at regenerating the original curve (Fig. 3.13) over the range proximal to M^*, but it too shows a flattening of the tail end of the curve when a void is present (Fig. 3.15).

In contrast, the M.L.F. method proved remarkably robust at extracting the original parameters put into the simulation, even when a void or cluster was present. Analysis showed this to be due to the weight given to galaxies falling on the knee of the Schechter curve, in the proximity of M^*, which were given greater emphasis than those at either extreme because of their greater numbers. The following tables list the results of several

31

Figure 3.14. A homogeneous V_{max} curve with a high $\alpha = -1.5$ tail. This may be compared with the same curve of Fig. 3.9, where a void is present.
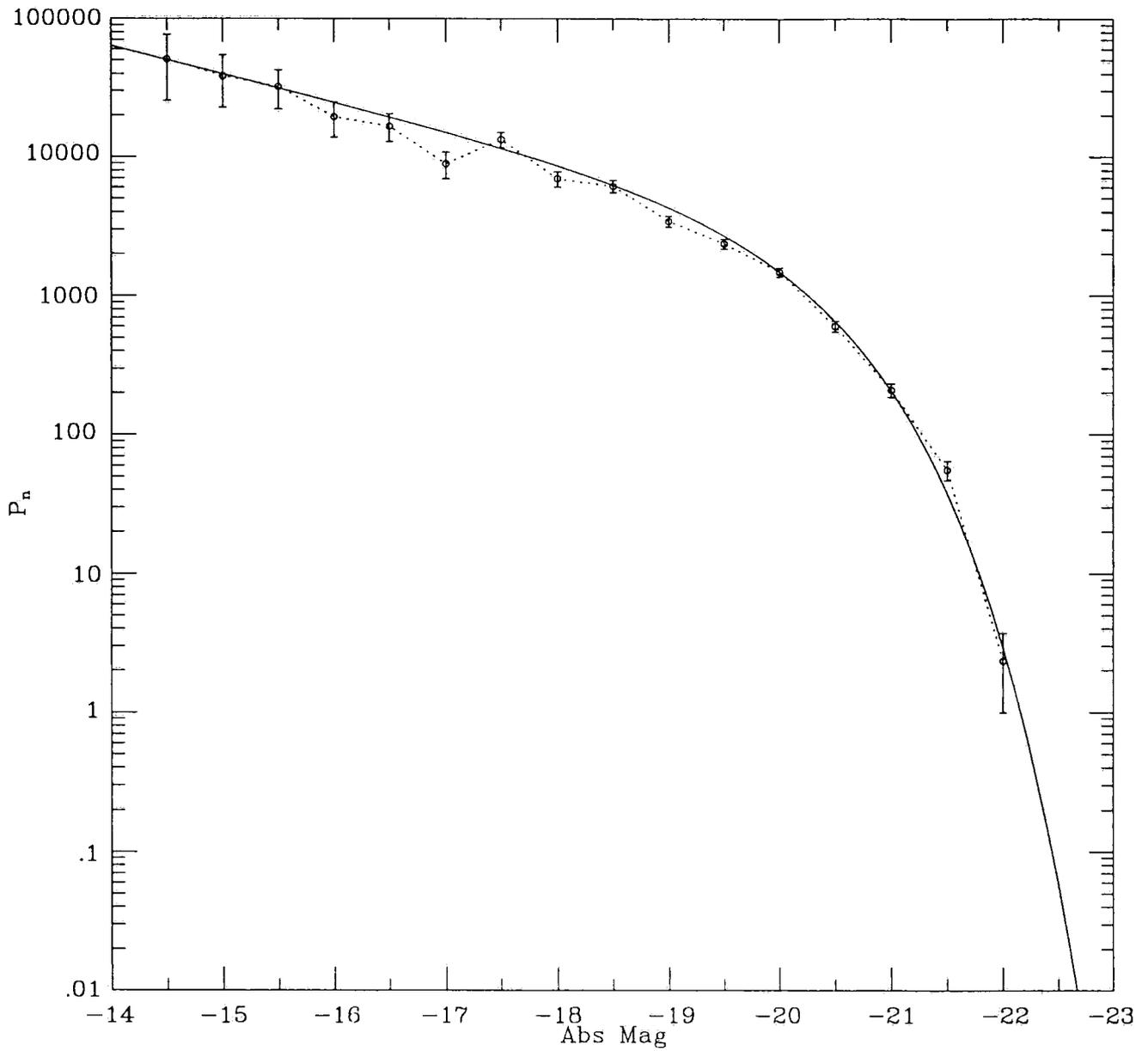
Schechter Curve for simulations ($\alpha = -1.5$, $M^* = -20.0$, $H_0 = 100$)

$mag_{lim} = 17$, K-correction = 3Z, Uniform density

(1000 galaxies, V/Vmax method)

Fig. 3.14

Figure 3.15. The Maximum Likelihood Method of plotting the data of Fig. 3.9, showing the void and a resulting small bright excess. There is rapid convergence over the ten runs shown.
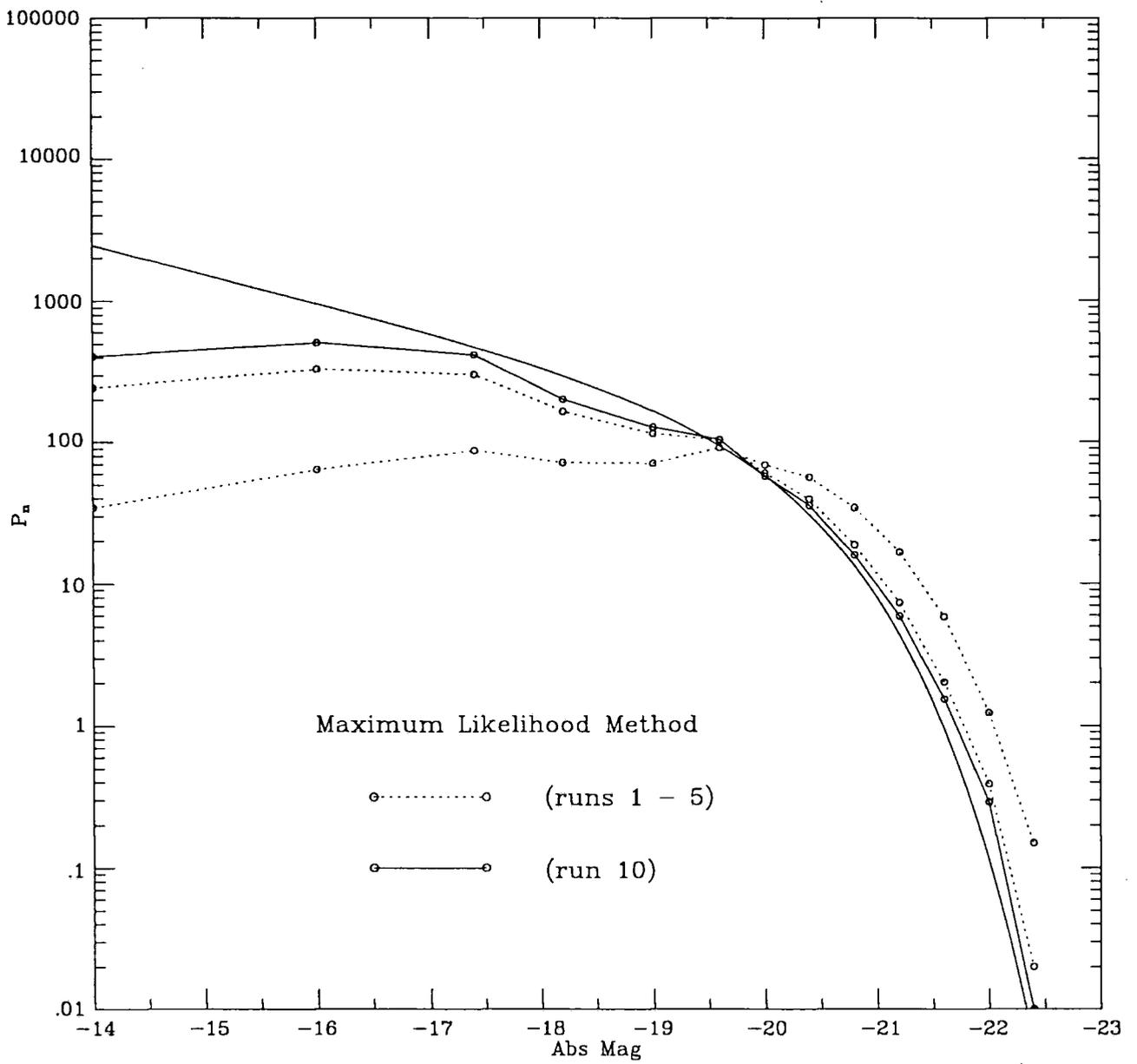
Schechter Curve for simulations ($\alpha = -1.5$, $M^* = -20.0$, $H_0 = 100$)

$\text{mag}_{\text{lim}} = 17$, K–correction = 3Z, Void X0.5 to 150Mpc

(Maximum likelihood method, free parameters)

Fig. 3.15

typical simulations using a homogeneous population (Table 3.2), and a void (Table 3.3) with different numbers of galaxies, and different values of α and M^*.

Table 3.2 Monte Carlo simulations for homogeneous populations

Galaxy numbers	Input α	Input M^*	Returned α	Returned M^*
100	-1.1	-20.0	-1.10	-19.80
500	-1.1	-20.0	-1.10	-19.95
1000	-1.5	-20.0	-1.50	-20.01
1000	-1.5	-20.0	-1.54	-20.16
1000	-1.5	-20.0	-1.53	-20.08
869	-1.8	-19.0	-1.74	-19.06

The last figure in Table 3.2 reflects tighter cutoff limits, which only include galaxies with derived absolute magnitudes fainter than -16.0 and brighter than -23.0. The input values of α and M^* were -1.8 and -19.0 from which we can confirm that the linear relationship $\Delta\alpha = -\Delta M^*$ may be used to correct one parameter of the derived results if the other is known with greater accuracy.

Table 3.3 Monte Carlo simulations with voids

Galaxy numbers	Input α	Input M^*	Returned α	Returned M^*
1000	-1.1	-20.0	-1.09	-19.94
1000	-1.5	-20.0	-1.50	-20.0
898	-1.8	-19.0	-1.72	-18.94

The mean deviation in α is $\pm 1.7\%$, and that for M^* is $\pm 0.36\%$. For the void models, the corresponding errors are $\pm 2.0\%$ and $\pm 0.2\%$, which do not differ significantly.

Two plots of $n - z$ are shown in Fig. 3.16, comparing a homogeneous model (solid curve) and a void model (dashed curve), using parameters $\alpha = -1.2$, $M^* = -19.9$ and $m_{lim} = 16^m.75$. There is a void of $\phi^* = 0.5\phi_0$ to a depth of $180h^{-1}$Mpc and its presence can be clearly seen in the sudden increase in overall counts at redshift $z = 0.06$, followed by a steeper high-redshift tail.

Figure 3.16. The $n - z$ plot for a homogeneous simulation (solid lines) and a void simulation (dashed lines). This is a simple step function model, and the crude jump in counts is clearly visible.
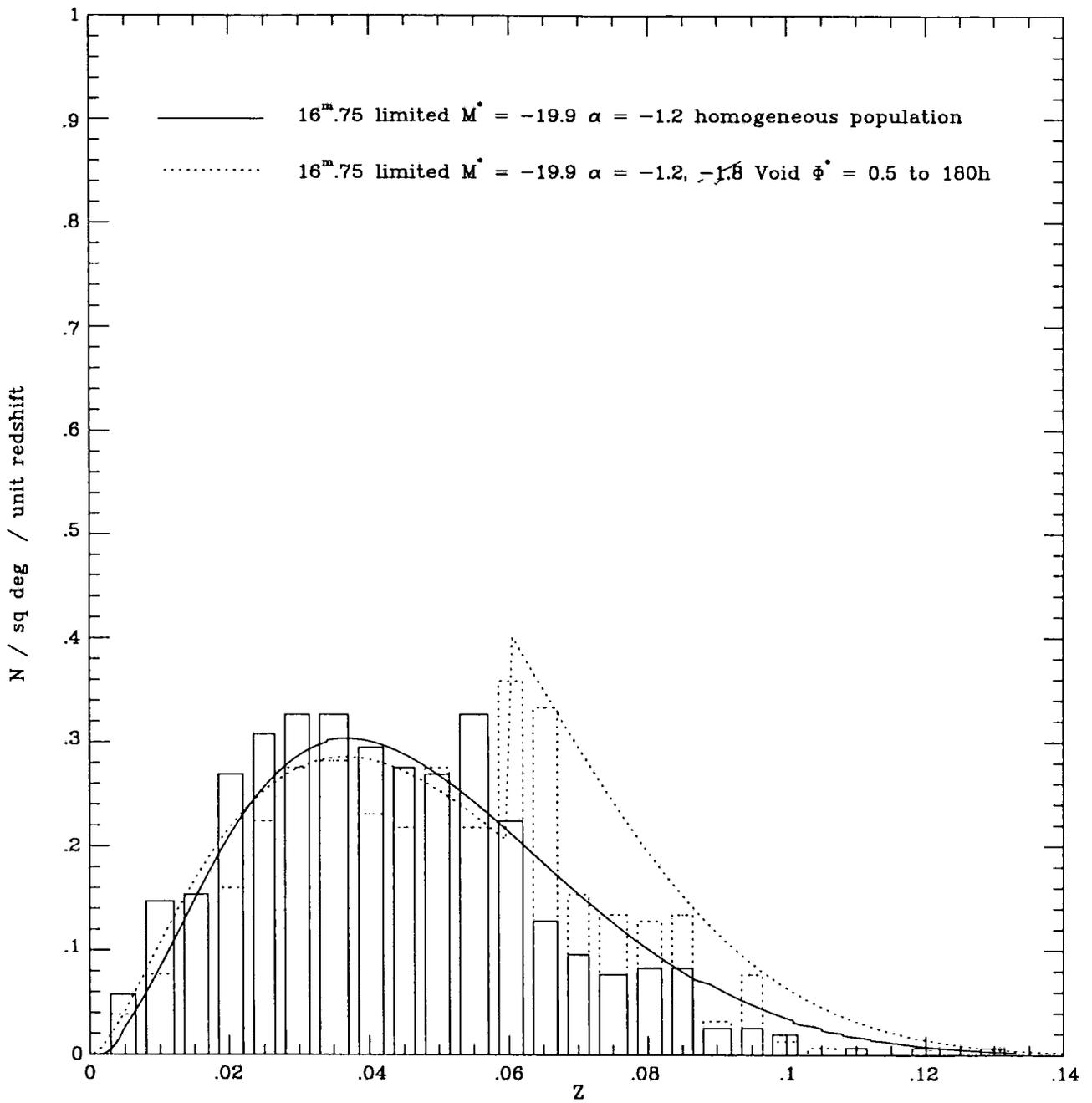
Fig. 3.16

3.5.3 Mixed populations with differing Schechter functions

Simulations were run combining two homogeneous populations of galaxies having the same M^* but differing values of α, as shown graphically in Figs. 3.17 and 3.18. Schechter curves do not add algebraically, and the resultant curves are seen to inflect upwards after the initial knee. The first curve combines a 50% population having $\alpha = -1.0$ and 50% having $\alpha = -1.5$; the second combines a 90% population with $\alpha = -1.0$ plus 10% having $\alpha = -2.0$ to examine the effect of extremes on this model. In both figures, the dotted lines show the input Schechter populations and the solid curve shows the resultant input curve. In contrast, the dashed lines show the results of the Sandage-Tammann-Yahil M.L.F. method. This predicts $\alpha = -1.1$ for both models, which follows from the method of the M.L.F. which has to assume that the curve is pure Schechter, and strongly weights data about the knee.

A curve of n-z is shown in Fig. 3.19 for the mixed equi-population model. The two populations (each with $M^* = -20$) are shown by the dashed lines, with $\alpha_1 = -1.0$ and $\alpha_2 = -1.5$; the composite curve is shown by the solid line and fits as might be expected, intermediate to the two. Its significance lies in the fact that if the Sandage M.L.F. method were taken to generate α and M^*, the predicted curve would lie closer to the low–α curve.

In Fig. 3.20, the effect of a void in a mixed population Monte Carlo simulation of 500 galaxies was studied; this shows an $n - z$ plot for a homogeneous mixed population model having $M^* = -19.9$, $\alpha_1 = -1.2$ (80%), $\alpha_2 = -1.8$ (20%), with $m_{lim} = 16^m.75$. Fig. 3.21 uses the same parameters but with a void of $\phi^* = 0.5\phi_0$ to $180h^{-1}$Mpc. The M.L.F. method of Sandage, Tammann and Yahil returns values of $M^* = -19.9$ and $\alpha = -1.2$ and -1.3 for the homogeneous and void models respectively (solid lines in Figs. 3.20, 3.21). This again emphasises that the M.L.E. method will not pick up a void, with or without a high α tail sub-population.

The influence of different αs on the $n - (b_j)$ number plots was examined in Fig. 3.22 for a wide range of αs, from $\alpha = -1.0 - -2.0$. These curves were all normalised to 19^m. The very extreme $\alpha = -2.0$ is seen to come closer to the observed data, but there is nothing in any of the published series to suggest that this is a realistic figure and the actual values of α are almost certainly much flatter. As discussed above, even if there be a high tail sub–population, this will form only a small percentage of the total population and does not significantly affect the overall shape of the curve.

Figure 3.17. Theoretical curves for a mixed–population model, showing the two independent Schechter curves put in (dotted lines, $\alpha = -1.0$ and $\alpha = -1.5$ respectively), the resultant curve (solid), and the parametrised curve extracted using the Sandage method (dashed line), which returns $\alpha = -1.1$.
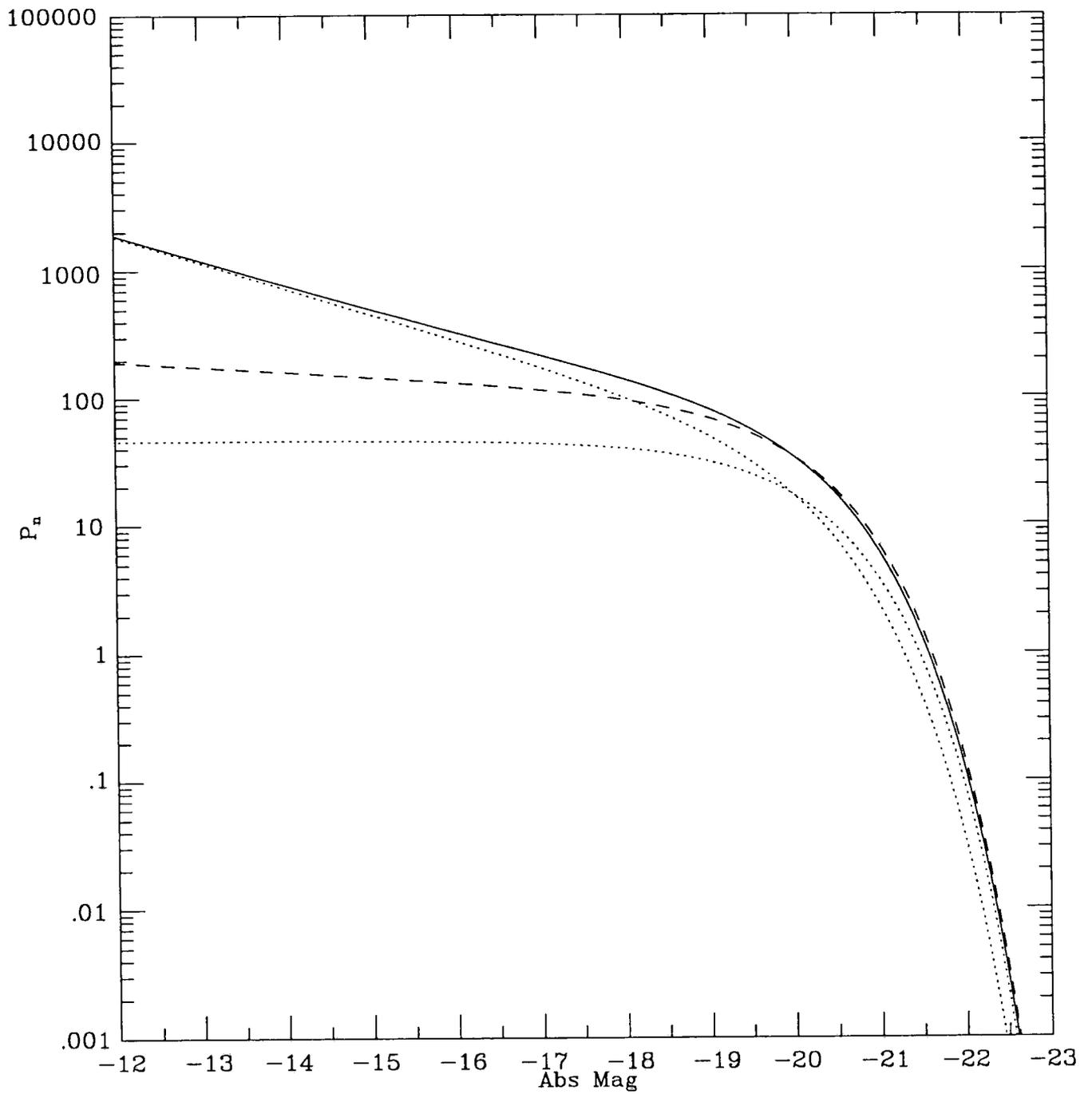
Mixed population model, $\alpha=-1.0$ 50%, $\alpha=-1.5$ 50% (both $M^{\bullet}=-20.0$)

(with Sandage–Tammann prediction, $\alpha = -1.1$)

Fig. 3.17

Figure 3.18. As Fig. 3.17, but with a higher slope ($\alpha = -2.0$) for one of the components, which also is present at a level of only 10%, and for which the Sandage method also returns $\alpha = -1.1$.
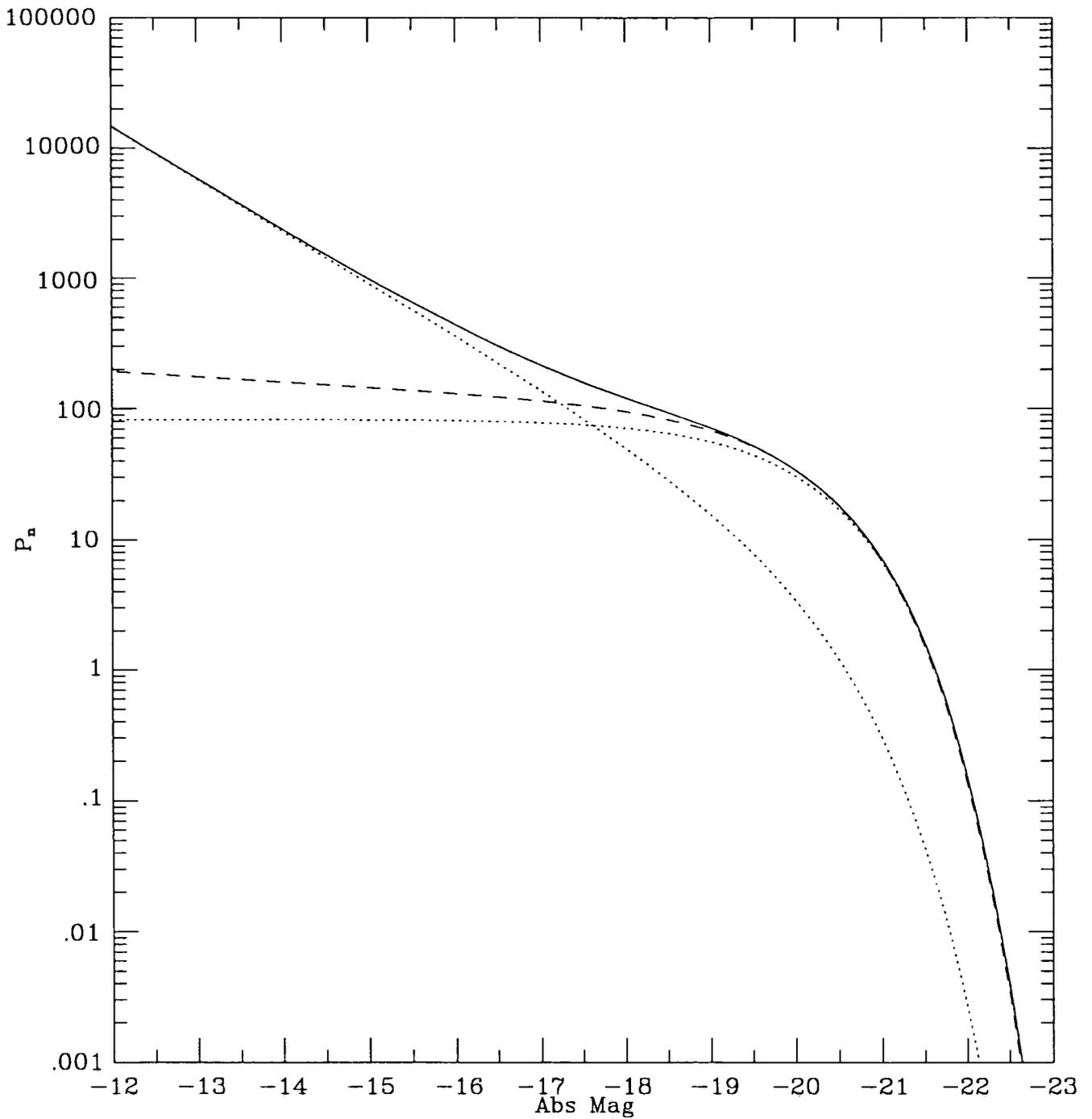
Mixed population model, $\alpha=-1.0$ 90%, $\alpha=-2.0$ 10% (both $M^*=-20.0$)

- - - - - - - = input model populations

———————— = resulting model

— — — — — = Sandage prediction

Fig. 3.18

Figure 3.19. The n-z curves for the mixed population model of Fig. 3.17, shown against the theoretical curves for the two populations (dashed lines) and the curve for the composite population (solid line).
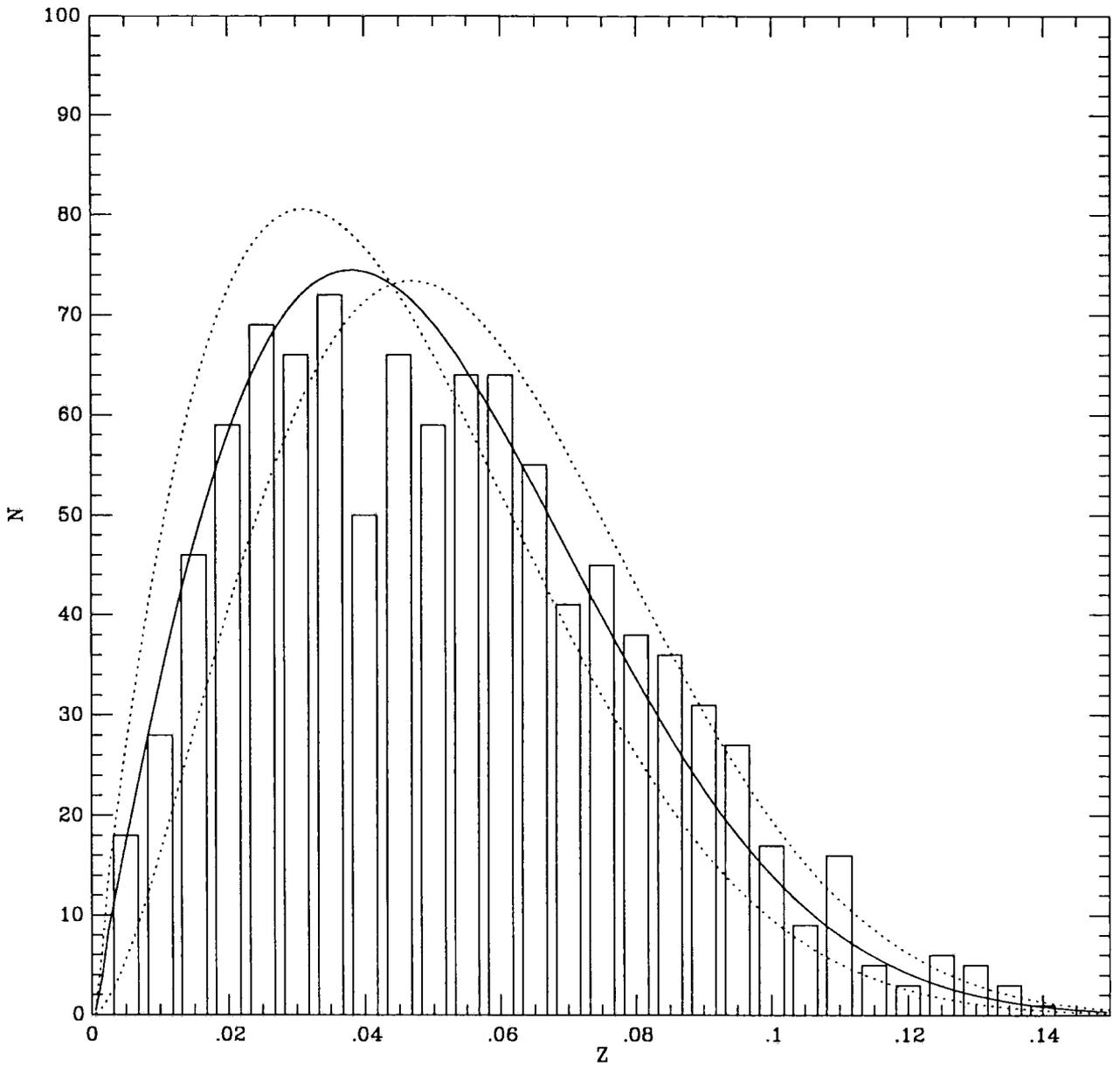
Number / Redshift plot, Mixed population model ($\alpha=-1.0$ / $\alpha=-1.5$)

Fig. 3.19

Figure 3.20. The n-z curves for a mixed homogeneous population model (dashed line) and the Sandage method predicted curve (solid line).
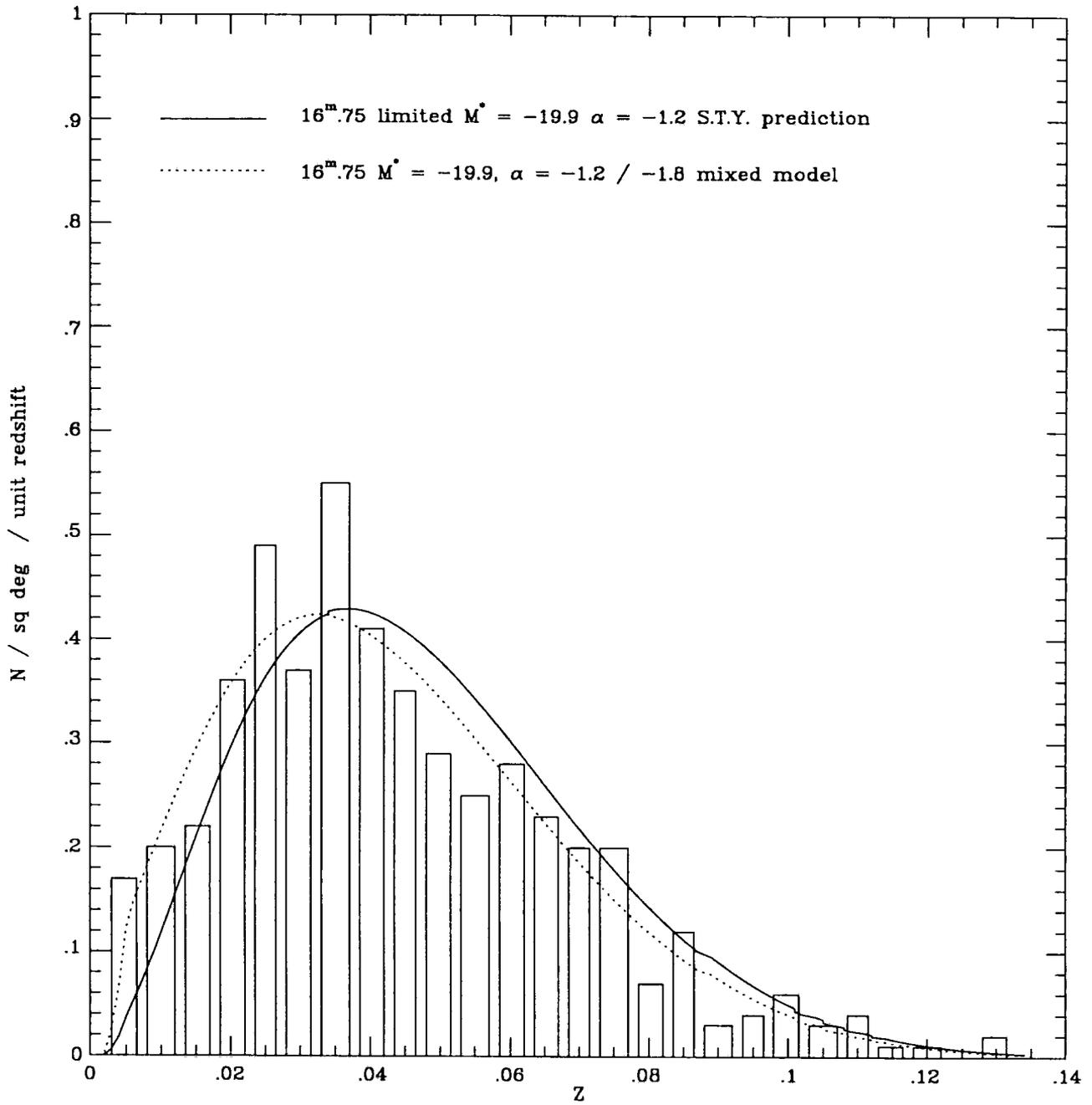
Number / Redshift plot homogeneous mixed alpha models

Fig. 3.20

Figure 3.21. As Fig. 3.20 but with a void of $0.5\phi_0$ to $180h^{-1}$Mpc.
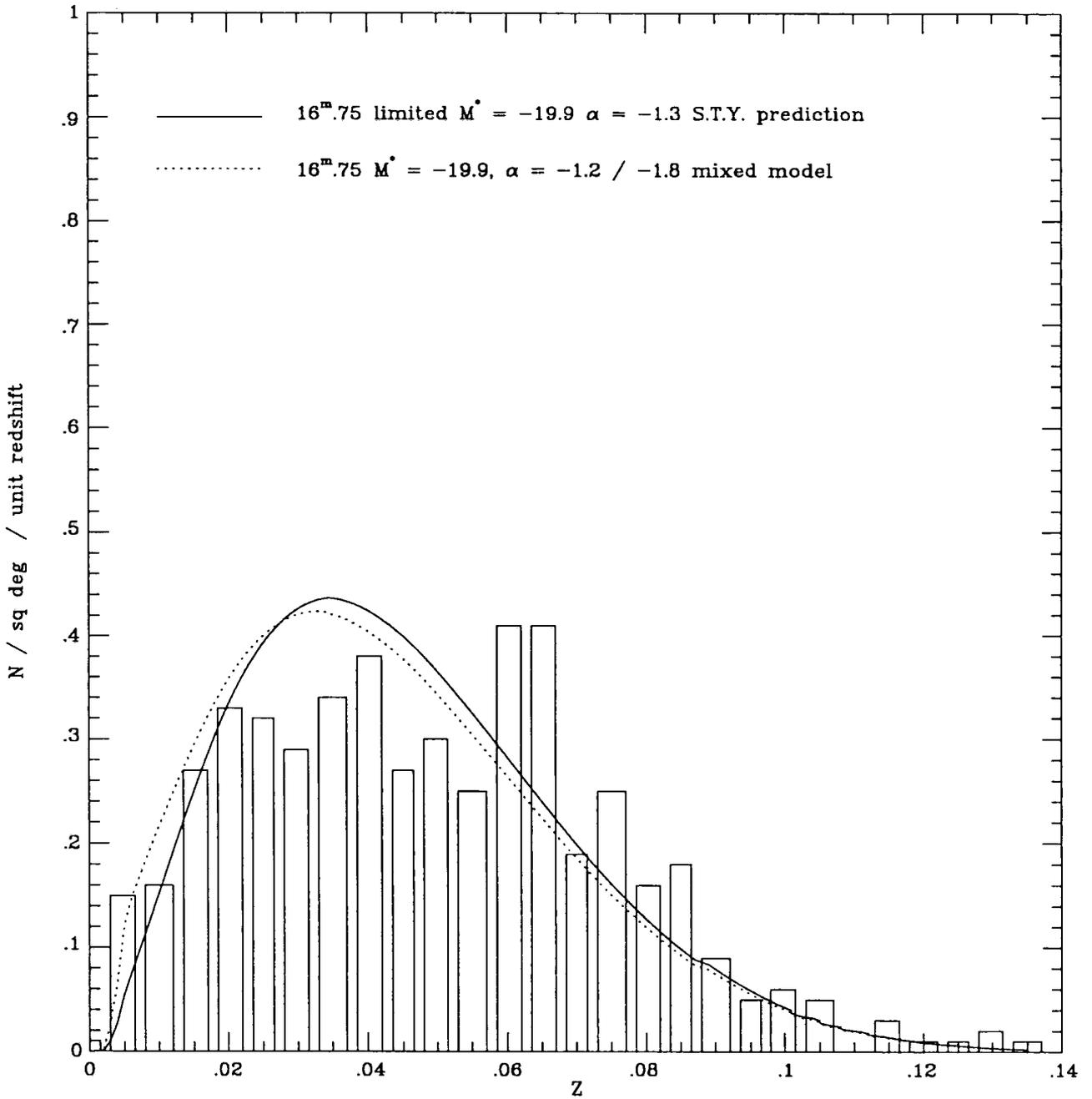
Number / Redshift plot mixed alpha models with void, $\Phi^{\bullet} = 0.5$ to 180h

Fig. 3.21

Figure 3.22. Variations across the bright part of the $n - b_j$ curve with α, normalised to 19^m.
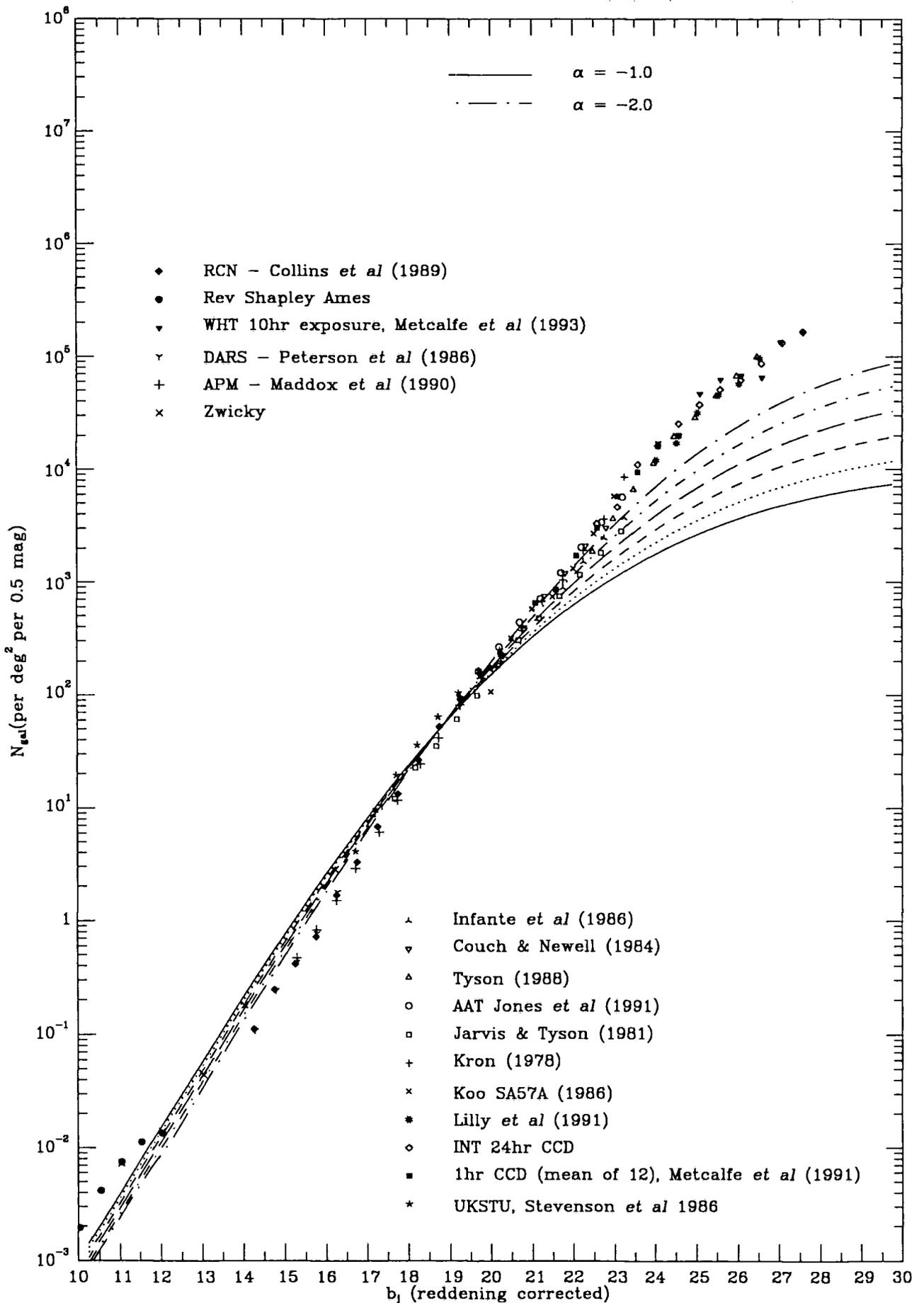
$M^{\bullet}=-20.0$, K-corr = 3z, for varied α models

Fig. 3.22

3.6 Conclusions

The method of Sandage, Tammann and Yahil (1979) has proved very robust and successful in returning the parameters α and M^* put into the Monte Carlo models, even with small numbers of galaxies and extreme values of α. Because of the assumptions inherent in the method (*i.e.* that the curve will be Schechter) and the great weight placed on galaxies whose absolute magnitude falls about the Schechter 'knee', the method tends to ignore any excess of faint galaxies. The method is also relatively insensitive to the presence of a 'void', and again returns the original parameters to within 5%, even with a void ($0.5\phi_0$ to $150h^{-1}$Mpc). Although the M.L.E. method of Peebles is theoretically the more accurate, it was found in practice that this method did not mimic the initial curves so well as the V_{max} method. It was particularly poor at regenerating the high-alpha tail of the composite simulations, which were much better represented by the V_{max} method, and this method was therefore used in the later sections when the analysis of real surveys is considered.

4. The survey data

The compilation of complete redshift catalogues of galaxies provides the only reliable means of determining the local luminosity function of field galaxies, which in turn is crucial to an understanding of the properties of more distant galaxy samples (Metcalfe, Fong, Shanks and Kilkenny, 1989). Such catalogues are also fundamental to understand the large–scale structure of the Universe (e.g. Peebles, 1980). To explore the full extent of the bright–galaxy deficit, and to evaluate its nature, this thesis has compiled as many surveys as possible from the available literature. Some of the most recent are statistically complete while others, for a number of reasons, are historically less reliable, having problems with completeness and photometrical standardisation. These surveys and some of their inherent problems are considered in more detail in this section.

The data points used in Fig. 1.3 are a composite from 16 surveys, with fuller details in Appendix 1. Deep Schmidt plates cover the brighter end to $\sim 21^m$. AAT plates extend from $\sim 20 - 23^m.5$, but there are currently only 5 plates covering an area of sky of $\sim 1^\circ$. The CCD plates extend from $22 - 27^m$, but the fields are only a few sq arc mins, eg 3×2 to 6×4 sq arc min. Table 4.1 is a resume of some of these fields.

Table 4.1

Survey	B_{mag}	No of plates	area (deg^2)	N_{gal}
UKSTU	14-20	20 plates	500	100000
AAT	20-23	5 plates	5	50000
INT CCD	23-25	12 frames	.08	4500
INT CCD	25-27.5	1 frame	.005	2500

The survey of Tyson and Seitzer (1988) was made in 1983 using 4m prime–focus CCD observations at CTIO in three bands: 27^m B_J, 26^m R and 25^m I. They derived a master sky frame by randomly moving the telescope up to $20''$ between exposures, to obtain sufficient information (sky plus fringing) to permit a unique determination for each pixel for systematic errors and subtraction. The images were then further processed to remove bad pixels and cosmic ray events, and flat-fielded to correct for instrumental response. The CCD images, typically 16 per band, were then automatically registered to fractional pixel accuracy and averaged by median filtering to produce the final images in each of the three bands B_J, R and I. Calibration was achieved by interspersing each

set of 8 or 16 object exposures with several short calibration star exposures. They claim a reproducibility at the $0^m.005$ level over a three year period.

Tyson (1988) limited his analysis to objects at least 2^m brighter than the survey surface-brightness limit, and imposed a minimum area for an object, so that the magnitude is isophotal down to a faint limit, and aperture at fainter magnitudes. He performed realistic simulations by adding galaxies and stars of known profile and magnitude to the data, to test the photometry.

Maddox $et\ al.$ (1990) analysed galaxy number–magnitude counts from 4300 deg^2 of the APM Galaxy Survey in the range $15 < b_J < 20.5$. Using CCD photometry of 339 galaxies to calibrate the APM magnitudes, they found the number counts at $b_J \sim 19 - 20$ close to the mean of previously published results. Their results for $b_J < 15$ are uncertain, as discussed in §3, but they consider the detection reliable from $b_J > 15$ to $b_J < 21.5$, with the only significant cause for incompleteness coming from their star–galaxy separation. Galaxies brighter than $b_J < 16.5$ were checked by eye, and the completeness is estimated at $> 95\%$ with zero stellar contamination. Over the range $16.5 < b_J < 19.5$, they estimate incompleteness and stellar contamination at $\sim 5\%$. For galaxies fainter than $b_J \sim 20$, they consider incompleteness to become progressively severe, being $\sim 27\%$ at $b_J = 20.5$, and 58% at $b_J = 20.9$. The uncertainties in this correction for $b_J < 20.5$ are smaller than their calibration uncertainties, and much smaller than the evolution seen in the counts over this range. Their counts fainter than $b_J = 20$ show a count slope $dN \propto 10^{0.45m}$, consistent with deeper studies, and they take this as confirmation that their correction is reliable to at least as faint as $b_J = 20.5$.

The survey of Metcalfe $et\ al.$ (1991) was taken on the Prime Focus CCD camera of the Isaac Newton Telescope in 1986, using 12 independent fields in the blue and red passbands for $21^m < B_{ccd} < 25^m$ and $19^m < R_{ccd} < 23^m.5$. Their galaxy count relations were found to lie within the middle of the wide range of previous photographic data, with reasonable agreement to the CCD galaxy counts of Tyson (1988) at corresponding depths. The field–to–field variation was small enough to define the faint galaxy count ($B < 24^m.5$) to $\pm 10\%$, consistent with that expected from galaxy clustering considerations. Their data confirmed that the B and R both show evidence for strong galaxy luminosity evolution, with the majority of the evolving galaxies of moderately blue colour ($0 < B - R < 1.4$).

Lilly $et\ al.$ (1991) examined three areas of sky to faint levels in four passbands (U',

B, V and H), reaching $\sim 27^{m}$. They found the fainter galaxies to be considerably redder than those of Tyson, with evidence of a decline in the steep slope of B-band number counts fainter than $B \sim 24$. Spectroscopic and imaging data indicate the median redshift of $B \leq 24$ galaxies is still low with $\langle z \rangle \sim 0.4$, as previously shown by Colless *et al.* (1989b) and close to that predicted from non–evolving models despite the considerable enhancement seen in the number counts relative to these models. They considered the low redshifts seen at $B \sim 24$ to confirm a trend noted by other workers, indicating that the evolution of galaxies to $z \sim 0.5$ is best characterised by an increase in ϕ^* rather than in L^*.

4.1 The Durham Anglo-Australian redshift survey (DARS)

This survey, undertaken over the period 1979–1983, is fully described by Peterson *et al.* (1986) and comprises a total of five fields and 322 objects having a well defined redshift out to limiting isophotal magnitudes of $B_J \sim 17.0$. Each field was selected from the unvignetted portion of a UK Schmidt plate, with a mean area of ~ 14.2 deg^2, all at high latitudes. The magnitudes are given as B_J total; corrections to convert the fields from B_{ccd} to b_J were made according to Table 4.2 (Metcalfe, personal communication), which also includes the galaxy numbers and the area for each field.

Table 4.2. Corrections to DARS survey fields

Field name	mag limit (B_J)	Field correction	Number	Area
GSA	17.00	0.02	73	14.06
GSD	17.00	−0.05	61	13.95
GSF	17.20	−0.1	57	15.17
GNA	17.20	−0.16	60	13.91
GNB	17.15	−0.1	71	13.50

The photometric exposures were made using Kodak emulsion IIIa-J photographic plates and GG395 filters. An additional correction of $-0^m.2$ had to be made to each field to transform them from total B–magnitude to b_J–magnitude. This gave a mean field magnitude limit of $16^m.88$ which was adopted as the b_J magnitude limit for the survey, assumed complete to this limit.

The catalogue quotes one or both of two velocities, an absorption–line velocity (cz) in km s^{-1} on a heliocentric corrected system, and an emission–line velocity; where both appear, the emission–line velocity was selected, this being assumed the more accurate.

Corrections to the photometry of other surveys was described by Peterson, with suggested figures of $B_j(25.6) = B_j(\text{AARS}) - 0.28$ and $J(\text{KOS}) = B_j(\text{AARS}) - 0.64$, though here there is much scatter at the faint end and it is thought that the KOS photometry is unreliable fainter than $J(\text{KOS}) \sim 15$. A determination of the luminosity function was made by Efstathiou *et al.* (1988).

4.2 The Durham A.A.T. faint galaxy survey, Broadhurst *et al.* (1988) (BES)

Spectroscopic observations were made of 230 galaxies in the magnitude range $20 \leq b_j \leq 21.5$, selected from five random AAT fields. Star/galaxy separation was based initially on standard algorithms, with each target visually checked before spectroscopy. This rejected a small number of misclassifications, merged objects and plate defects; in addition, for object pairs closer than $18''$, only one object could be chosen. It was estimated that these final selections affected $< 10\%$ of the sample. Subsequent re-examination of the fields have inevitably revealed some galaxies misclassified as stars, and not surveyed; again, this is estimated to be $< 10\%$ of the total; however, there may be a residual incompleteness from these combined effects of $\sim 15\%$. Additionally, some larger field areas were sampled at a lower rate, and some smaller fields were sampled nearly to completeness. A further limitation of the survey was the bright cut-off limit; in general this was one magnitude brighter than the faint limit (which varied across the survey fields), but for one field (MT, centre $22h03'03''-18° 54'42''$) it was only $0^m.85$ brighter. Table 4.3 summarises the five fields used in the survey. Photometric calibration in each field was based on CCD photometry of stars and galaxies taken under good conditions, and adjusted to the b_j passband; it should be noted that two fields are in common with the DURSAAO survey (529≡GSG and 419≡GSP) and the same magnitude corrections are applied.

Table 4.3. Field details from BES survey

Name	Mag Lim (b_j)	Correction	Area (sq$'$)	Completeness	Fraction sampled	$\bar{z}$
SGP	20.5 – 21.5	+.21	216.6	59/70	0.68	.225
197	20.5 – 21.5	0	400.0	31/38	0.79	.249
MT	20.5 – 21.35	0	776.2	30/35	0.12	.235
529	20.0 – 21.0	−.04	275.5	35/41	0.80	.193
419	20.0 – 21.0	+.02	501.8	32/36	0.25	.193

4.3 The KOS (1979) and KOSS (1983) surveys

Kirschner, Oemler and Schechter (1979) (usually referred to as KOS) took deep pencil beam surveys in a number of randomly chosen fields, surveying 164 galaxies to a maximum depth of $\sim 200h^{-1}$Mpc. This was continued by Kirshner et $al.$ (1983) (the KOSS survey) in a further and deeper study to ~ 350 h^{-1}Mpc.

4.4 The Durham 1984 (DURSAAO) survey

The extended galaxy redshift survey of Metcalfe, Fong, Shanks and Kilkenny (1989) was undertaken in 1983–1984. It continued the approach of the DARS survey, sampling to fainter magnitudes over small areas of sky to produce as full a sample as possible, with a limiting magnitude of $b_j \approx 16^m.80$ from nine UK Schmidt (UKST) fields. Each field was of area $\sim 3^\circ.75 \times 3^\circ.75$. Star–galaxy separation was done initially with an automated routine, then checked by eye to pick up very bright galaxies, and to eliminate non-galactic contaminants. A one–third sampling rate was used, selecting every third galaxy in magnitude order in each field for spectroscopy. This gave approximately 30 galaxies per field, with a total of 260 galaxies.

4.4.1 Photometry of the DURSAAO survey

Accurate photometry was acquired from UKST blue plates, which were scanned by the COSMOS measuring machine to produce photographic isophotal b_j magnitudes for all objects to the plate limit. The isophotal thresholds were set so that isophotal magnitudes of galaxies in the survey would be within $\approx 0.1 - 0.2^m$ of 'total' magnitudes. Zero–point scales were initially obtained by setting the galaxy number–counts at $b_j = 19^m$ to agree with those of the South Galactic Pole (SGP) survey (Shanks *et al.* 1984). However, the final magnitude scale of each field was calibrated accurately to $\pm 0^m.1$ by taking B and V CCD photometry for several galaxies in each field. The zero point for each field was then determined by comparing the COSMOS magnitudes with their CCD values, corrected for differences between the photographic (b_j) and CCD passbands, using a colour equation of the form $b_j = B_{CCD} - 0.17(B - V)_{CCD}$. This correction gave a residual overall scatter of $\pm 0^m.15$, mostly from photographic errors (errors in CCD magnitudes were estimated at $\pm 0^m.05$). The zero points used here are revised versions of those given in Metcalfe *et al.* (1989), using the corrections in Table 4.4 (Metcalfe, personal communication).

Table 4.4. Field corrections to the DURSAAO survey

Field name	mag limit (b_j)	field correction
GNX	16.86	−0.01
GNY	17.24	−0.10
GNH	17.24	−0.07
GNZ	17.08	−0.16
GSG	17.10	−0.04
GSM	16.92	−0.03
GSI	17.05	no change
GSN	17.01	+0.25
GSP	17.09	+0.02

These corrections are the ones used in this paper to derive the L.F. and the appropriate number counts.

4.5 The Colless *et al.* (1990) survey

The LDSS deep redshift survey of Colless *et al.* (1990) sampled 149 objects selected randomly in three high-latitude fields from the magnitude range $21 \leq b_j \leq 22.5$, with an overall success rate of 81%, comparable to that of Broadhurst *et al.* . Its significance is that the survey was representative of galaxies over this magnitude range, and their observed redshifts were in the range $0 < z < 0.7$, effectively ruling out a significant excess of high-redshift galaxies. This provided significant restraints on models where galaxy luminosities evolve monotonically with redshift in a luminosity–independent way, suggesting that the steep slope of the number–magnitude counts is mostly due to the evolution of galaxies at the faint end of the galaxy luminosity function.

4.6 The Third Reference Catalogue of Bright Galaxies survey (1993)

The original Shapley and Ames (1932) Harvard Survey of Galaxies contained 1,249 objects brighter than 13^m, of which five were not galaxies. The First Reference Catalogue (RC1) (G. and A. de Vaucouleurs 1964) included 2,599 objects of which six were not galaxies. The Second Reference Catalogue (RC2) (G. and A. de Vaucouleurs and H.G. Corwin 1976) listed 4,364 objects, but both RC1 and RC2 are incomplete beyond the Shapley–Ames limit.

The Third Reference Catalogue of Bright Galaxies (RC3) (de Vaucouleurs, de Vaucouleurs, Corwin, Buta, Paturet and Fougué, 1991) assembles an amalgam of reference sources to give a comprehensive whole–sky coverage for galaxies fulfilling the limiting criteria of apparent diameter > 1 min at the D_{25} isophotal level, total B-band magnitude $B_T \leq 15.5$, and a velocity < 15000 km/sec (equivalent to redshift $z < 0.05$). The two principle surveys used are The European Southern Observatory Catalogue (ESO) and The Uppsala General Catalogue of Galaxies (UGC) which cover the sky for $\delta \leq -17.5°$ and $\delta \geq -2.5°$ respectively, with other surveys filling the gaps such as The MCG Russian survey and The Corwin and Skiff Equatorial Catalogue. This produces a catalogue with potentially serious errors for any comparison across the whole sky, as independent authors use differing photographic plates and emulsions, and sometimes idiosyncratic criteria for determining magnitudes, angular diameters, classifications and colours; but with this proviso, it claims to be 'reasonably complete', listing 11,897 objects conforming to the above limits. Additional objects not meeting all these conditions bring the total number to 23,024. This represents a substantial body of data for bright galaxies, and makes analysis potentially fruitful if homogeneity between the fields can be demonstrated, or compensated for in a systematic manner. With this in mind, an attempt was made to analyse the data in the catalogue to produce a number–magnitude relationship, remembering that Schechter's original derivation used RC1 and a sample of only 184 galaxies, limited to $m_B \leq 11.75$.

The angular diameters listed in the principle catalogues are visual estimates, and Lauberts (1982) noted a decline in ESO counts setting in below 1.4 min. Hudson and Lynden–Bell (1991) have analysed the completeness of the UGC and ESO catalogues, and Hudson considers that RC3 is probably 95% complete for $B_T \leq 14.5$, but may be only ~ 70% complete for the smallest galaxies in the survey, with 'face–on' diameters ≈ 1 min corresponding to $B_T \leq 15.5$ (personal communication).

The catalogue was accessed in its revised tape format using SCAR extraction routines on the STARLINK system. Analysis was limited to $|b| \geq 30°$ to reduce the inhomogeneities of galactic extinction, and the catalogue was divided into Northern and Southern hemispheres for systematic analysis of biases and differences within the catalogue.

4.6.1 Calibration of RC3 to the b_j magnitude system

The RC3 survey gives three different measures of magnitude for each object:

a) BT_{mag} — defined as the total (asymptotic) magnitude in the B-system, derived by extrapolation from photoelectric aperture–magnitude data

b) MB_{mag} — photographic magnitude from Ames (1930), Shapley and Ames (1932), CGCG, Buta and Corwin (1986), and/or Lauberts and Valentijn (1989) reduced to the B_T system

c) B_T-magnitude, defined as the total "face–on" magnitude corrected for Galactic and internal extinction and for redshift.

In attempting to determine the most appropriate system to use for conversion to the b_j scale, a total of 42 galaxies from the DURSAAO survey were found to match PCG reference galaxies in the RC3 catalogue. Details are given in Table 4.5. A ? indicates uncertainty in the position identification, leaving a total of 35 galaxies from seven fields for which there is definite positional correlation. For identification within RC3, the PCG reference number designation (Paturel *et al.* 1989) is given. Where available, the NGC or IC designations are also given.

Table 4.5. Calibration of RC3 magnitude system to b_j

Name	b_j	PCG-number	NGC/IC Name	BT_{MAG}	MB_{MAG}	B_T	ΔBT	ΔMB
?GNX 003	14.25	PCG 34006		14.10		13.81	0.15	
GNY 013	14.98	PCG 42109			14.92			0.06
?GNY 018	15.40	PCG 42393			14.40	14.07		1.00
?GNY 004	13.69	PCG 42199	NGC 4581	13.32	13.11	13.20	0.37	0.58
?GNY 017	15.31	PCG 42255			14.93	13.65		0.38
GNY 006	14.07	PCG 42453	NGC 4599		13.61	13.32		0.46
GNY 003	13.68	PCG 40564	NGC 4385	13.20	12.88	12.90	0.48	0.80
GNY 012	14.93	PCG 42305			14.90	14.80		0.03
GNY 001	11.27	PCG 41618	NGC 4517	11.10	11.30	9.93	0.17	−0.03
?GNY 015	15.12	PCG 42202			14.88			0.24
?GNY 005	13.98	PCG 41911	NGC 4514		13.84	13.20		0.14
GNY 011	14.88	PCG 41788			14.36			0.52
?GNY 009	14.54	PCG 40762	NGC 4418		13.99	13.60		0.55
GNH 001	13.31	PCG 52825	NGC 5756	12.34	13.22	12.31	0.97	0.09
GSM 006	14.32	PCG 68201		14.59	14.69	14.11	−0.27	−0.37
GSM 002	12.85	PCG 67892	NGC 7183		12.93	12.84		−0.08
GSM 007	14.32	PCG 67956			14.37	13.65		−0.05
GSM 004	13.79	PCG 67943	NGC 7188		14.02	13.46		−0.23
GSM 003	13.55	PCG 67919	NGC 7185	13.40	13.11	13.16	0.15	0.44
GSM 005	13.87	PCG 67890	NGC 7180	13.56	13.59	13.47	0.31	0.28
GSM 001	11.74	PCG 67904	NGC 7184	11.65	11.86	10.79	0.09	−0.12
GSM 008	14.67	PCG 68082			14.96	14.19		−0.29
GSI 002	13.33	PCG 69661	NGC 7368		13.15	12.11		0.18
GSI 003	14.09	PCG 69578			13.21	13.15		0.88
GSI 005	14.93	PCG 69480			15.03	14.87		−0.10
GSI 001	13.01	PCG 69161	NGC 7307	12.92	12.90	12.02	0.09	0.11
GSI 008	15.29	PCG 69665			15.40			−0.11
GSN 003	13.66	PCG 4646	NGC 461		14.08	13.85		−0.42
GSN 004	13.78	PCG 4799	NGC 491A	14.30	14.28	13.83	−0.52	−0.50
GSN 001	13.26	PCG 4914	NGC 491	13.21	13.23	13.01	0.05	0.03
GSN 002	13.61	PCG 4731			13.72	13.62		−0.11
GSN 017	14.82	PCG 4787			15.14	15.04		−0.32
GSN 008	14.00	PCG 3822	NGC 365		14.21			−0.21
GSN 006	13.93	PCG 4161	NGC 415		14.28	13.86		−0.35
GSN 007	13.94	PCG 4132	NGC 409		14.00	13.88		−0.06
GSN 009	14.02	PCG 4881			14.22	13.59		−0.20
GSN 013	14.62	PCG 4073			14.57	14.45		0.05
GSN 011	14.59	PCG 4900			14.64	14.53		−0.05
GSN 020	14.87	PCG 4924			15.14			−0.27
GSN 021	14.89	PCG 3971			14.58			0.31
GSP 001	13.97	PCG 14110	IC 2007		13.68			0.29
GSP 002	14.64	PCG 14151			14.15	13.29		0.49

Only the BT_{mag} and the MB_{mag} were found to be within reasonable calibration range of the b_j system. As might be expected, the B_T system with its applied corrections varied by too large and unreproducible a margin for reliable use in any conversion model. The BT_{mag} was available for 10 objects with a mean offset of $+0^m.15$. The MB_{mag} system was obtained for 35 objects, with an r.m.s. scatter of $0^m.056$, comparable with the internal r.m.s. errors in ΔMB of $0^m.058$ ($n = 41$), and this magnitude was therefore the one selected to bring it into the b_j system.

4.6.2 $n(b_j)$ from the RC3 survey

The following table (Table 4.6) lists the final results for the RC3 survey analysis. For the northern hemisphere survey (declination $> 0°$), 10,133 objects were found to be in range of the specified criteria. For the southern hemisphere (dec $\leq 0°$), 6,184 objects were found to be in the range. Of these, 1,878 had no MB_{mag} in the southern group and similarly 1,958 were excluded in the northern group. The errors shown are the magnitude errors for the system used averaged over the total number of objects falling into each b_j magnitude band.

Table 4.6. Total counts and calculated n(b) for RC3 catalogue

b_j	Counts North	South	n/sq deg/0.5 mag North	South	Mean errors North	South
10.25	23	6	0.00223	0.00058	0.17	0.14
10.75	39	17	0.00378	0.00165	0.16	0.17
11.25	61	39	0.00591	0.00378	0.17	0.14
11.75	93	83	0.00902	0.00805	0.19	0.15
12.25	163	114	0.01581	0.01105	0.19	0.15
12.75	250	180	0.02424	0.01745	0.19	0.16
13.25	349	297	0.03384	0.02880	0.20	0.18
13.75	667	497	0.06468	0.04819	0.21	0.20
14.25	1326	802	0.12858	0.07777	0.21	0.20
14.75	2040	1056	0.19781	0.10240	0.21	0.21
15.25	2470	906	0.23950	0.08785	0.25	0.23

This data is shown plotted in Fig. 4.1, where it may be compared to other data over this range, while Fig. 4.2 shows the same data in the context of the overall survey plots. Table 4.7 lists the log counts, and the fractional errors measured for the northern and southern surveys compared to the predicted model counts ($q_0 = 0.5$) normalised to 17^m.

Table 4.7. Fractional errors in RC3 counts

bj	model	RC3N	RC3S	err N	err S	N/S excess
10.25	−2.99	−2.651	−3.236	2.17	.566	3.83
10.75	−2.69	−2.422	−2.782	1.85	.808	2.29
11.25	−2.39	−2.228	−2.422	1.45	.927	1.56
11.75	−2.10	−2.044	−2.094	1.13	1.01	1.12
12.25	−1.81	−1.801	−1.956	1.02	.713	1.43
12.75	−1.52	−1.615	−1.758	.802	.577	1.39
13.25	−1.23	−1.470	−1.540	.574	.489	1.17
13.75	−0.95	−1.189	−1.317	.576	.429	1.34
14.25	−0.67	−.8908	−1.109	.601	.363	1.65
14.75	−0.39	−.7037	−.9897	.485	.251	1.93

This table is of particular interest as it demonstrates clearly the wide variation between counts in the two hemispheres over the full magnitude range of the surveys. One might expect gross discrepancies at the brightest end from local clustering effects; these should progressively reduce with increasing faintness and increasing numbers of contributing galaxies, as indeed they do over the range 10—$11^m.75$. The best correlation is at $11^m.75$, where the counts agree to within 12%; fainter than this, there is a steady divergence reaching a factor of 2 at $14^m.75$, where incompleteness still ought not to be a problem.

Possible causes of such differences between the surveys have already been discussed (§1.3.1 and 1.3.2); the mean photometry errors at this level are $0^m.21$ for both hemispheres, which corresponds to a count differential of 1.34 times. This suggests that the surveys might be pulled into agreement on the basis of photometry differences down to $13^m.75$, with the implied deficiencies in the southern hemisphere attributable to systematic differences between the two principal surveys.

The real problem is that even the northern survey shows a mean under–density over

Figure 4.1. The RC3 survey plots, compared with other bright galaxy surveys. The $q_0 = 0.5$ model and the Euclidean $10^{0.6m}$ line are also shown.
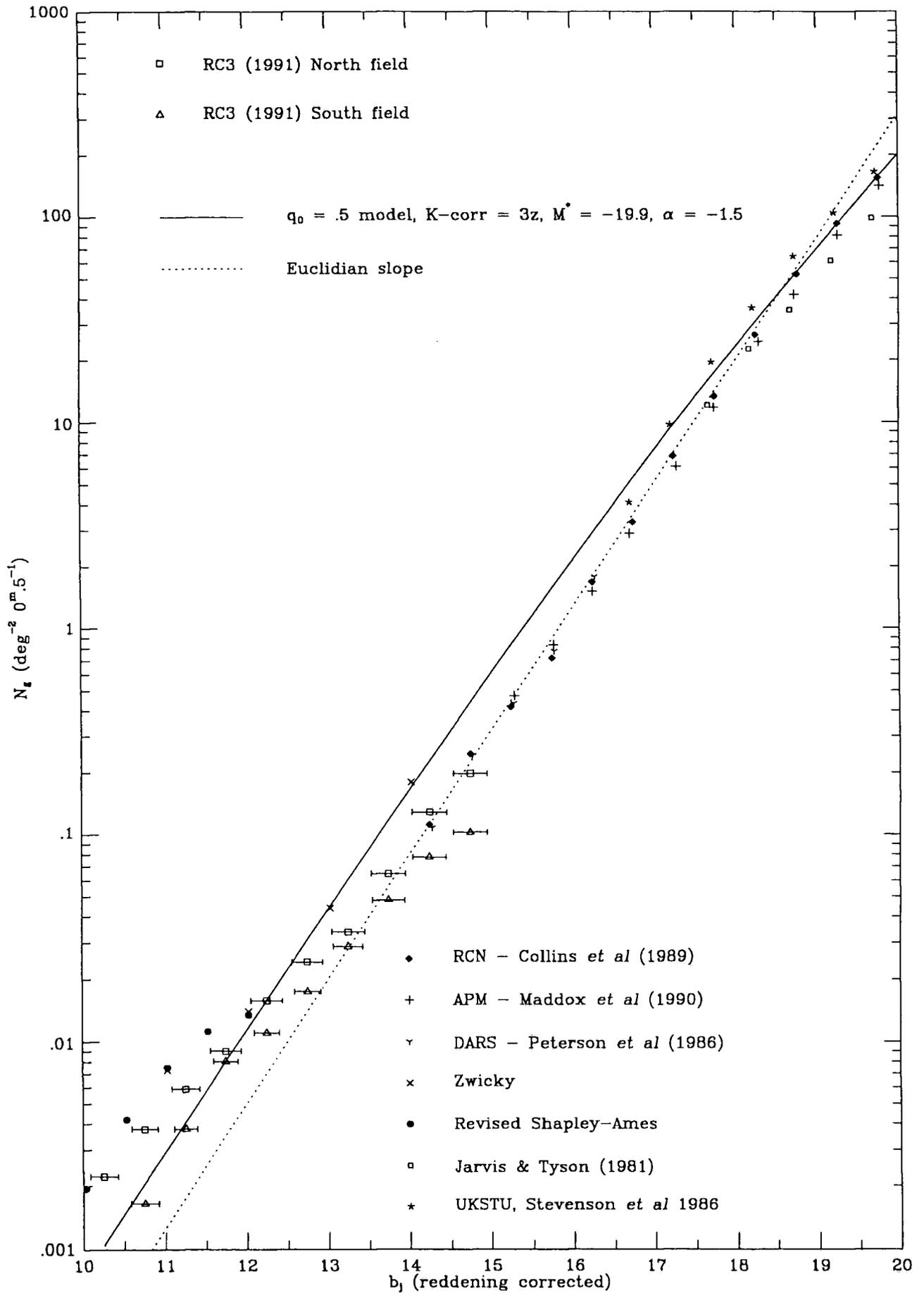
Data from The Third Reference Catalogue of Bright Galaxies

Fig. 4.1

Figure 4.2. The RC3 survey in the context of the full survey plots.

The figure is a log-linear plot with axis label N_{gal}(per deg^2 per 0.5 mag) on the vertical axis and b$_j$ (reddening corrected) on the horizontal axis.

Legend entries:

——— $q_0 = 0.02$

- - - - Euclidean slope

□ RC3 (1991) North field
△ RC3 (1991) South field

◆ RCN — Collins *et al* (1989)
● Rev Shapley Ames
▼ WHT 10hr exposure, Metcalfe *et al* (1993)
Y DARS — Peterson *et al* (1986)
+ APM — Maddox *et al* (1990)
× Zwicky

⅄ Infante *et al* (1986)
▽ Couch & Newell (1984)
△ Tyson (1988)
○ AAT Jones *et al* (1991)
□ Jarvis & Tyson (1981)
+ Kron (1978)
× Koo SA57A (1986)
∗ Lilly *et al* (1991)
◇ INT 24hr CCD
■ 1hr CCD (mean of 12), Metcalfe *et al* (1991)
★ UKSTU, Stevenson *et al* 1986

Data from The Third Reference Catalogue of Bright Galaxies

Fig. 4.2

the range $12^m.75$—$14^m.25$ of a factor of 0.64, although it must be noted that this is in good agreement with other surveys continuing beyond this, such as the RCN, DARS and the APM.

Coupled with the remarkably good fit to a standard Euclidean $10^{0.6m}$ slope over this range, these figures do suggest that, over the wide magnitude range 14—19^m, the surveys cannot be far wrong. In particular, there is unlikely to be such a uniform and continuous smooth void over such a wide range of magnitudes. The inference from this is that the normalisation of the number–magnitude curve is correct at these brighter magnitudes, with the implication that it is either some systematic observational error, or markedly wrong theoretical models, which may be introducing the pronounced count excess at the fainter end, beyond 19^m.

5. Analysis of the survey data

5.1 Derived luminosity functions for DURSAAO and DARS

The analytical methods described in §3 were applied to several surveys (DARS, KOSS, DURSAAO, BES) to extract estimates for α and M^* using Sandage's M.L.F. method, the $1/V_{max}$ method and Peebles' MLE method. The curves derived by these methods were compared with standard Schechter curves using the calculated parameters. The DURSAAO survey contained 246 usable objects with a corrected magnitude limit of $16^m.88$. Using the technique outlined in §(3.4.2), the M.L.F. gave the values $\alpha = -1.15 \pm 0.05$, $M^* = -19.93 \pm 0.08$. Fig. 5.1 shows the resultant $1/V_{max}$ curve for this data, with the derived Schechter curve normalised to this about M^*. Fig. 5.2 is for the DARS survey, with 306 usable galaxies, for which Peebles' M.L.E. gives $\alpha = -1.18 \pm 0.05$, $M^* = -20.05 \pm 0.07$.

Fig. 5.3 shows the same survey data for the DURSAAO (circles) and the data for the DARS survey (squares) with an additional combined survey (stars), which yielded a total of 552 usable objects. The error bars are for the combined survey. Peebles' M.L.E. method now gives values for α and M^* of -1.16 ± 0.03 and -19.99 ± 0.06 respectively, which is the curve used in the figure.

Fig. 5.4 shows a best-fit model to the combined data obtained by assuming a mixed population model (solid line — in effect, this is equivalent to a non-Schechter function). The two populations used were 90% with $\alpha = -1.0$ (short dashed line) and 10% with $\alpha = -2.0$ (medium dashed line), both with $M^* = -20.0$. The long dashed line is the best fit M.L.E. curve described above ($\alpha = -1.16$ and $M^* = -19.99$). The presence of a high α tail has been noted in a number of surveys and, although its statistical significance has been questioned because of the small volume and hence low numbers of galaxies present, it does seem to be a genuine feature of the surveys, which suggests that the luminosity function may not be a pure Schechter function over the range of fainter absolute magnitudes. Similar curves have been noted for other series of observations such as KOS and KOSS and this type of curve is subjectively similar in shape to the composite curve function derived by Shanks (1990) for galaxy types by colour (Fig. 2.3). He noted that the reddest galaxies ($B - V > 0.85$) seem to show a turnover in their luminosity function (with $\alpha = -0.7$) whereas the bluest galaxies ($B - V < 0.6$) seem to rise steeply toward fainter magnitudes ($\alpha = -1.5$). Galaxies of intermediate colour ($0.6 < B - V < 0.85$) also have an intermediate slope.

Figure 5.1. The DURSAAO survey binned in absolute magnitude. The best–fit Schechter curve is overlaid.
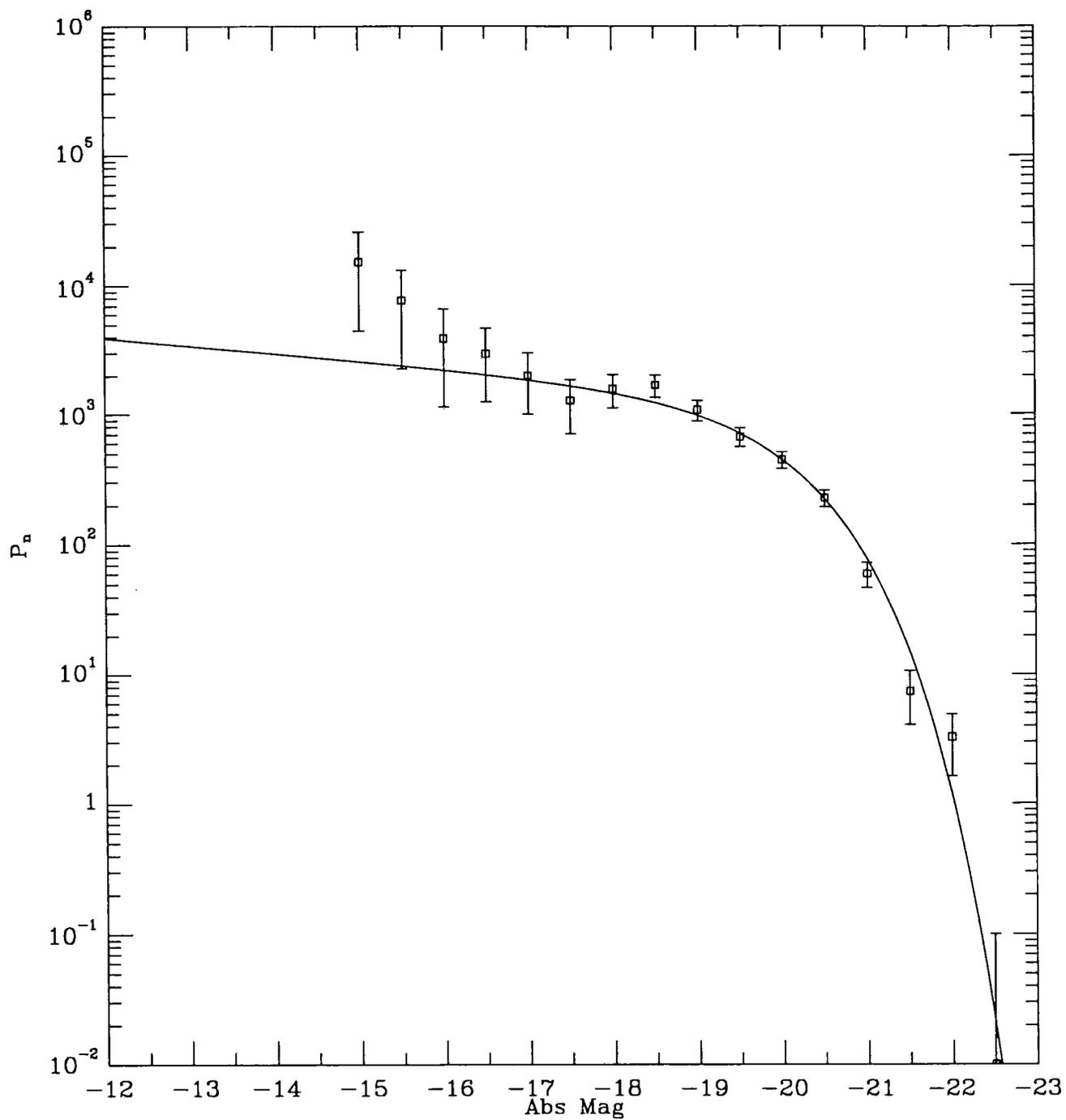
Best fit Schechter curve ($\alpha = -1.15$, $M^* = -19.93$, $H_0 = 100$)

$mag_{lim} = 16.88$ DURSAAO survey

(246 galaxies, V/Vmax method)

Fig. 5.1

Figure 5.2. As Fig. 5.1 for the DARS survey data.
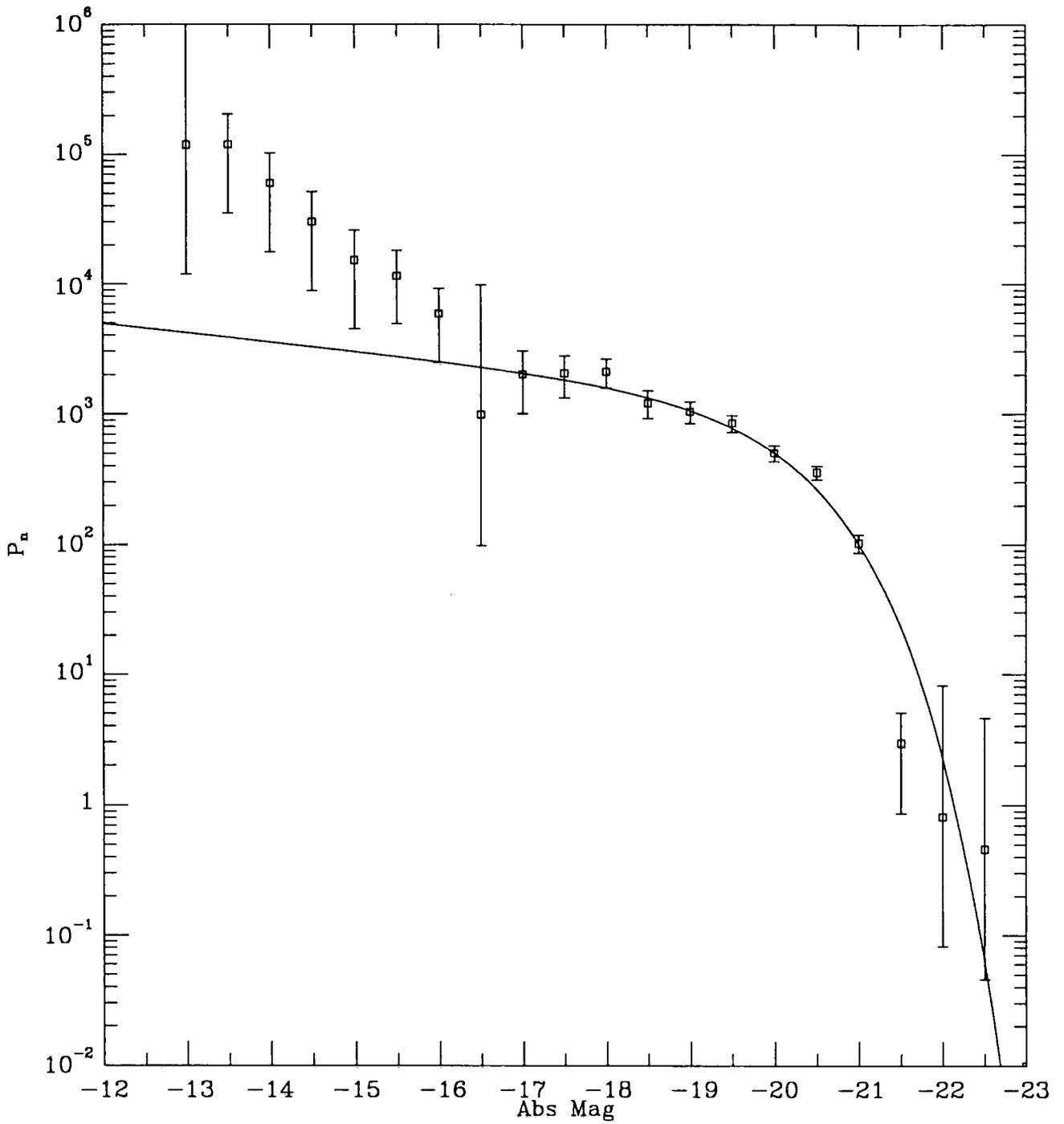
Best fit Schechter curve ($\alpha = -1.18$, $M^{*} = -20.05$, $H_0 = 100$)

$mag_{lim} = 16.88$ DARS survey

(306 galaxies, V/Vmax method)

Fig. 5.2

Figure 5.3. Combined survey data for DARS and DURSAAO, with the best–fit Schechter curve overlain.
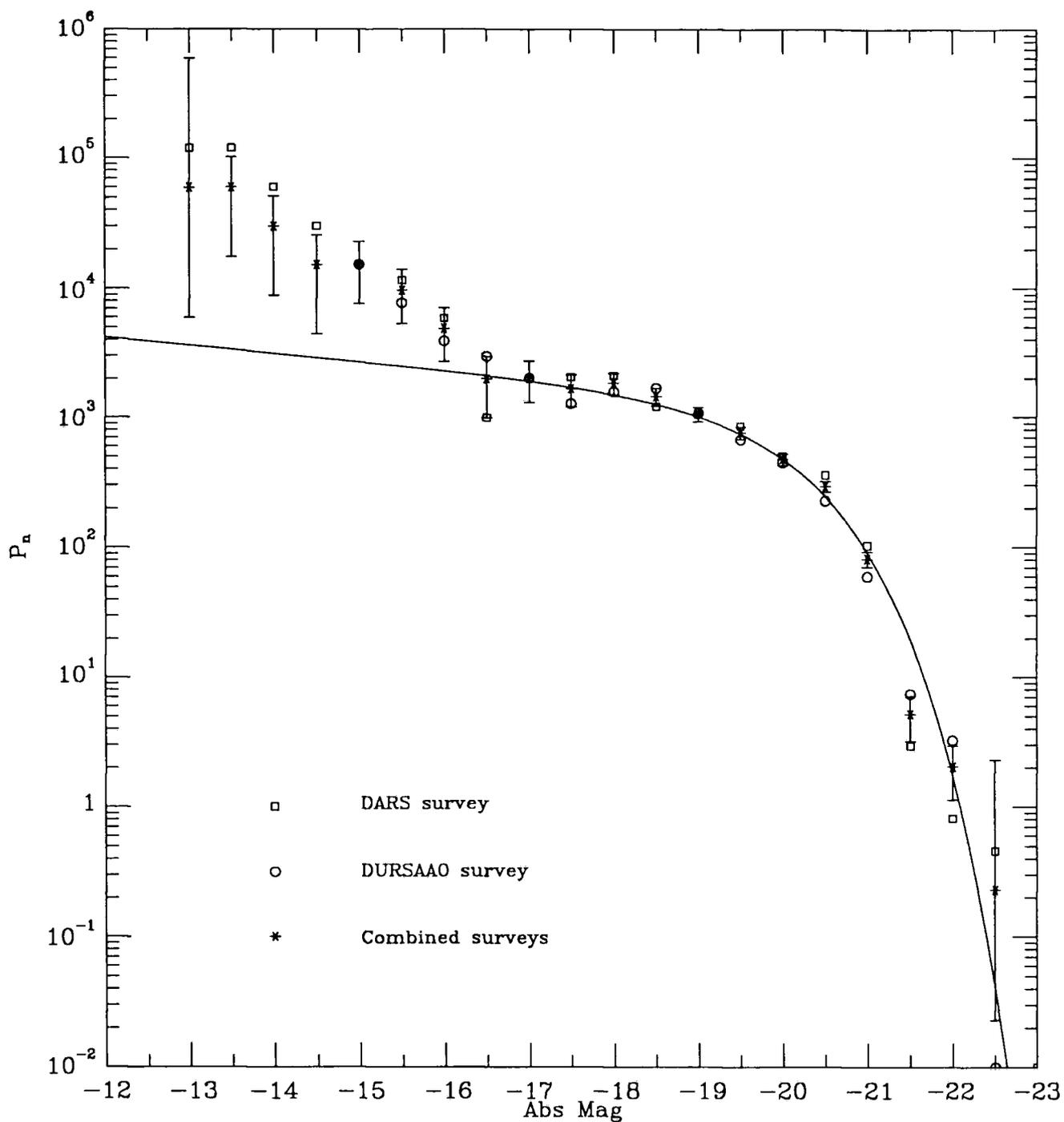
Best fit Schechter curve ($\alpha = -1.16$, $M^* = -19.99$, $H_0 = 100$)

$mag_{lim} = 16.88$ DARS + DURSAAO survey

(552 galaxies, V/Vmax method)

Fig. 5.3

Figure 5.4. The combined data of Fig. 5.3, with a mixed population model compared to the best–fit Schechter curve obtained by the Sandage–Tammann–Yahil method.
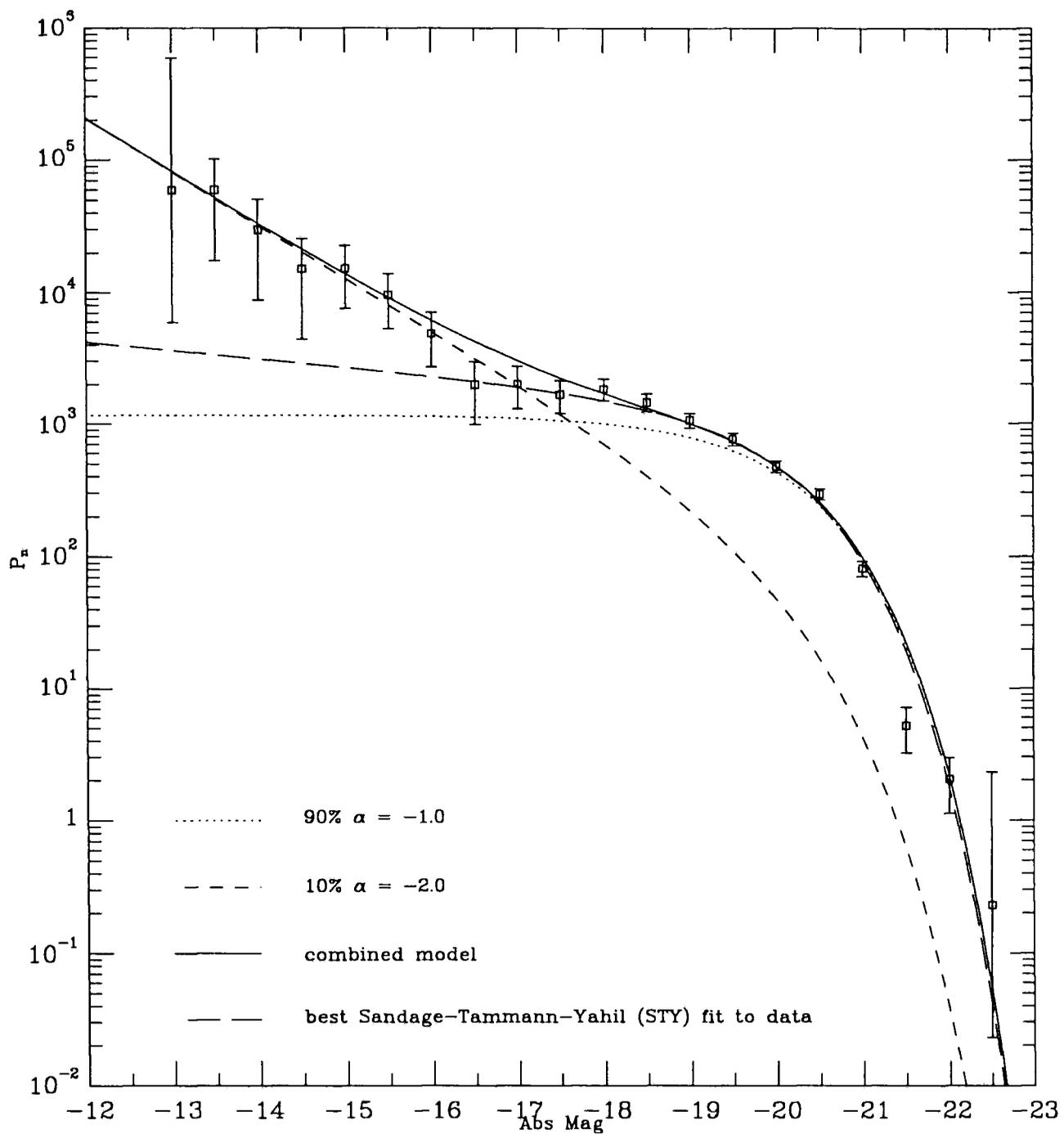
Best fit Schechter curves, mixed population models

$mag_{lim} = 16.88$ DARS + DURSAAO survey

(552 galaxies, V/Vmax method)

Fig. 5.4

5.2 Derived luminosity function for the B.E.S. survey

Similar methods were applied to the B.E.S. redshift survey, again using the M.L.E. method of Sandage to derive best fit values assuming the luminosity function to be Schechter. This is a magnitude slice survey, with derived magnitude limits of 20.0— 21.5 containing 179 usable galaxies which yielded values of $M^* = -19.5 \pm 0.06$ and $\alpha = -1.1 \pm 0.04$. The survey is plotted in $1/V_{max}$ form in Fig. 5.5, with the best fit Schechter curve overlaid. The overall fit is quite good; it may be noted that in this survey there is no evidence for a high faint–end tail, but they have virtually no galaxies with $M_B < -16.0$.

5.3 n–z curves for DURSAAO and DARS surveys

One $n - z$ curve for the combined series (Shanks *et al.* , unpublished), and calibrated in Mpc, is shown in Fig. 5.6 with two theoretical curves. Fig. 5.7 shows the combined plots for the 802 galaxies of the DURSAAO and DARS surveys with a theoretical curve (solid) assuming a calculated magnitude limit to the survey of $16^m.81$ with Sandage best–fit parameters of $M^* = -19.9$ and $\alpha = -1.01$. It may be seen that the overall fit of the model is remarkably good, especially over the range $z = 0.06 - 0.12$; there is, however, considerable variation between bins, especially in the nearer volumes which show a variation of over 200% in some adjacent bins. For completeness, a mixed population model is also shown (dashed line). This has been normalised to the total counts, but it may be seen that, if normalised over the brighter region of the curve (high z), then such a curve would show a substantial local void.

5.4 Experimental constraints on model parameters

It is usually held that the number/magnitude plots will harbour some intrinsic statistical variation at the bright end because of clustering and the low numbers involved; generally this effect will diminish as one moves to increasingly fainter magnitudes where the numbers increase substantially. As described in the introduction, this has frequently led to the arbitrary normalisation of the curves in the range $18^m - 22^m$; for the $n - z$ plots, this suggests that more accurate normalisation might be achieved by taking the bright end of the plots as correct (*i.e.* that region where the absolute brightness approximates M^*, which is at higher z on the curves) rather than, as was done with the theoretical curve-fitting of Figs. 5.7, normalising to the area under the curve or total

Figure 5.5. The Broadhurst *et al.* survey data, and best–fit Schechter curve.
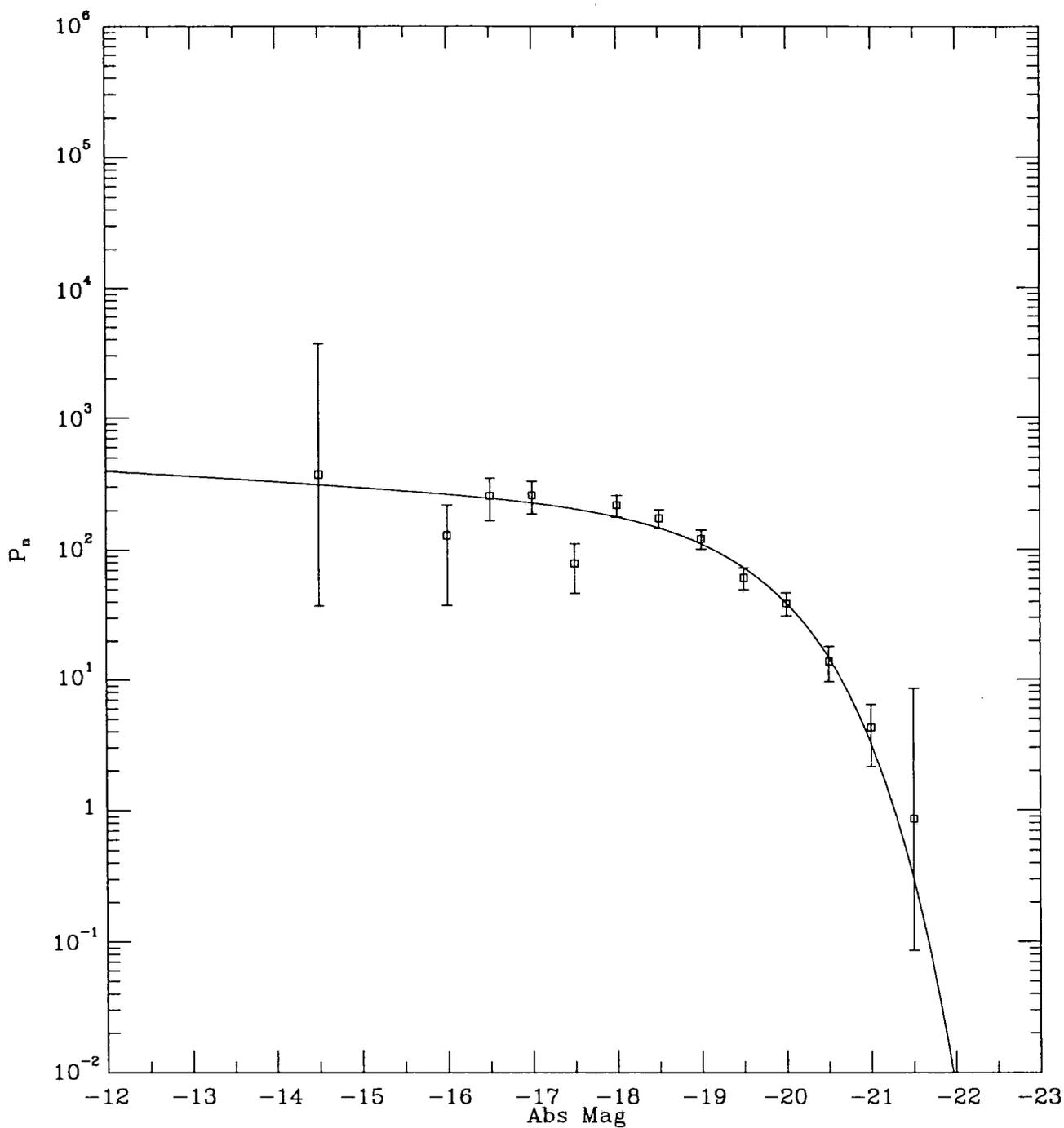
Best fit Schechter curve ($\alpha = -1.1$, $M^* = -19.5$, $H_0 = 100$)

$mag_{lims} = 20.0 - 21.5$ BROADHURST *et al* survey

(179 galaxies, V/Vmax method)

Fig. 5.5

Figure 5.6. $n - z$ plot for combined DARS and DURSAAO, (Shanks)
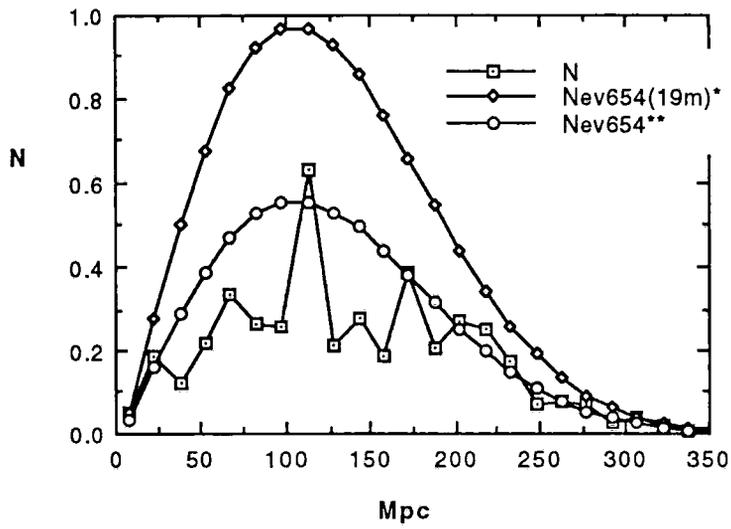
Fig. 5.6

Figure 5.7. As Fig. 5.6, with STY best–fit magnitude limited curve and a mixed population model curve.
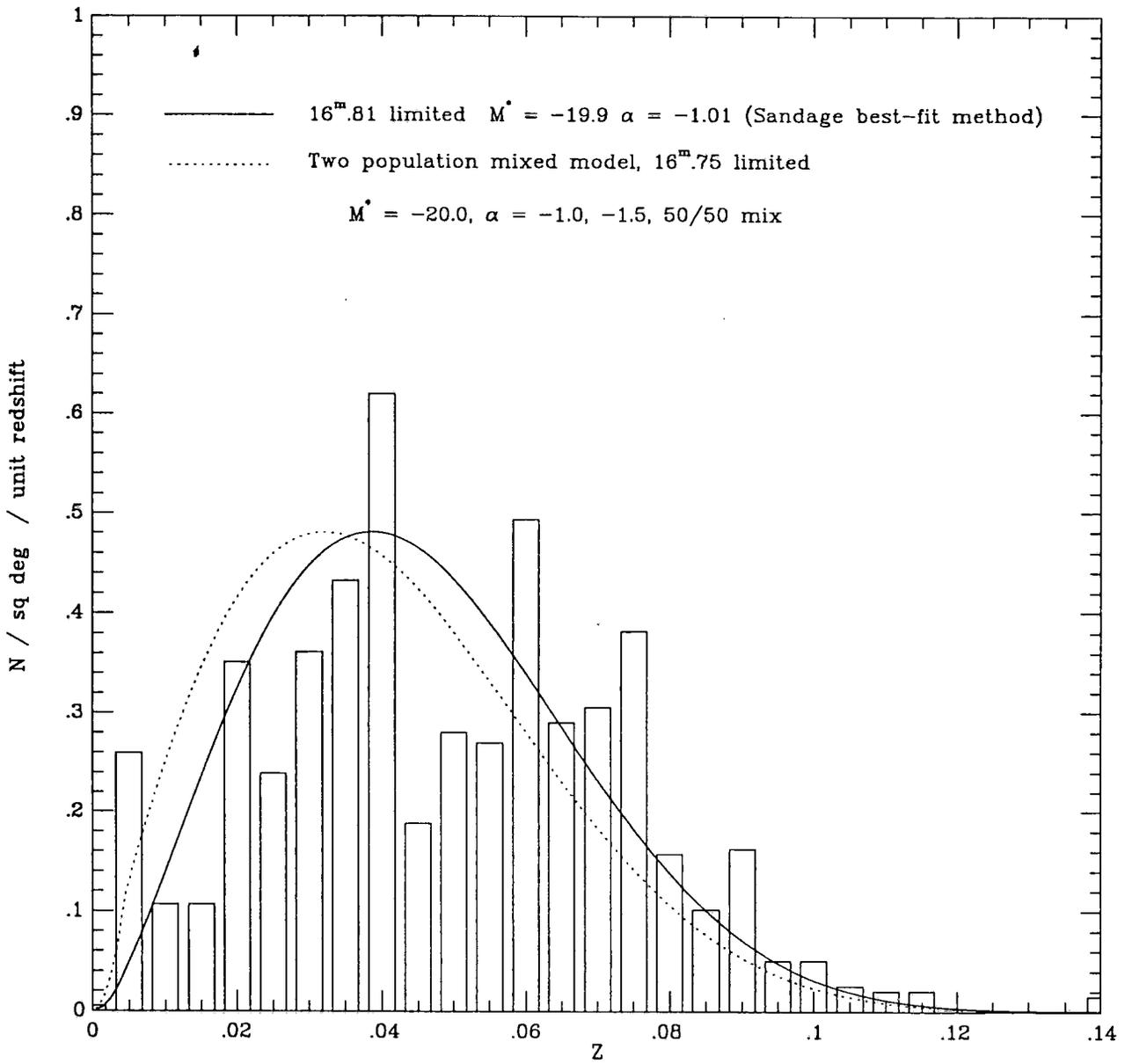
Number / Redshift plot (14 fields, 802 galaxies) — DARS+DURSAAO surveys

Fig. 5.7

counts. The independent parameters varied for this study were: (a) the magnitude limit, from $16^m.7 - 16^m.9$, (b) the K-correction, from $K = 0$ to $K = 4z$, (c) M^* and (d) α. Two such curves are shown in Fig. 5.8, for $M^* = -19.6$ to -20.0 and Fig. 5.9, for $\alpha = -1.0$ to -1.8. Varying the curves within the predicted errors of the derived parameters about such a normalisation has a profound effect; when the overall errors in M^*, α and M_{lim} are combined algebraically there is evident room for a void to be masked in the intrinsically faint low- z region.

5.5 n–z curves for the BES survey

Fig. 5.10 is the observed $n - z$ plot for the BES survey; the presence of two dense clusters may be seen clearly in what is otherwise a smooth curve. Two theoretical curves are also shown: (1) for $M^* = -20.0$, $\alpha = -1.0$ (dashed line) and (2) for the 5-galaxy type model of Shanks, as previously described, normalised to equal areas under the curve. At these depths the cosmological curvature is becoming significant, and the curve is shown assuming an open universe with $q_0 = 0.2$. Similarly, K-corrections are of greater importance varying as they do as a function of z, and the standard correction $K = 3z$ used in model (1) may be too simplistic. Indeed, it may be seen that such a naive model is unable to explain the bright–end of the histogram where clearly the more sophisticated model is more appropriate.

5.6 Conclusions

Several surveys, such as DARS, DURSAAO, KOS and KOSS, are seen to have a high-alpha tail on the V_{max} plots. Although this may be an artefact of galaxy clustering at low redshift, it is an effect which has been observed for several surveys, and is also present using Peebles' M.L.E. method. The five-galaxy model of Shanks (Metcalfe *et al.* 1991), which was plotted in Fig. 2.3, also suggests a small tail with $\alpha = -1.5$. As was concluded in §3, the values for α and M^* returned by the M.L.F. method of Sandage will ignore this tail, and give values which are accurate to within a few percent for the majority of galaxies which have their loci about the Schechter 'knee'. The galaxies in the tail have low intrinsic luminosity and their absolute numbers are small, however, reflecting the relatively small volume of space in which they can be seen and consequently they do not greatly influence the overall shape of the $n - z$ and $N(m)-$apparent magnitude plots.

What is of significance is the shape of the $n - z$ curves, and the remarkably good fit of the curves derived from the M.L.F. method over many surveys (e.g. Fig. 5.7). In

particular, the 5–galaxy type curves of Shanks fit the observed data remarkably well (e.g. Figs. 5.6, 5.10). The normalisation on these curves is to the area beneath the counts so, if any void is present, this must extend uniformly across the surveys, which is to a depth of $z = 0.45$ for the data of Broadhurst *et al.* The implications of these findings are discussed in the final section (§6).

Figure 5.8. $n - z$ fit to DARS + DURSAAO data, using variable M^*.
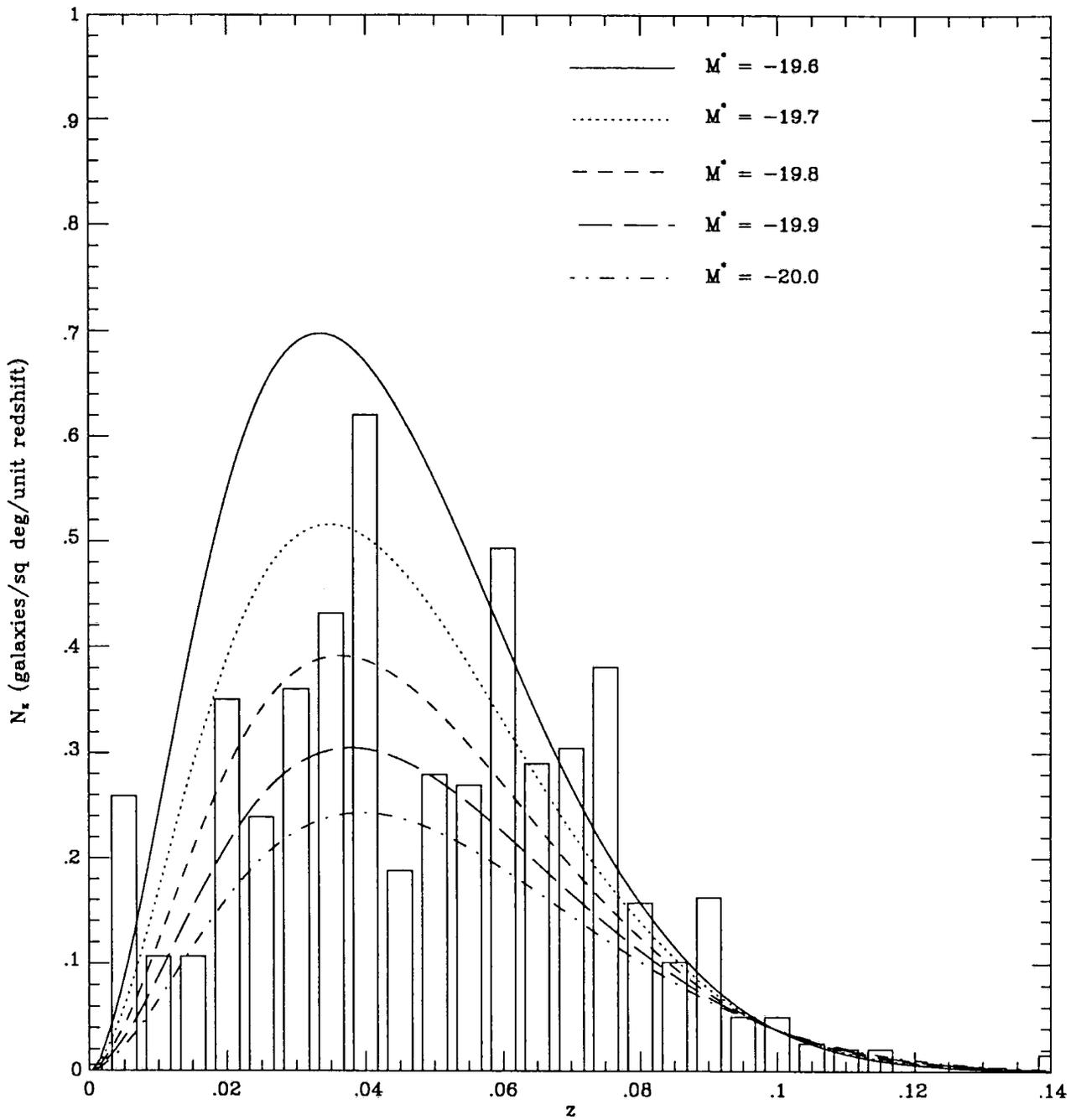
Number / Redshift models (K-corr = 3z, q_0 = 0.5, H_0 = 100)

for DARS and DURSAAO data. Mlim = 16.8 α = −1.2, variable M^*

Fig. 5.8

Figure 5.9. As Fig. 5.8 but using variable α.
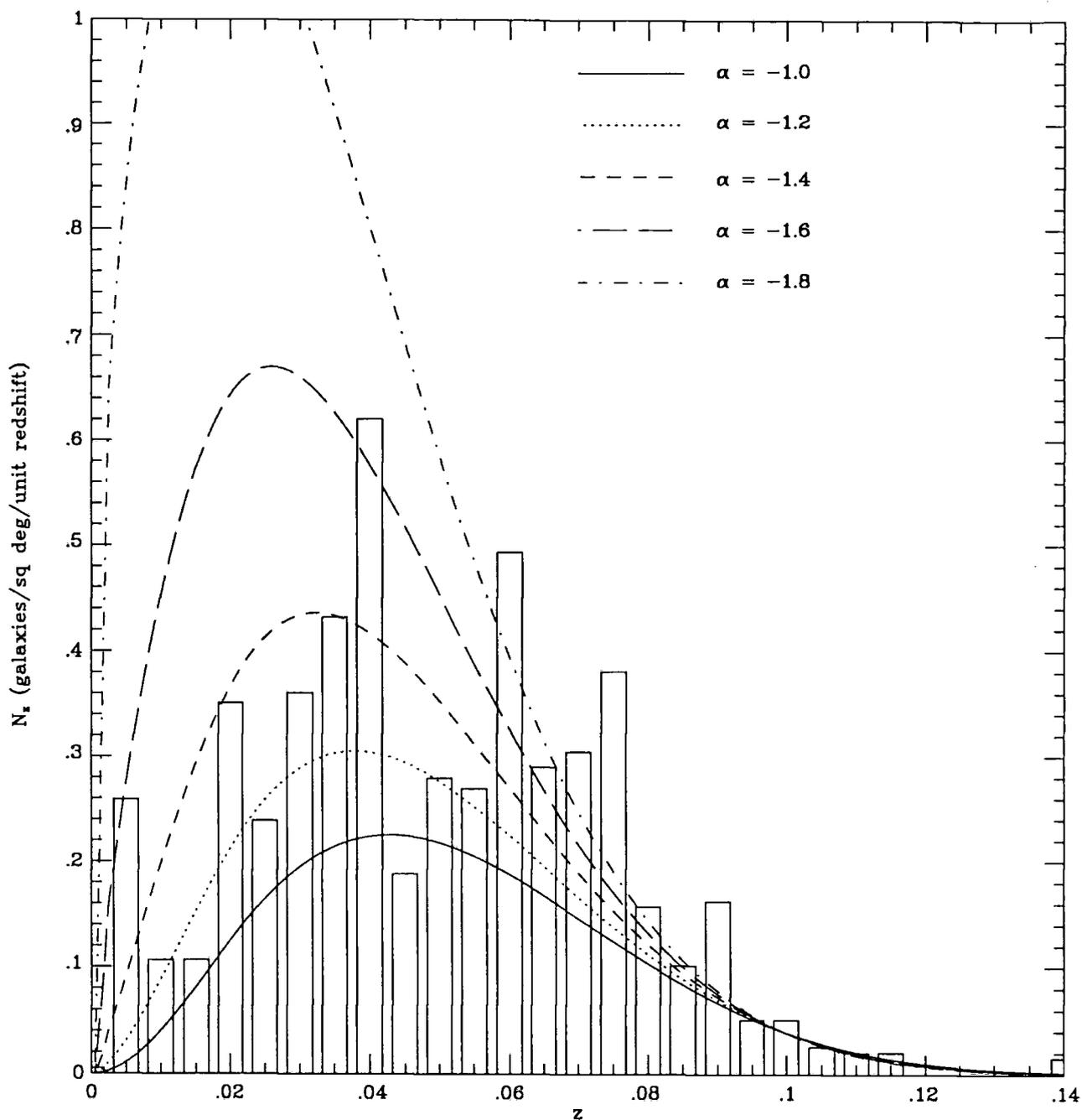
Number / Redshift models (K-corr = 3z, q_0 = 0.5, H_0 = 100)

for DARS and DURSAAO data. M^* = −19.9, Mlim = 16.8, variable α

Fig. 5.9

Figure 5.10. Fitting two $n - z$ curves to the data of Broadhurst *et al.* .
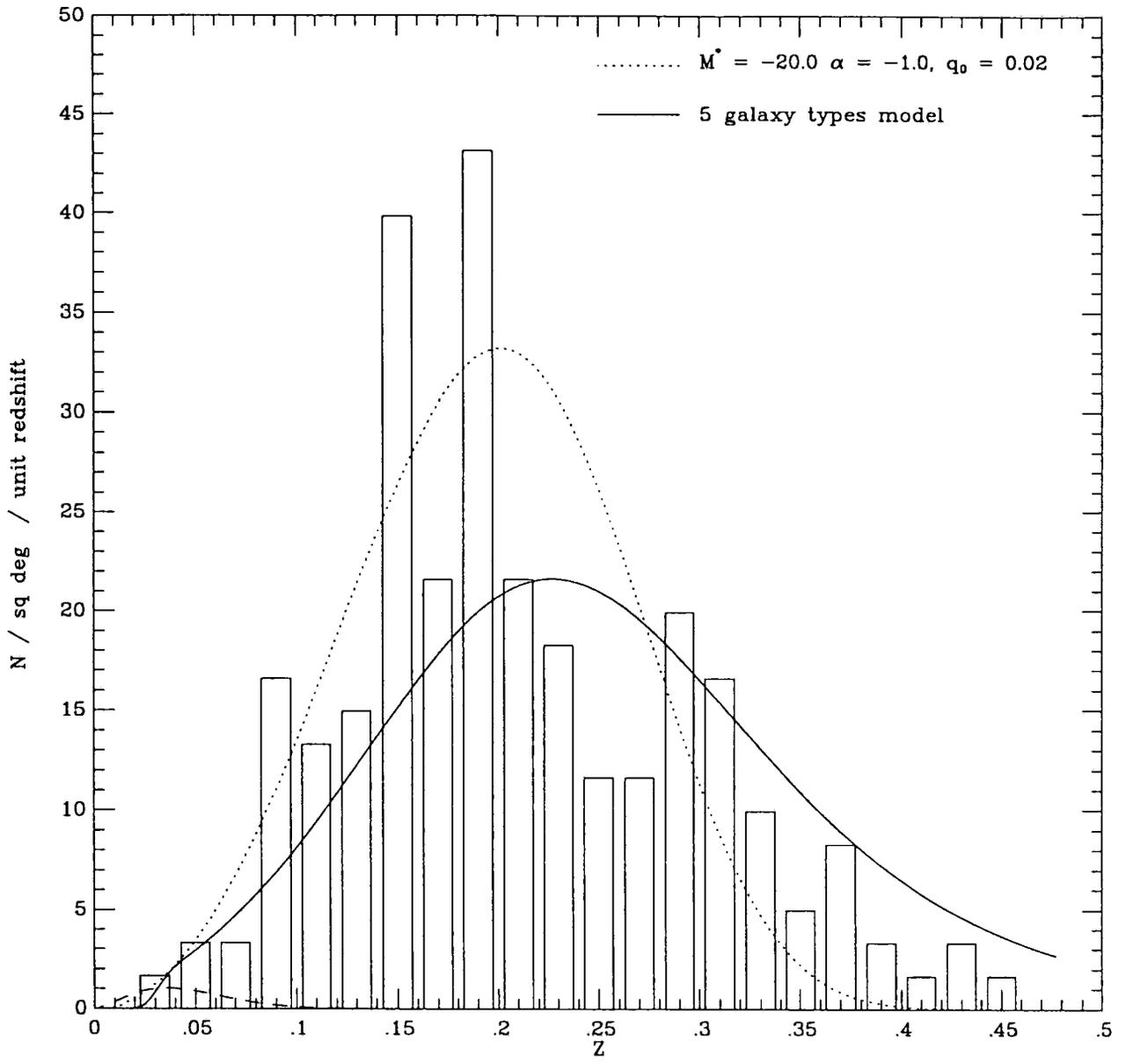
Number / Redshift plot — Broadhurst *et al* 1988 survey

No evolution model, with individual field limits, $20 < B < 21^m.5$

Fig. 5.10

6. Discussion

This thesis has attempted to address the problems found when endeavouring to reconcile the observed under–density of counts in the brighter $n(b_j)$ region ($b_j < 17^m$) with the number anticipated from standard theoretical predictions for the number counts.

The first section reviewed the historical basis for considering inhomogeneity in the universe as a possible factor to account for the variation in counts, before looking at other factors such as photometry errors and incompleteness in the surveys which might account for the problem. It next examined the theoretical basis for predicting number counts, looking at the classical Euclidean model and the standard G–R models for differing density parameters. The thesis then assessed the rationale of the Schechter model for luminosity distribution, and looked at how likely this is to represent galaxies in the actual universe. Methods of extracting the Schechter parameters were considered, and Monte Carlo simulations were performed to see how faithfully the input parameters could be reconstructed using these methods.

Some of the recent surveys were then reviewed in detail; the types of error which can creep into presented figures were enumerated, and an estimate was made of the cumulative effect of these on the number counts they produce. The new Third Reference Catalogue of Bright Galaxies (RC3) was examined and a new set of number counts for the north and south polar hemispheres was obtained, with a constraint of galactic latitude $b > |30°|$ to minimise the effect of galactic extinction. This fresh data was added to that already obtained from other sources for the bright end of the plots; comparisons were then made on the observed variations between the different catalogues, and between the northern and southern hemisphere plots in RC3.

6.1 The validity of a Schechter–type luminosity function

There seems little doubt that a Schechter type luminosity function gives an excellent first approximation to the observed galaxy distribution of luminosities. Monte Carlo simulations suggest that the methods used to extract the Schechter parameters are intrinsically sound, and return the values put into the models with a fair degree of precision which is independent of the presence of a void or local cluster, and typically better than 5%.

Some of the series (e.g. DARS, DURSAAO, KOS, KOSS) suggest that the faint tail may rise more steeply than a simple one–population Schechter model. If this is a genuine

observation rather than some statistical chance finding, then there is no doubt that the simple methods of the M.L.F. — which assumes the function *is* Schechter — will not pick this up; nevertheless this does not affect the number–magnitude curve greatly. Fig. 3.22 illustrated this effect for a wide range of αs, from $\alpha = -1.0 - -2.0$, all normalised to 19^m; the very extreme $\alpha = -2.0$ did indeed come closer to the observed data, but there is nothing in the measured observations to suggest that this is a realistic figure. The actual values of α are almost certainly much flatter ($\bar{\alpha} = -1.07 \pm 0.05$, see Appendix); and even if there is a high tail sub–population (as considered in §3), this will be only a small percentage of the total population and does not significantly affect the overall shape of the curve.

Shanks has proposed that the best approximation is to take five seminal galaxy types, each with its characteristic values of α, M^*, ϕ^* and K-corrections. On this basis he has produced an excellent approximation to the observed $n - z$ distribution for several series of observations (Fig. 5.6).

Test plots of Monte Carlo–generated galaxy populations suggest that the number–magnitude curve is remarkably robust to variations in the Schechter parameters over the bright end. Below 19^m, quite large variations in α, M^* or K-corrections produce only small changes in the slope or offset of the number–magnitude curve, and the error from this is estimated to be less than $0^m.1$, or — equivalently — to a number–count error of less than $\times 0.15$ at 15^m. The only parameter which directly affects the curves is the distribution density, ϕ^*, and varying this as a function of distance enables the deficit in the number counts (and the local excess at the bright end) to be mimicked to any required degree (Figs. 1.6,7,8).

6.2 Photometric errors

The possibility of different photometric errors being responsible for discrepancies in the number counts was considered in detail. The overall conclusion is that this source of error is unlikely to account for more than $\sim 0.2 - 0^m.3$, equivalent to a number–count error of $\times 1.32 - 1.5$. Although large in itself, this is still considerably less than the observed discrepancy of $\times 2$.

6.3 Incomplete surveys

The RC3 surveys over the range brighter than $\sim 14^m.5$ have been estimated to be better than 95% complete. Errors from incompleteness for the other major surveys is estimated to be $\sim 10\%$. This translates into a magnitude error better than $\pm 0^m.07$.

6.4 Inhomogeneities as a source of error

The observation of large inhomogeneities at all scales in nature has already been discussed (§1.1), and there is no doubt that such inhomogeneities extend at least to the scale of super–clusters. The effect of this may be seen particularly well at brighter than 12^m, where the local cluster dominates the counts, producing a significant local over–density with a factor of $\times 2.5 - 3$. Statistical averaging leads to the expectation of a corresponding void or under–density between clusters, assuming an overall uniform density distribution; but in agreement with Maddox *et al.* (1990b), it is suggested that a large void can be firmly excluded because:

(i) the distribution in the sparse-sampled redshift survey of APM galaxies to $b_j \sim 17$ (Maddox *et al.* 1990b) does reveal a weak local underdensity in the APM survey area, but this can account for a reduction of at most 10% in the number counts at $b_j \sim 17$;

(ii) the correlation function measured from the whole APM survey (Maddox *et al.* 1990a) implies that the rms variation in galaxy density in a $150h^{-1}$Mpccube is only $\sim 7\%$;

(iii) inhomogeneity estimates based on a series of 2-point correlation functions for several series by Hale–Sutton (1990) suggest that inhomogeneities are not a big factor at these depths.

(iv) simple calculations for the expectation value of this under–density suggest that it can only be a significant factor to a depth of $\sim 50h^{-1}$Mpc, which is too shallow for the required depth of $\sim 300h^{-1}$Mpc.

Maddox *et al.* (1990b) conclude that their survey constitutes a fair sample of the Universe, and they suggest that in the most conservative interpretation of the data, the bright counts are low by 10% due to a local underdensity, and by a further 10% due to non-linearities in the photometric calibration.

6.5 Overall errors

The cumulative errors over the range $12^m.0 - 17^m.0$ from all sources may be summarised as:

1) Errors in luminosity function: < 0.1

2) Errors in photometry: $0.2 - 0.3$

3) Errors from incompleteness: < 0.07

4) Errors from local voids: reducing from $<\sim 0.5$ for magnitudes $< 13^m.5$ to $<\sim 0.1$ for magnitudes in the range $13.5 - 17.0$

These suggest that total errors over this magnitude range might combine to a maximum magnitude error of $\pm 0^m.57$ down to 17^m. This is equivalent to an error in the number counts of a factor of $\times 1.9 - 2.2$, which would be just sufficient to account for the observed discrepancy.

This is an uncomfortable result for several reasons. First, it depends on the arithmetic sum of all the errors being of the same sign, *i.e.* none of the errors cancel each other; in reality they should be combined in quadrature. Second, every source of error must contribute the maximum in its range. Third, there is no margin for improvement of errors: the range quoted must reflect an absolute underlying error rather than mere caution on the part of an observer, otherwise subsequent improvements in errors will worsen the misalignment. Fourth, the same 'cumulative maximum–error bias' must extend over much of the range of interest. Fifth, the errors show remarkable homogeneity: *i.e.* they do not show much degree of spread about the Euclidean line that can be drawn through the data.

Overall, the data does seem to suggest that, brighter than $\sim 14^m$, inhomogeneities are becoming apparent which dominate the curve brighter than $12^m.5$. Fainter than 14^m, the curve is reasonably tight with little spread up to $\sim 18^m.5$, after which data begins to show more divergence and inconsistency.

6.6 The influence of evolution

If the data is accepted as accurate over the range $14.0 - 18^m.5$, then the implication is that the theoretical curve ought to be normalised over this range rather than at the fainter end. This does allow a good fit to the data over the bright range, but would need considerable modification to fit at the fainter end.

The standard models, even with normalisation to 19^m and individual K-corrections according to galaxy type, still require considerable modification to account for the huge increase in counts at fainter magnitudes, and this correction is particularly severe if the canonical $\Omega_0 = 1$ parameter is applied. One such correction based on Bruzual (1983)-type luminosity evolution was shown in Fig. 1.4; this is a considerable improvement to the no-evolution models, but with an $\Omega_0 = 1$ model it also under-predicts the number counts at faint magnitudes. Furthermore, the redshift surveys of Broadhurst, Ellis and

Shanks (1988) and Colless *et al.* (1990) show that the redshift distribution, $n(z)$, to $b_j = 22.5$ is very similar to the no-evolution prediction, despite the excess in the counts compared to no-evolution models, and BES showed that this is inconsistent with such simple luminosity-evolution models which match the number counts, since these models predict a substantial high-redshift tail in $n(z)$ to $z > 0.5$ which is not observed. They suggest that the overall evolution of the galaxy luminosity function must look much more like pure density evolution than pure luminosity evolution.

Another model, applying a $(1 + z)^3$ correction for merging, was shown in Fig. 1.5. This later model fits the faint counts well with $\Omega_0 = 1$ and in addition, when normalised to 19^m, it does predict fewer galaxies at the bright end than do the standard curves, which suggests that there has been galaxy evolution at low redshift. This last feature is consistent with:

(i) evidence for galaxy evolution at low redshift from the IRAS Faint Source Catalogue which shows a number count excess of $\sim 100\%$ at 0.3 Jy corresponding to $z \sim 0.1$ (Lonsdale *et al.* 1990);

(ii) the rapid evolution of galaxies suggested by Maddox *et al.* (1990b) from the APM Galaxy Survey;

(iii) Lonsdale and Chokshi (1993) found evidence for density evolution for moderate luminosity galaxies at a rate of $(1 + z)^\sigma$, with a best fit of $\sigma = 4 \pm 2$ between the current epoch and $z \sim 0.1$. Using the local luminosity functions of Efstathiou, Ellis and Peterson (1988) and Loveday *et al.* (1992), they concluded that no additional luminosity evolution is required to fit the $M_b < -22(H_0 = 50)$ data;

(iv) Eales (1993), in a review of three faint galaxy redshift surveys, has also reported evidence of evolution at low redshifts, though he suggests that only starburst models are consistent with the observations.

These results suggest that, if a factor of $(1 + z)^3$ does have to be applied and there has been little recent luminosity evolution, then most of the evolution is in the form of continual merging down to the present epoch.

6.7 Conclusions

General observations of clustering hierarchies in the Universe lead to the expectation that we live in a region of space with a local excess of galaxies (the Virgo cluster), and with voids extending beyond the local region. Such strong inhomogeneities are confirmed by comparing surveys in the Northern and Southern hemispheres from the Third Reference Catalogue of Bright Galaxies (de Vaucouleurs 1991), which show an excess of counts in the Northern surveys ranging from $\times 2.29$ at $10^m.75$ to $\times 1.34$ at $13^m.75$. However, large voids in the range $14 < b_j < 18$ can generally be excluded, and are probably $< 10\%$ by $b_j = 17$ (e.g. Maddox et $al.$ 1990b). The inclusion of a theoretical local void (say $\times 0.7\phi_0$ out to $150 h^{-1}$Mpc) can account for some of the bright number count deficit. Moreover, such voids will be missed when values for the Schechter parameters are calculated using the L.F.E. method; if, however, such voids are genuinely present, they are too small to show up in the $n - z$ curves out to $z = 0.45$.

The combination of small cumulative errors in photometry, luminosity function parameters, incompleteness, and inhomogeneities is insufficient to account for the observed deficit in bright counts when the standard theoretical curves are normalised in the range $18 - 22^m$. In conjunction with the strong correlation of the bright counts to the Euclidean $10^{0.6m}$ slope over the magnitude range $14 - 18^m$, this suggests that the bright galaxy number counts are substantially correct, and normalisation to the fainter magnitudes (e.g. 19^m) may be wrong. This implies that the models used may need additional corrections from evolution at low redshifts (e.g. Maddox et $al.$, 1990b) to lift their predicted count values brighter than $\sim 17^m$. One simple evolutionary model based on the density merging parameters of Lonsdale and Chokshi (1993), and ignoring luminosity evolution, was shown in Fig. 1.5. This assumes that the number density is proportional to distance ($i.e.$ a linear proportionality between probability of merging and time), which implies a correction factor of $(1 + z)^3$. Such a correction is consistent with Lonsdale and Chokshi's density evolution parameter $(1 + z)^\sigma$, with $\sigma = 4 \pm 2$; it can be normalised closer to the bright galaxies, coming within the overall errors of observation and inhomogeneity; it shows a steep rise in counts beyond 21^m, consistent with the observations; and it allows the canonical value of $q_0 = 0.5$ to be applied, rather than some of the very low values (e.g. $q_0 = 0.02$) which are used with several other models.

The overall conclusion of this thesis suggests that the observations of counts over the magnitude range $14.0 - 18^m$ are reasonably robust and fit the theoretical Euclidean

slope well. The counts beyond $b_j = 21$ are considerably greater than the theoretical curves (especially using $q_0 = 0.5$) and it will require substantial modification to the theoretical curve, either through luminosity evolution models or through merging, to make these fit. When combined with suitable luminosity evolution, a simple merging model with a factor of $(1 + z)^3$ may closely fit the observed data over a wide range of magnitudes, and at the bright end it may fit the observations within the relatively small band of fluctuations allowed by observational error and local inhomogeneities.

7. Acknowledgements

8. References

Abell, G.O. (1958) *ApJ*, **31**, III 243–244

Bean, J. *'A Complete Redshift Sample of Galaxies'*, PhD Thesis, Durham University, U.K., 1983.

Bondi, H. *'Cosmology'*, Cambridge University Press, (1952).

Bonometto, S.A., Iovino, A., Guzzo, L., Giovanelli, R. and Haynes, M. (1993) *ApJ*, **419**, 2,1

Broadhurst, T.J., Ellis, R.S., Shanks, T. (1988) *MNRAS*, **235**, 827–856

Bruzual, G. (1981) *Ph.D. thesis*, Univ. of California, Berkeley.

Choloniewski, J. (1985) *MNRAS*, **214**, 2

Cochran, W.C. (1977) *'Sampling Techniques'*, Wiley & Sons, .

Colless, M., Ellis, R.S. and Taylor, K. (1989) *'The Epoch of Galaxy Formation'*, eds Frenk, C.S., Ellis, R.S., Shanks, T., Peacock, J.A. and Heavens, A., Kluwer, Dordrecht. p.359.

Colless, M., Ellis, R.S., Taylor, K. and Hook, R.N. (1990) *MNRAS*, **244**, 408 (Paper I)

Colless, M., Ellis, R.S., Taylor, K. and Shaw, G. (1991) *MNRAS*, **235**, 686-702

Colless, M., Ellis, R.S., Broadhurst, T.J., Taylor, K. and Peterson, B.A. (1992) *'Faint Blue Galaxies: High or Low Redshift?'*, **MNRAS**, Pre-print

Davis, M., Huchra, J., Latham, D.W. and Tonry, J. (1982) *ApJ*, **253**, 423-425

de Sitter, W. *Kosmos*, Harverd University Press, 1932.

de Vaucouleurs, G. (1971) *PASP*, **83**, 113

de Vaucouleurs, G. and de Vaucouleurs, G. *'Reference Catalogue of Bright Galaxies'*, University of Texas Press, 1964.

de Vaucouleurs, G. de Vaucouleurs, A., Corwin, H.G., *Second Reference Catalogue of Bright Galaxies*, University of Texas Press, 1976.

de Vaucouleurs, G. de Vaucouleurs, A., Corwin, H.G., Buta, R.J., Paturel, G. and Fouqué, P. *Third Reference Catalogue of Bright Galaxies*, Springer–Verlag, 1991.

Eales, S. (1993) *Astrophys.J.*, **404**, 51

Eddington, A.S. (1939) *Science Progress*, **34**, 225

Efstathiou, G., Ellis, R.S. and Peterson, B.A. (1988) *MNRAS*, **232**, 2

Einstein A., (1917) *S-B Preuss Akad Wiss*, **1,3,4**, 142

Einstein A., (1933) *'Structure Cosmologique de l'Espace'*, Paris: Hermann et Cie, (§2).

Ellis, R.S. (1979) *Phil. Trans. R.Soc. Lond. A.*, **296**, 355

Ellis, R.S. (1982) *'The Origin and Evolution of Galaxies'*, ed Jones and Jones, Dordecht:Reidel, 255.

Ellis, R.S., Gray, P.M., Carter, D. and Godwin, J. (1984) *MNARS*, **206**, 285

Fath E.A., (1914) *AJ*, **28**, 75

Ferguson, H.C. and Sandage, A. (1991) *AJ*, **101**, 3

Fong, R., Godwin, J.G., Green, M.R. and Shanks, T. (1983) *'Occ. Reports of ROE, Edinburgh'*, 10, p. 61.

Fong, R., Godwin, J.G. and Metcalfe, N. (1984) *'Occ. Reports of ROE, Edinburgh'*, 14, p. 207.

Gardner, J.P., Cowie, L.L and Wainscoat, R.J. (1993) *'Galaxy Number Counts from K=10 to K=23'*, **Preprint**,

Garilli, B., Maccagni, D. and Vettolani, G. (1991) *AJ*, **101**, 3

Hale-Sutton D., *'Galaxy Clustering and Dynamics from Redshift Surveys'*, PhD Thesis, Durham University, UK, 1990.

Heydon-Dumbleton, N.H., Collins, C.A. and MacGillivray, H.T. (1989) *MNRAS*, **238**, 379–406

Hubble E., (1926) *ApJ*, **64**, 321

Hubble E., (1931) *Proc NAS*, **15**, 168

Hubble E., (1934) *ApJ*, **79**, 8

Hubble E., (1936) *ApJ*, **84**, 517

Huchra, J.P. (1985) *'The Virgo cluster redshift survey'*, Editor(s): Richter, O.G., Binggeli, B, ESO Workshop on the Virgo Cluster of Galaxies, Proceedings p.181-200.

Hudson, M.J., and Lynden-Bell, D. (1991) *MNRAS*, **252**, 219-228

Jarvis, J.F. and Tyson, J.A. (1981) *AJ*, **86**, 476

Kiang, T. and Saslaw, W.C. (1969) *MN*, **143**, 129

King, C.R. and Ellis, R.S. (1985) *ApJ*, **288**, 456

Kirshner, R.P., Oemler, A., Schechter, P.L., (1979) *AJ*, **84**, 7

Kirshner, R.P., Oemler, A., Schechter, P.L., Shechtman, S.A., (1983) *AJ*, **88**, 9

Koo, D.C. (1988) *'The Epoch of Galaxy Formation'*, eds Frenk, C.S., Ellis, R.S., Shanks, T., Peacock, J.A. and Heavens, A., Kluwer, Dordrecht p.71.

Koo, D.C. and Kron, R. (1988) *'Towards Understanding Galaxies at High Redshift'*, eds Kron, R. and Renzini, A, Kluwer, Dordrecht p.209.

de Lapparent, V., Geller, M.J. and Huchra, J.P. (1989) *ApJ*, **343**, 1,1

Lauberts, A *'The ESO-Uppsala Survey of the ESO(B) Atlas*, European Southern Observatory, 1982.

Lebofsky, M.J. (1981) *ApJ*, **303**, L59

Ledermann, W. (1984) *'Handbook of Applicable Mathematics'*, Pt A (Statistics) Vol VI, John Wiley & Sons.

Lilly, S.J., Cowie, L.L and Gardner, J.P. (1991) *ApJ*, **369**, 79

Lonsdale, C.J., Hacking, P.B., Conrow, T.P. and Rowan-Robinson, M. (1990) *Astrophys.J.*, **358**, 60

Lonsdale, C.J. and Chokshi, A. (1993) *AJ*, **105**, 4

Loveday, J., Peterson, B.A., Efstathiou, G. and Maddox, S.J. (1992) *ApJ*, **390**, 338

Maddox, S.J., Efstathiou, G., Sutherland, W.J., and Loveday, J. (1990a) *MNRAS*, **242**, 43p

Maddox, S.J., Sutherland, W.J., Efstathiou, G., Loveday, J. and Peterson, B.A. (1990b) *MNRAS*, **247**, 1-5

Metcalfe, N., Fong, R., Jones, L.R. and Shanks, T. (1987) *'High Redshift and Primeval Galaxies'*, eds Bergeron, J. *et al.* , Editions Frontières, Gif sur Yvette, France p.37.

Metcalfe, N., Fong, R., Shanks, T. and Kilkenny, D. (1989) *MNRAS*, **236**, 207

Metcalfe, N., Shanks, T., Fong, R. and Jones, L.R. (1991) *MNRAS*, **249**, 498-522

Metcalfe, N., Shanks, T., Roche, N. and Fong, R. (1992) *Conference Proceedings, in press*, ,

Oegerle, W.R., Hoessel, J.G. and Ernst, R.M. (1986) *AJ*, **91**, 4

Oegerle, W.R. and Hoessel, J.G., Jewison, M.S. (1987) *AJ*, **93**, 3

Oemler, A. (1974) *ApJ*, **194**, 1–19

Peebles P.J.E., *'The Large–Scale Structure of the Universe'*, Princeton University Press, 1980.

Peterson, B.A., (1970) *AJ*, **75**, 695

Peterson, B.A., Ellis, R.S., Efstathiou, G., Shanks, T., Bean, A.J., Fong, R. and Zen-Long, Z. (1986) *MNRAS*, **221**, 233–255

Phillipps, S., Fong, R., Ellis, R.S., Fall, S.M. and MacGillivray, H.T. (1978) *MNRAS*, **182**, 673–685

Phillipps, S., Shanks, T. (1987) *MNRAS*, **227**, 1

Phillipps, S. (1992) *'Large Scale Inhomogeneities and Number Counts'*, , In press

Picard A. (1991) *AJ*, **102**, 445

Ramella, M., Geller, M.J. and Huchra, J.P. (1989) *ApJ*, **344**, 1

Reshetnikov, V.P. (1986) *Astrofizika*, **24**, 1 (Translated in: Astrophys **24**,1 1986)

Robertson, H.P. (1935) *ApJ*, **82**, 284

Sandage, A. and Tammann, G.A. (1981) *'A Revised Shapley-Ames Catalog of Bright Galaxies'*, Carnegie Institution, Washington.

Sandage, A., Tammann, G.A. and Yahil, A., (1979) *ApJ*, **232**, 352

Schaeffer, R. (1987) *Astronomy and Astrophysics*, **180**, L5–8

Schechter, P. (1976) *ApJ*, **203**, 297–306

Sears F.H., (1925) *ApJ*, **62**, 168

Shanks, T. (1990) *'Galaxy count models and the extragalactic background light'*, 'The Galactic and Extragalactic Background Radiation', ed Bowyer and Leinert.

Shanks, T., Fong, R., Ellis, R.S. and MacGillivray, H.T. (1980) *MNRAS*, **192**, 209

Shanks, T., Metcalfe, N., Hale-Sutton, D. and Fong, R. (1989) , ,

Shanks, T., Stevenson, P.R.F., Fong, R. and MacGillivray, H.T., (1984) *MNRAS*, **206**, 767

Shapley H., (1938) *Proc NAS*, **24**, 287

Shapley H., Ames A., (1932) *Harvard Annals*, **88**, II

Stevenson, P.R.F. *'Faint Galaxy Photometry and Cosmology'*, PhD Thesis, Durham University, U.K., 1985.

Stobie, R.S. *'Application of moments to the analysis of panoramic astronomical photographs'*, Applications of Digital Image Processing to Astronomy, NASA, 1980.

Tinsley, B.M. (1977) *Ap J.*, **211**, 621; **216**, 349

Thompson, L.A. and Gregory, S.A. (1980) *ApJ*, **242**, 1

Tolman, R.C. (1949) *R.M.P.*, **21**, 374

Tyson, J.A. (1988) *AJ*, **96**, 1

Tyson, J.A., Seitzer, P. (1988) *ApJ*, ,

Turner, E.L. and Gott, J.R., (1976) *ApJ*, **209**, 1

Tully, R.B. (1988) *AJ*, **96**, 1

Watson, J.M. and Rowan-Robinson, M (1993) *MNRAS*, **265**, 4

Weinberg, S. (1972) *'Gravitation and Cosmology'*, Wiley, New York.

White, S.D.M. (1990) *'Physics of the Early Universe'*, ed. Peacock, J.A., Heavens, A.F., Davies, A.T., SUSSP Publications.

Yoshii, Y. and Takahara, F (1988) *ApJ*, **326**, 1–18

9. Appendix. A Summery of Values for α and M^* from the major surveys

The Durham/Anglo–Australian Telescope faint galaxy redshift survey (Broadhurst, Ellis and Shanks 1988)

This looked at over 200 field galaxies, with apparent magnitude slices in the range $20.0 < b_j < 21.5$ mag in five fields. Uses $H_0 = 50$. Suggests star-forming galaxies which produce count excess, at $b_j \sim 21 - 22$ mag. No–evolution parameters.

Table A1. The AAT results.

Galaxy type	$M_{b_j}^*$ $(H_0 = 100)$
E/S0	-20.09
Sab-Sbc	-19.64
Sc-IM	-19.34

B-K Limits	$M_{b_j}^*$ $(H_0 = 100)$
> 3.65	-19.88
2.9–3.65	-19.73
< 2.9	-19.01

The M_{50}^* of their results are here converted to M_{100}^* using $M_{100} = M_{50} + 5\log 2 = M_{50} + 1.505$. They also found the faint end slope $\alpha = -1.25$, using the technique of Ellis *et al.* (1984) to parametrise the distributions in terms of an expected Schechter function.

Table A2. Y & T summary of results.

alpha	M_{bj}^{*}	ϕ^{*} (gal Mpc^{-3})	n_0 (gal Mpc^{-3})	References
-1.11	-21.1	$1.4E-3$	$5.4E-3$	E
-1.11	-21.1	$2.3E-3$	$8.9E-3$	KOS (adopted)
-1.25	-21.28	$2.2E-3$	$1.1E-2$	F
-1.25	-21.1	$5.0E-3$	$2.6E-2$	S

Refs: E= Ellis 1983, KOS=1979, F=Felton 1977, S=Schechter, 1976

They normalise to 0.5 gals deg^{-2} in 0.5 magnitude intervals centred on $B_J = 15$ mag. Using $H_0 = 50$, they obtain

$$\phi_{50}^{*} = 2.3 \times 10^{-3} \, \mathrm{Mpc}^{-3}$$

Table A3. Relative proportion of Galaxy Types

E/S0	Sab	Sbc	Scd	Sdm	References
0.215	0.185	0.160	0.275	0.165	P
0.321	0.281	0.291	0.045	0.061	T (adopted)
0.28	0.47		0.25		E

P=Pence(1976) - Bright Galaxy Catalogue, de Vaucouleurs 1963,

T=Tinsley(1980) - KOS 1978,

E=Ellis - DARS 1983

The KOS survey

Their sample contained approximately 155 galaxies in eight fields from de Vaucouleurs Second Reference Catalogue (1976) (RC2), 5 without z, and was almost complete to a magnitude limit of $M_{J_{KOS}} = 14.9$. The J_{KOS} photometric system differs considerably from that used in the AAT survey, and also one field was in error. Efstathiou *et al.* (1988) correct for these errors, and apply the k—corrections shown in Table 2.1.

Table A4. The KOS results

Type	J^*_{KOS}	α
ALL	-20.23	-1.64
E-S0	-20.01	-1.04
S	-19.87	-1.72
ALL (F^*_{KOS})	-21.48	-2.08

They assume $H_0 = 50$, with best fits of:

$$\alpha = -1.36 \pm 0.29,$$

$$M^*_J = -21.35 \pm 0.20$$

Assuming $\langle B - V \rangle = 0.7$ for their galaxies, they convert to the B_T photometric system of de Vaucouleurs with:

$$M^*_{B_T} = -21.00 \pm 0.25$$

They also calculate a luminosity function for the completeness limit of RC2:

$$\alpha = -1.02 \pm 0.18,$$

$$M^*_{B_T} = -20.99 \pm 0.13$$

These results are within $1\,\sigma$, and combining the results:

$$\alpha = -1.10 \pm 0.15,$$

$$M^*_{B_T} = -21.00 \pm 0.11$$

$$\text{or} \quad M^*_J = -21.35 \pm 0.11$$

KOSS (1983)

KOSS extended the original KOS survey to a limit of $F_{KOS} \approx 16$ in six fields containing ~ 280 galaxies.

They used six fields, each 2 sq deg; photoelectrically calibrated photographic magnitudes; and $J - F$ colours for 512 galaxies brighter than completeness limits of $F = 16.5$ to $F = 17.2$. Redshifts were determined for 280 of the brighter galaxies, with the results:

They obtained:

$$\alpha_J = -1.25$$

$$M_J^* = -21.70, \qquad M_F^* = -22.70.$$

$$\phi^* = 1.50 \times 10^{-3} \, \text{Mpc}^{-3} \qquad (H_0 = 50)$$

The analysis of Efstathiou *et al.* gives the results:

Table A5. The KOSS results

Type	M^*	α
ALL (F_{KOS}^*)	-21.07	-1.04
ALL†	-21.34	-1.20
ALL (J_{KOS}^*)	-19.88	-0.92

$\dagger$ this includes 3 bright galaxies with $z > 0.117$ not used by KOSS.

The RSA catalogue

Efstathiou *et al.* (1988) also analysed the RSA sample (Sandage and Tammann 1981). This becomes progressively incomplete at $B_T > 12.5$, and is supplemented by a redshift catalogue compiled by Huchra which is limited to $B(0) = 13.2$. The two catalogues were cross-correlated to the limit $B_T \leq 12.5$, and $|b| \geq 30°$. The authors adopt a linear Virgo-infall model based on the equation of Schechter (1980) with $\gamma = 2$, and the mean recession velocity of the Virgo cluster taken to be 1019 km s^{-1}.

Phillipps and Shanks (1987)

Use correlation function to include all galaxies within a circle of fixed metric radius, $1h^{-1}$ Mpc, centred on a bright galaxy of measured redshift, from the Durham Redshift Surveys (regions GSN, GSP, GNX, GNY, GNZ, GSM, GSI) and three regions (GSA, GSD, GSF) from AAT Redshift Survey (AARS). Use $H_0 = 100$, $\mathrm{k - corr} = 3z$. This method assumes all galaxies visible within the $1h^{-1}$ Mpc circle are part of a cluster centred on the known galaxy, and at the same redshift. This gives much larger numbers of faint galaxies from which the L.F. may be calculated, assuming it is Schechter.

They take a conservative magnitude limit of $b_J = 20.5$ for the samples, and a bright end limit at $b_J = 16.0$ to the UKSTU data to avoid the small number statistics. Quote apparent magnitudes to be accurate to better than 0.2 mag rms, even at $b_J = 20.5$, and field to field uncertainty in the zero points should be less than 0.1 mag. They find the differential L.F. is essentially flat fainter than $M(b_J) = -18.5 + 5\log h$. Their best fits are:

$$\alpha = -1.0, \qquad M^*(b_J) = -19.8 \pm 0.2$$

They also determine a best value for the mean density, assuming a known excess of galaxies in a cluster from the standard correlation form $\xi(r) = (r/r_0)^{-\gamma}$ (Peebles 1980) with $\gamma = 1.8$ and $r_0 = 1h^{-1}$ Mpc:

$$\phi^* = 0.015\, h^{-3} \quad \mathrm{Mpc}^{-3}$$

Efstathiou, Ellis and Peterson (1988)

Analyses five magnitude–limited surveys. Use maximum-likelihood methods which provide unbiased estimates of the L.F. for spatially inhomogeneous distributions under the assumption that luminosity is uncorrelated with position. The methods are checked against Monte Carlo simulations, and show that the L.F.s from the AARS, KOS and KOSS redshift surveys are all compatible with Schechter functions. The L.F. for the CfA survey does not fit a Schechter function; the bright end falls off less steeply than if it were Schechter. They argue that this is caused by the large random errors in the Zwicky magnitudes: there is no evidence for morphological differences in type for types earlier than Sc. Later type galaxies (Sc-I) are significantly fainter than earlier types.

The AARS

Contains 340 galaxies in five fields. Assumes Hubble flow, and luminosity distance for a Friedmann model with $q_0 = 0.5$. Uses k–corrections:

Table A6. AARS k–corrections

Galaxy type	$k\,B_J$	$k\,J_{KOS}$
E-S0	$4.14z$	$3.3z$
Sa-Sb	$2.90z$	$2.2z$
Sc	$2.25z$	$1.7z$
Sd-Sm	$1.59z$	$1.1z$

Table A7. The AARS results

Type	B_J^*	α
ALL	-19.56	-1.04
E-S0	-19.37	-0.48
S	-19.64	-1.24

The CfA survey

The sample size is large ($\sim$ 2000 galaxies), and systematic uncertainties in the Zwicky magnitude system and the Virgo 0 infall model are much larger than the random errors. Their analysis suggests that the CfA L.F. differs significantly from a Schechter form, with a more abrupt change of slope, and an excess of bright galaxies at $M_Z < -21$. Efstathiou *et al.* attribute the apparent discrepancies with the results from the RSA and deep surveys to errors in the Zwicky magnitudes.

The overall survey results

Any inter-comparison of L.F. results must be considered as only approximate, due to difficulty in correcting precisely for the different photometric systems. Transforms between these systems will need colour (or morphological type) terms, isophotal corrections, etc. Transforming from M^* of one system to another by simply adding an offset constant is a gross simplification, but it is attempted by Efstathiou *et al.* on the basis that the size of the error ellipses is so large, while differences between the L.F.s of different morphological types is small. With this proviso, they give the following offset correction table:

$$B_T = m_Z - 0.29$$

$$B_T = J_{KOS} + 0.35$$

$$B_T = B_J - 0.29$$

and this is adapted to give corrections in terms of B_J:

$$B_J = B_T + 0.29$$

$$B_J = J_{KOS} + 0.64$$

$$B_J = F_{KOS} + 1.64$$

$$B_J = m_Z$$

The following summary table was prepared using these conversion figures.

Table A8. The collected results

Survey	Type	B_J^*	α
AARS	ALL	−19.56	−1.04
	E-S0	−19.37	−0.48
	S	−19.64	−1.24
KOS	ALL	−19.59	−1.64
	E-S0	−19.37	−1.04
	S	−19.23	−1.72
KOSS	ALL	−19.43	−1.04
	ALL[†]	−19.70	−1.20
RSA	ALL	−19.27	−1.12
	E-S0	−19.58	−1.36
	Sa-Sb	−19.21	−0.72
	Sc-SI	−18.69	−1.16
Phillipps & Shanks	ALL	−19.8	−1.0
CfA	ALL	−19.16	−0.96

Given the large error ellipses, and with the exception of the CfA survey, Efstathiou *et al.* (1988) consider that the L.F.s derived from the redshift surveys are compatible with each other and give mean values of:

$$\alpha = -1.07 \pm 0.05$$

$$M_{B_J}^* = -19.68 \pm 0.10 \quad (H_0 = 100)$$

$$\phi^* = (1.56 \pm 0.34) \times 10^{-2} \ \mathrm{Mpc}^{-3}$$

Efstathiou concludes that one cannot significantly improve the results by combing surveys, since we lack accurate transforms between the surveys. Any generalisation of the luminosity function for galaxies at the present time is therefore problematical and, to a certain degree, arbitrary. The division into five different galaxy types by Metcalfe *et al.* (1991), each with its own ϕ_0^*, M^*, and α is probably the best overall method available.